

**NASA CONTRACTOR
REPORT**

NASA CR-1292



NASA CR-1292

NASA
CR
1290
v.3
c.1



TECH LIBRARY KAFB, NM

LOAN COPY: RETURN TO
AFWL (WLIL-2)
KIRTLAND AFB, N MEX

**HIGH-PERFORMANCE
TURBOALTERNATOR AND
ASSOCIATED HARDWARE**

III - DESIGN OF BACKUP GAS BEARINGS

by W. Shapiro, J. T. McCabe, T. W. Chu, and V. Castelli

Prepared by
UNITED AIRCRAFT CORPORATION
East Hartford, Conn.

NATIONAL AERONAUTICS AND SPACE ADMINISTRATION • WASHINGTON, D. C. • FEBRUARY 1969



0060595

NASA CR-1292

HIGH-PERFORMANCE TURBOALTERNATOR AND ASSOCIATED HARDWARE

III - DESIGN OF BACKUP GAS BEARINGS

By W. Shapiro, J. T. McCabe,
T. W. Chu, and V. Castelli

Distribution of this report is provided in the interest of information exchange. Responsibility for the contents resides in the author or organization that prepared it.

Prepared under Contract No. NAS 3-6013 by
THE FRANKLIN INSTITUTE RESEARCH LABORATORIES
Philadelphia, Pa.

under Subcontract to Pratt & Whitney Aircraft,
Division of United Aircraft Corporation, East Hartford, Conn.

for Lewis Research Center

NATIONAL AERONAUTICS AND SPACE ADMINISTRATION

For sale by the Clearinghouse for Federal Scientific and Technical Information
Springfield, Virginia 22151 - CFSTI price \$3.00

ABSTRACT

The National Aeronautics and Space Administration is conducting an evaluation of candidate Brayton Cycle Turbomachinery. As part of this program, Pratt & Whitney Aircraft has delivered a turboalternator incorporating a two stage axial-flow turbine driving a four pole inductor alternator supported on gas bearings. A backup gas bearing system was designed by the Franklin Institute Research Laboratories. Steady-state and dynamic operating characteristics were established by numerical methods programmed on a digital computer. A comprehensive description of the analysis and results are presented along with assembly design drawings of the selected journal and thrust bearings.

FOREWORD

The research described herein was conducted by the Franklin Institute Research Laboratories under subcontract to Pratt & Whitney Aircraft, Division of United Aircraft Corporation (NASA Contract NAS 3-6013). The project was managed by Mr. Henry B. Tryon, Space Power Systems Division, NASA-Lewis Research Center. The report was originally issued as Pratt & Whitney PWA-3070, volume 3 (Franklin Institute Research Laboratories F-B2263).

TABLE OF CONTENTS

SUMMARY	xxi
I. INTRODUCTION.	1
II. JOURNAL BEARINGS.	3
A. Basic Configuration	3
B. Specifications and Performance Requirements.	5
C. Analytical Approach	5
D. Steady-State Analysis	5
E. Results - Steady-State Analysis	14
F. Dynamic Analysis.	28
G. Results - Dynamic Analysis.	36
H. Rigid Rotor Dynamics.	48
I. Mechanical Design	50
J. Conclusions and Recommendations	50
III. THRUST BEARING.	53
A. Configuration	53
B. Specifications and Performance Requirements.	56
C. Analytical Approach	56
D. Main Hybrid Bearing - Steady-State and Stability Analysis.	57
E. Bi-Directional Pair Steady-State and Stability Analysis.	67
F. Determination of Viscous Friction Losses.	75
G. Determination of Bearing Righting Moment Capability.	80
H. Synchronous Vibrations of Thrust Bearing.	80
I. Thermal Distortion.	84
J. Main Thrust Bearing - Analytical Results.	88
K. Bi-Directional Pair - Analytical Results.	108
L. Mechanical Design - Hybrid Thrust Bearing	116
M. Conclusions and Recommendations - Hybrid Thrust Bearing	123
IV. REFERENCES.	125
APPENDIX A - Calculations of Synchronous Vibrations and Thermal Distortions	126
APPENDIX B - Final Design and Performance of Thrust Bearing.	129

LIST OF FIGURES

<u>Figure</u>		<u>Page</u>
A	Sectional View of Turbine-Alternator.	2
1	Hybrid Journal Bearing.	4
2	Geometric Parameters - Hybrid Journal Bearing	7
3	Conceptual Flow Chart - Steady-State Program.	13
4	Steady-State Computer Output - Hybrid Journal Bearing	15
5	Attitude Angle and Load Coefficient vs Groove Location Angle - Hybrid Journal Bearing	16
6	Attitude Angle and Load Coefficient vs Flow Coefficient - Hybrid Journal Bearing.	18
7	Attitude Angle and Load Coefficient vs Eccentricity Ratio-Hybrid Journal Bearing	19
8	Dimensionless Flow vs Eccentricity Ratio-Hybrid Journal Bearing	21
9	Dimensionless Friction Moment vs Eccentricity Ratio- Hybrid Journal.	22
10	Dimensionless Recess Pressure vs Eccentricity Ratio- Hybrid Journal Bearing.	23
11	Load and Attitude Angle vs Eccentricity Ratio-Hybrid Journal Bearing	24
12	Flow vs Eccentricity Ratio-Hybrid Journal Bearing.	25
13	Friction Horsepower vs Eccentricity Ratio-Hybrid Journal Bearing.	26
14	Coordinate System.	29
15	Flow Chart - Dynamics Program.	35
16	Dynamic Program Computer Output I - Hybrid Journal Bearings	37

LIST OF FIGURES (CONT.)

<u>Figure</u>		<u>Page</u>
17	Dynamic Program Computer Output II - Hybrid Journal Bearings	38
18	Orbit of Shaft Mass Center - Hybrid Journal Bearings	39
19	Orbit of Shaft Mass Center - Hydrodynamic and Hybrid Journal Bearings.	41
20	X and Y Displacement of Mass Center vs Shaft Revolutions - Hybrid Journal Bearings.	42
20a	X and Y Forces vs Shaft Revolutions - Hybrid Journal Bearings	43
21	Relative Angular Displacement Between Shaft and Bearing 1 vs Shaft Revolutions - Hybrid Journal Bearings	44
22	Relative Angular Displacement Between Shaft and Bearing 2 vs Shaft Revolutions-Hybrid Journal Bearings	45
23	Shaft Angular Displacements vs Shaft Revolutions	46
24	Bearing Angular Displacements vs Shaft Revolutions.	47
25	Rigid Rotor Analysis - Amplitude vs Shaft Speed.	49
26	Mechanical Design - Hybrid Journal Bearing	51
27	Hybrid Thrust Bearing.	54
28	Reaction Thrust Bearing.	55
29	Load Factor vs Compression Ratio - Spiral Groove Thrust Bearing	63
30	Flow Chart - Main Hybrid Thrust Bearing.	68
31	Bi-Directional Pair - Schematic.	69

LIST OF FIGURES (CONT.)

<u>Figure</u>		<u>Page</u>
32	Flow Chart - Bi-Directional Opposed Thrust Pair.	76
32B	Flow Chart - Bi-Directional Opposed Thrust Pair.	77
33	Friction Factor vs Clearance - Spiral Groove Bearing.	79
34	Restoring Moment - geometric parameters.	81
35	Synchronous Vibration of Thrust Bearing.	83
36	Thermal Distortion - Analytical Model.	85
37	Groove Depth vs Compression Ratio - $W_H = 30$ lbs.	89
38	Groove Depth vs Compression Ratio - $W_H = 86$ lbs.	90
39	Program Output - Hybrid Thrust Bearing $D_o = .020$, $h_o = .008$	92
40	Program Output - Hybrid Thrust Bearing $D_o = .031$, $h_o = .0095$	93
41	Program Output - Hybrid Thrust Bearing $D_o = .020$, $h_o = .0044$	94
42	Program Output - Hybrid Thrust Bearing $D_o = .031$, $h_o = .005$	95
43	Load vs Clearance - Hybrid Thrust Bearing ($R_2 = 3.0$ in for W_{SG} curve).	96
44	Load vs Clearance - Hybrid Thrust Bearing ($R_2 = 2.5$ in for W_{SG} curve).	98
45	Stiffness vs Clearance - Hybrid Thrust Bearing	99
46	Flow vs Clearance - Hybrid Thrust Bearing.	101
47	Friction Horsepower vs Clearance - Hybrid Thrust Bearing.	102

LIST OF FIGURES (CONT.)

<u>Figure</u>		<u>Page</u>
48	Load vs Clearance - Hybrid Thrust Bearing ($D_o = .020$)	103
49	Stiffness vs Clearance - Hybrid Thrust Bearing ($D_o = .020$)	104
50	Comparison of Critical Recess Depths Between Orifice Compensated and Inherently Compensated Thrust Bearings.	106
51	Program Output I - Bi-Directional Pair ($N = 12,000$)	109
52	Program Output II - Bi-Directional Pair ($N = 12,000$)	110
53	Program Output III- Bi-Directional Pair ($N = 12,000$ RPM)	111
54	Program Output IV - Bi-Directional Pair ($N = 12,000$ RPM)	112
55	Load vs Clearance - Bi-Directional Pair ($N = 0$ RPM)	113
56	Load vs Clearance - Bi-Directional Pair ($N = 12,000$ RPM)	114
57	Flow vs Clearance - Bi-Directional Pair.	115
58	Axial Stiffness vs Clearance - Bi-Directional Pair	118
59	Axial Stiffness vs Load - Bi-Directional Pair.	119
60	Mechanical Design - Hybrid Thrust Bearing.	120
61	Groove Geometry - Hybrid Thrust Bearing.	121
62	Tabulation of Groove Coordinates - Hybrid Thrust Bearing	122

NOMENCLATURE

Steady State Journal Bearing Analysis

- A_1 = dimensionless angular excursion in x-z plane = $\frac{L}{C} \alpha_1$
- A_2 = dimensionless angular excursion in y-z plane = $\frac{L}{C} \alpha_2$
- A_o = orifice area
- BFC = bearing flow coefficient
- C = bearing radial clearance
- C_D = orifice coefficient of discharge
- C_L = dimensionless total load capacity
- C_N = dimensionless load capacity normal to line of centers
- C_T = dimensionless load capacity tangent to line of centers
- COE = BFC/OFC
- D = shaft diameter
- f_L = bearing mass flow
- $f_{L\theta}$ = mass flow normal to circumferential line
- $f_{L\eta}$ = mass flow normal to axial line
- FHP = friction horsepower loss
- FMOM = dimensionless friction moment = M_s
- G = orifice coefficient = $\sqrt{\frac{2\gamma}{(\gamma-1)R_g T_g}}$
- H = dimensionless clearance (non dimensionalized with respect to C)
- $K = 1/R_g T_g$
- L = bearing length
- M_B = dimensionless bearing mass flow

NOMENCLATURE

Steady State Journal Bearing Analysis (Cont'd)

- M_o = dimensionless orifice mass flow
 M_{xx} = moment about x-x axis through center of bearing
 M_{yy} = moment about y-y axis through center of bearing
 M_s = dimensionless friction moment (non dimensionalized with respect to $P_a RCL$)
 N = shaft RPM
 N_o = no. of orifices per sector
 OFC = orifice flow coefficient = $\frac{N_o A_o C_d P_s G}{K P_a^2 C^3}$
 P_a = ambient pressure
 P = dimensionless pressure (non-dimensionalized with respect to P_a)
 P_r = dimensionless recess pressure (non-dimensionalized with respect to P_a)
 P_s = dimensionless supply pressure (non-dimensionalized with respect to P_a)
 p_s = supply pressure
 $Q = P^2 H^2$
 R = shaft radius
 R_g = gas constant
 $RESFLO$ = dimensionless bearing mass flow = M_B
 $RESPR$ = dimensionless recess pressure = P_r
 T_g = absolute gas temperature
 $TORX$ = dimensionless torque about x-x axis through center of bearing = $\frac{M_{xx}}{P_a R^2 L}$

NOMENCLATURE

Steady State Journal Bearing Analysis (Cont'd)

TOR_Y = dimensionless torque about y-y axis through center of

$$\text{bearing} = \frac{M_{yy}}{P_a R^2 L}$$

W = Bearing Load

X = dimensionless x displacement (non-dimensionalized with respect to C)

Y = dimensionless y displacement (non-dimensionalized with respect to C)

Z = dimensionless axial distance from bearing center plane (non-dimensionalized with respect to L)

α = sector included angle

α_1 = angle between shaft and bearing in x-z plane

α_2 = angle between shaft and bearing in y-z plane

β = angle between load vector and nearest groove

ξ = angle between line of centers and beginning of first sector

δ = bearing attitude angle

ϵ = eccentricity ratio

γ = ratio of specific heats

η = axial coordinate (non-dimensionalized with respect to L)

Λ = compressibility No. = $\frac{6\mu\omega}{P_a} \left(\frac{R}{C}\right)^2$

μ = absolute viscosity

ω = shaft speed

ψ = PH

θ = circumferential coordinate

NOMENCLATURE

Journal Bearing - Dynamics Analysis

A_1, A_2 = dimensionless conical motion of shaft. Defined as
 $\frac{\alpha_1 L}{C}, \frac{\alpha_2 L}{C}$

A_r = recess area

B = dimensionless shaft mass parameter

$$B = \frac{P_a R L}{M C \frac{\Omega}{2}^2}$$

B_{1j}, B_{2j} = dimensionless conical motion of j^{th} bearing. Defined as
 $\beta_1 \frac{L}{C}, \beta_2 \frac{L}{C}$

C = radial clearance

d_r = recess depth

D_r = dimensionless recess depth = d_r/c

f_L = bearing mass flow rate out of recess

f_o = restrictor mass flow rate into recess

F_L = dimensionless bearing mass flow rate = $\frac{2R T}{\Omega P_a C R^2} f_L$

F_o = dimensionless restrictor flow rate = $\frac{2R T}{\Omega P_a C R^2} f_o$

G = dimensionless shaft gyroscopic parameter = $\frac{2I_p}{I_t}$

h = clearance

H = dimensionless clearance = h/c

h_r = average film over the recess

H_r = dimensionless clearance over recess = h_r/c

NOMENCLATURE

Journal Bearing - Dynamics Analysis

$$I_{Bj} = \text{dimensionless inertia parameter of } j^{\text{th}} \text{ bearing} = \frac{P_a PL^3}{I_{tj} C \left(\frac{\Omega}{2}\right)^2}$$

I_p = polar moment of inertia

I_t = transverse moment of inertia

I_s = dimensionless shaft inertia parameter

$$= \frac{P_a RL^3}{I_t C \left(\frac{\Omega}{2}\right)^2}$$

L = bearing length

M = bearing mass

m = unbalance mass on the mass center plane

NB = number of bearings

NS = number of sectors in a bearing

$$O_F = \text{orifice flow parameter} = \frac{2N_o A_o C_d P_s}{\Omega R^2 C P_a} \sqrt{\frac{2\gamma R T_g}{(\gamma-1)}}$$

p = dimensional pressure

p_r = dimensional recess pressure

p_s = dimensional supply pressure

p_a = ambient pressure

P = dimensionless pressure = p/P_a

P_r = dimensionless recess pressure = p_r/P_a

P_s = dimensionless supply pressure = p_s/P_a

$r = P_r/P_s$

R = bearing radius

t = time

NOMENCLATURE

Journal Bearing - Dynamics Analysis (Cont'd)

T = dimensionless time = $t \frac{\Omega}{2}$

U_f = dimensionless unbalance in plane of center of mass = $\frac{MR\Omega^2}{P_a RL}$

U_m = dimensionless unbalance moment = $\frac{LR\Omega^2}{P_a RL^2}$

V_r = recess volume

W_y = dimensionless external load (non-dimensionalized with respect to $P_a RL$)

X-Force = dimensionless Force in x direction (non-dimensionalized with respect to $P_a RL$)

Y-Force = dimensionless Force in y direction (non-dimensionalized with respect to $P_a RL$)

Z_{Bj} = dimensionless position of j^{th} bearing measured from shaft center of mass = Z_{bj}/L

α_1, α_2 = angles between shaft axis and bearing center axis in x-x and z-y planes respectively

β_1, β_2 = angles between bearing axis and bearing center axis for bearings 1 and 2 respectively

ΔT = time increment for computer program

γ = ratio of specific heats

Λ = bearing compressibility number = $\frac{6\mu\Omega}{P_a} \left(\frac{R}{C} \right)^2$

η = axial coordinate (non-dimensionalized with respect to L)

Ω = shaft speed

ρ_r = recess density

θ = circumferential coordinate

τ = unbalance moment

NOMENCLATURE

Rigid Rotor Program

M = shaft mass

ΔM_1 = unbalanced mass 1

ΔM_2 = unbalanced mass 2

R = shaft radius

ϕ_M = angle between unbalanced masses 1 and 2

Thrust Bearing

a_1 = groove width - in.

a_2 = ridge width - in.

A = effective bearing area - in.²

A_o = orifice area - in.²

A_R = groove area = $(\pi R_2^2/2)$ in.²

A_P = projected area of bearing = (πR_4^2) - in.²

C_D = orifice discharge coefficient = 0.8

C_L = load factor = $\frac{W_{SG} h^2}{\mu \omega R_2^4}$

D = bearing diameter - in.

D_o = orifice diameter - in.

h = clearance - in.

h_o = groove depth - in.

h' = clearance variation about equilibrium position - in.

H_T = total axial clearance of Bi-Directional Pair - in.

NOMENCLATURE

Thrust Bearing

k = number of grooves

m = mass of rotor - lb-sec²/in.

M = mass constant - lb-sec²/in.

N_o = number of orifices

P_a = ambient pressure - psia

P = pressure - psia

P_r = recess pressure - psia

P_s = supply pressure - psia

P_{rh} = equivalent hybrid recess pressure - psia

$(P_r/P_s)_{crit}$ = critical pressure ratio for choked flow

p = pressure variation in recess about equilibrium position -psia

q = variation in bearing mass flow- lb-sec/in.

Q_o = mass flow through orifice - lb-sec/in.

Q_B = mass flow through bearing - lb-sec/in.

Q_T = total mass flow of bi-directional pair - lb-sec/in.

R = electrical resistance of analog model

r = electrical resistance of unit square of conducting sheet

R_1 = inside radius of grooved region - in. (Hybrid Bearing)
inside radius-in (Reaction Bearing)

R_2 = outside radius of grooved region - in. (Hybrid Bearing)
radius to inside of orifice, in. (Reaction Bearing)

R_3 = radius to orifice circle - in. (Hybrid Bearing) radius
to outside of orifice, in (Reaction Bearing)

R_4 = outside radius of bearing - in.

R_g = gas constant $\frac{\text{in.}^2}{\text{sec}^2-\text{°F}}$

NOMENCLATURE

Thrust Bearing

T = temperature °F

T_g = absolute temperature °R

V_B = volume flow through bearing - in.³/sec

W_{EP} = load carrying capacity of Main Thrust Bearing due to external pressurization - lbs

W_H = total load capacity of hybrid bearings - lbs

W_{SG} = load capacity of spiral-groove bearing - lbs

W_T = load capacity of bi-directional pair - lbs

α = angle between tangent to spiral groove and normal to radius - rad

δ = compression ratio = h/h_o

Δ = recess depth = h_o - in

γ = a_2/a_1 , ratio of specific heats

λ = R_1/R_2

μ = viscosity lb-sec/in.²

ω = angular velocity - rad/sec

ρ = mass density - lb-sec²/in⁴

NOMENCLATURE

Righting Moment

- k = stiffness of one orifice sector of gas film - lbs/in
- K'_{EP} = axial stiffness of single orifice sector - externally pressurized bearing - lbs/in
- K_T = tilting stiffness of bearing fluid film - in-lb/rad
- S_{EP} = axial stiffness of externally pressurized bearing-lb/in.
- S_{SG} = axial stiffness of spiral groove bearing-lb/in.

Synchronous Vibrations

- D = diameter of thrust bearing - in
- I_T = transverse moment of inertia of thrust bearing - lb-in-sec²
- K_T = tilting stiffness of bearing plus self aligning support in-lb/rad
- ϵ = relative angle of swash - rad
- ξ = angle of swash in plane of paper - rad
- ζ = angle of swash perpendicular to plane of paper - rad
- ω = swashing frequency - rad/sec
- ω_c = natural frequency in swashing mode - rad/sec

Viscous Friction

- F = viscous shear stress - lb/in²
- G_2 = friction factor
- HP = friction horsepower
- h = clearance - in
- N = shaft RPM
- r = radius - in

NOMENCLATURE

Viscous Friction

R_{in} = inside radius - in

R_{out} = outside radius - in

T_f = friction torque - in-lbs

$(T_f)_{sg}$ = friction torque - grooved section - in-lbs

v = relative velocity - in/sec

μ = absolute viscosity friction - lb-sec/in²

ω = angular velocity - rad/sec

$\lambda = R_2/R_1$

Thermal Distortion

a = thickness of bearing = in.

F = heat generation - $\frac{BTU}{hr-ft^2}$

K = thermal conductivity BTU/Hr-in-°F

K_1 = const.

P = power generation - BTU/Hr

R = radius of curvature - in.

r = radial distance - in.

y = total distortion - in.

α' = coefficient of thermal expansion in/in-°F

ΔL = differential increase in length of bearing - in.

ΔT = temperature differential - °F

SUMMARY

This report presents a detailed description of a program, conducted by The Franklin Institute Research Laboratories (FIRL) for the analysis and design of a gas (argon) bearing system for a Brayton Cycle turbo-alternator that is to produce electric power in a space vehicle. The overall bearing program was a parallel effort by a group of organizations so that alternatives would be available in case of difficulties with the primary system. To insure against duplication of effort the objectives of the FIRL program were specified as the design and analysis of hybrid journal and thrust bearings.

Because of the complex nature of the lubrication problem, the analysis (comprehensively described in the body of the report) was accomplished by numerical methods programmed on a digital computer. For both the thrust and journal bearings steady-state and dynamic analyses were accomplished. The steady-state results provided parametric performance over a wide range of operating conditions; the more complicated and lengthy dynamic analysis was used to establish the stability of the bearings and bearing-rotor system using geometric variables selected on the basis of steady-state results. Assembly drawings of the bearing configurations are included in sufficient detail to readily permit the production of final shop drawings.

Steady-state performance of both the journal and thrust bearings is considered excellent. Stability characteristics of the journal bearings are marginal; recommendations for an extended effort designed to improve stability are referred to.

1. INTRODUCTION

One of the candidate machinery configurations for application in a Brayton cycle space vehicle power source employs a turbine driven compressor and a turbine driven alternator on separate shafts. The cycle fluid, argon, enters the compressor at approximately 75°F and is discharged at higher pressure to a regenerator and the heat source where the fluid is heated to 1490°F. The argon flows through the turbine which drives the compressor at high speed and then passes through a two-stage axial flow turbine which drives the alternator. The gas is cooled in the regenerator and in the heat rejection system before being returned to the compressor. A 4-pole alternator was selected, which is driven at 12,000 rpm to provide three-phase, 400 cycles per second electric power. Gas bearings on each side of the alternator provide radial rotor support and the turboalternator thrust is supported by a gas bearing on the free end of the alternator. The bearings are required to support the rotor on the ground in various orientations and in space with nominally no gravitational forces.

The turboalternator was developed for a Brayton cycle space power plant by Pratt & Whitney Aircraft under contract for the National Aeronautics and Space Administration. Under subcontract, the Franklin Institute Research Laboratories has provided one of two gas bearing designs for this unit. The Franklin Institute Research Laboratories was assigned the task of the design and analysis of hybrid journal and thrust bearings. In the hybrid bearing the purely hydrodynamic or self-generating capacity is supplemented by the introduction of pressurized lubricant into the bearing clearance volume. With a small expenditure of supply gas a considerable increase in load capacity and an improvement stability characteristics can be achieved. Figure A is a sectional view of the turboalternator.

In this report, the journal and thrust bearing analysis and design are discussed. In broad perspective the analysis is separated into two major categories, the steady-state (or equilibrium) and the dynamic. Dynamic analysis is especially significant in gas bearing investigations because the inherent low damping properties of gas bearings enable self-excited instabilities to be easily initiated.

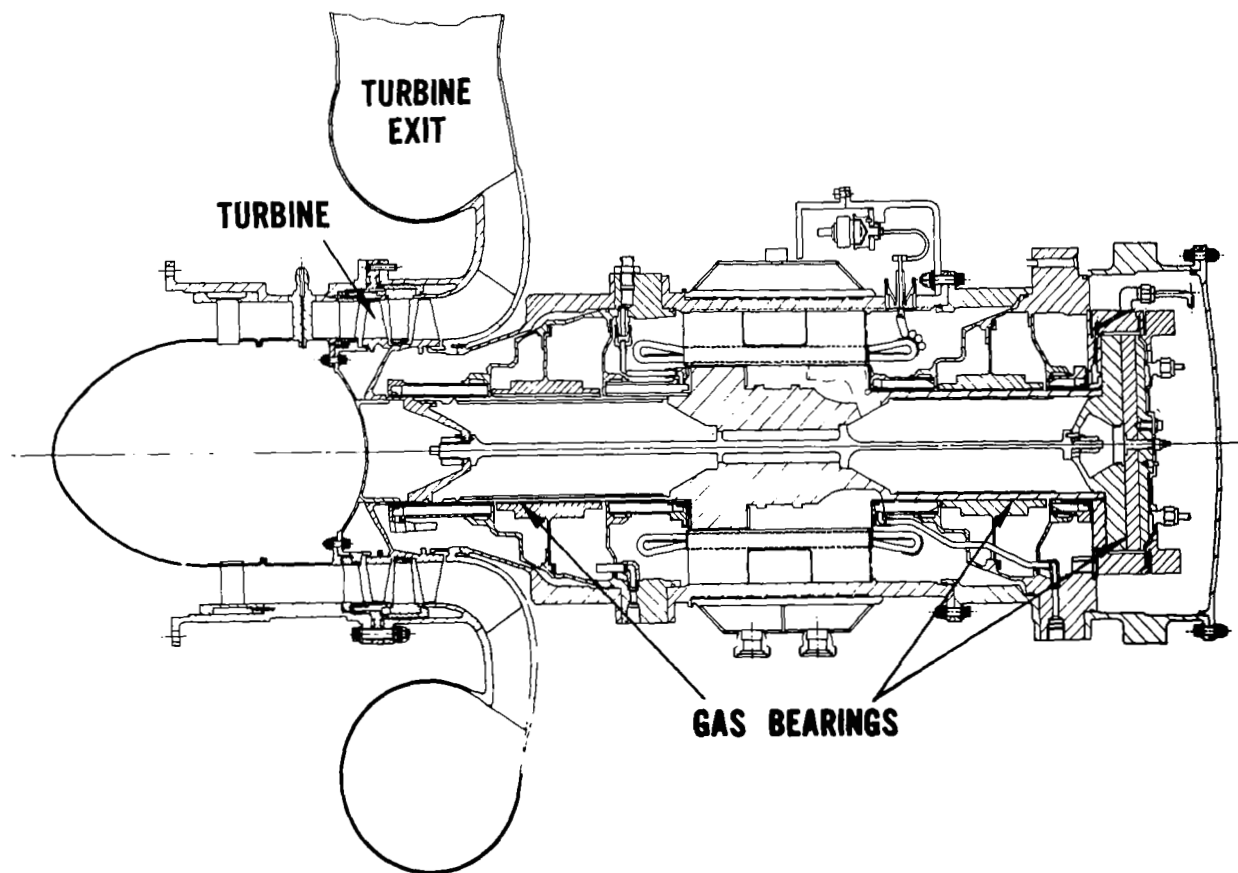


Fig. A - Sectional View of Turbine-Alternator

II. JOURNAL BEARINGS

A. Basic Configuration

Figure 1 schematically represents the journal bearing configuration. The total angular extent of the bearing is 360° , but three axial grooves extending the full length of the bearing trisect the bearing into geometrically equivalent sectors. The axial grooves have included angles of 5° each. In each sector of the bearing, 20° from the leading edge, are axially aligned recesses through which externally pressurized gas is introduced. The external gas is supplied from a common source and passes through an orifice restrictor prior to entering each recess. The bearing shell is supported by an alignment mechanism that will allow rotation but not translation. Some of the advantages of this type of bearing are:

- (1) It is a simple configuration with a minimum number of parts. At installation the journal bearings can be line bored in place to ensure an accurate set up; the absence of final adjustment removes much of the chance of installation errors.
- (2) Segmentation of the bearing will reduce attitude angles and improve stability characteristics.
- (3) Introduction of the external gas near the leading edge feeds the natural pumping action of the bearing. In addition to the benefits derived from external pressurization, the external gas essentially raises the ambient pressure level for the hydrodynamic action.
- (4) The recesses located near the leading edge ensure good separation of maximum hydrodynamic and hydrostatic pressures. This is especially significant to this application because of the low supply to ambient pressure ratio of two to one. It would be quite possible that, if the recesses were located further inside the bearing area, hydrodynamic pressures would exceed the external pressure causing reverse flow through the orifice.

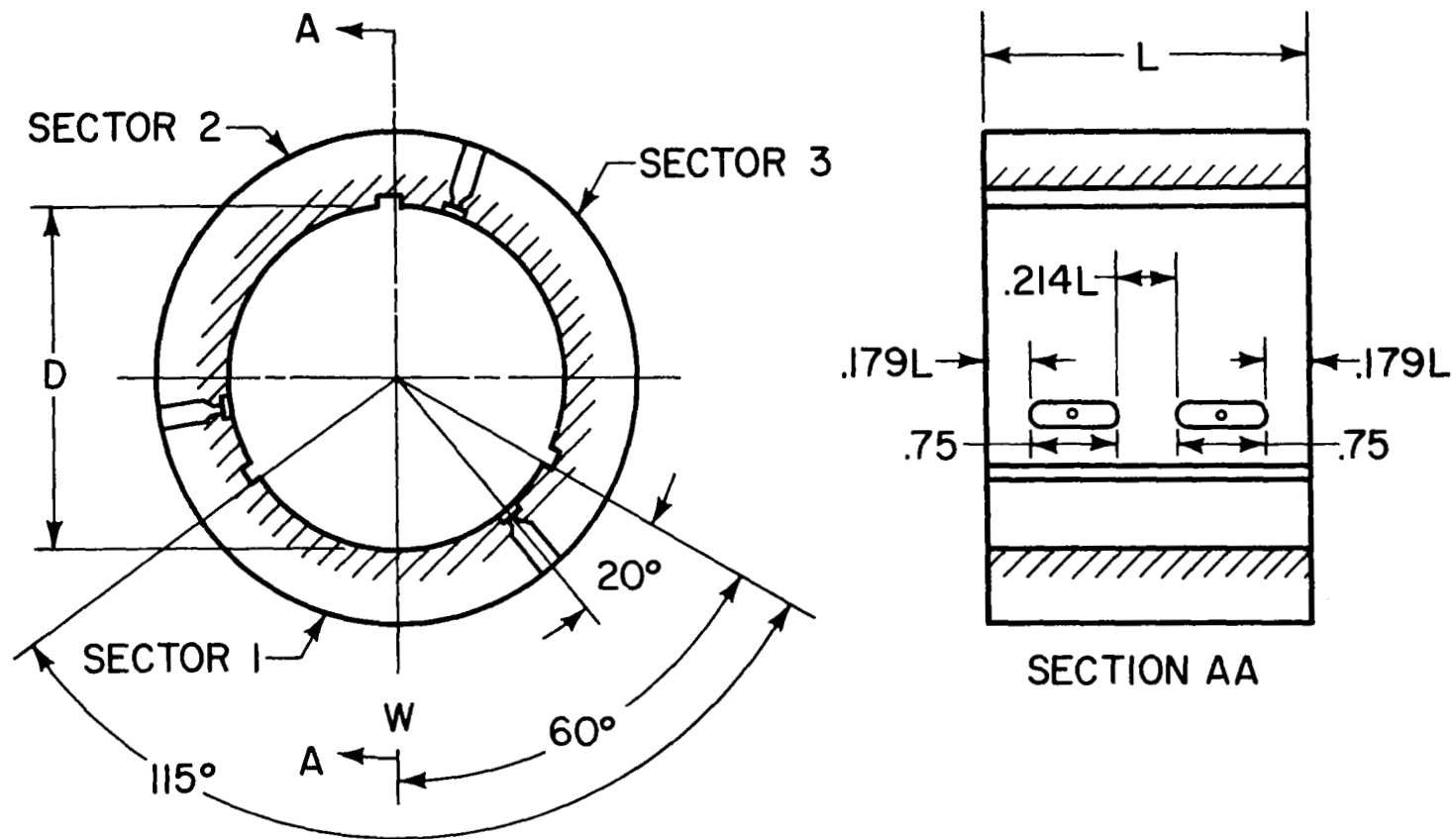


Figure 1 - Hybrid Journal Bearing

B. Specifications and Performance Requirements

The following specifications were used for performing the analysis:

- (1) Lubricant - argon gas
- (2) Operating temperature, $T = 760^{\circ}\text{R}$ (300°F)
- (3) Operating shaft speed, $N = 12,000$ RPM (normal), $14,400$ RPM (overspeed)
- (4) Supply pressure, $P_s = 12$ psia (normal), 13.8 psia (Max)
- (5) Ambient pressure, $P_a = 6$ psia
- (6) Journal diameter, $D = 3.5$ in
- (7) Bearing length, $L = 3.5$ in
- (8) Bearing load, $W = 0-35$ lbs.

The target performance parameters were

- (1) Minimum operating clearance $h = 1$ mil
- (2) Maximum allowable flow $f_L = 0.006$ lbs/sec (1% of compressor flow)
- (3) Minimum orifice diameter, $D_o = 0.015$ in
- (4) Maximum friction loss, $\text{FHP} = 0.1$ HP

To accomplish these performance requirements, a preferred load direction was permitted when the alternator was operating in the horizontal attitude.

C. Analytical Approach

The journal bearing analysis was accomplished by two digital computer programs. A purely steady-state investigation produced operating performance parameters. Stability of the rotor bearing system was tested by a separate time-transient dynamic investigation. To handle both problems simultaneously is not practical since the required computer time would be monumental. The dynamic analysis, in addition to the solution of the Reynold's lubrication equations containing the time transient terms, requires solution of the equations of motion applied to

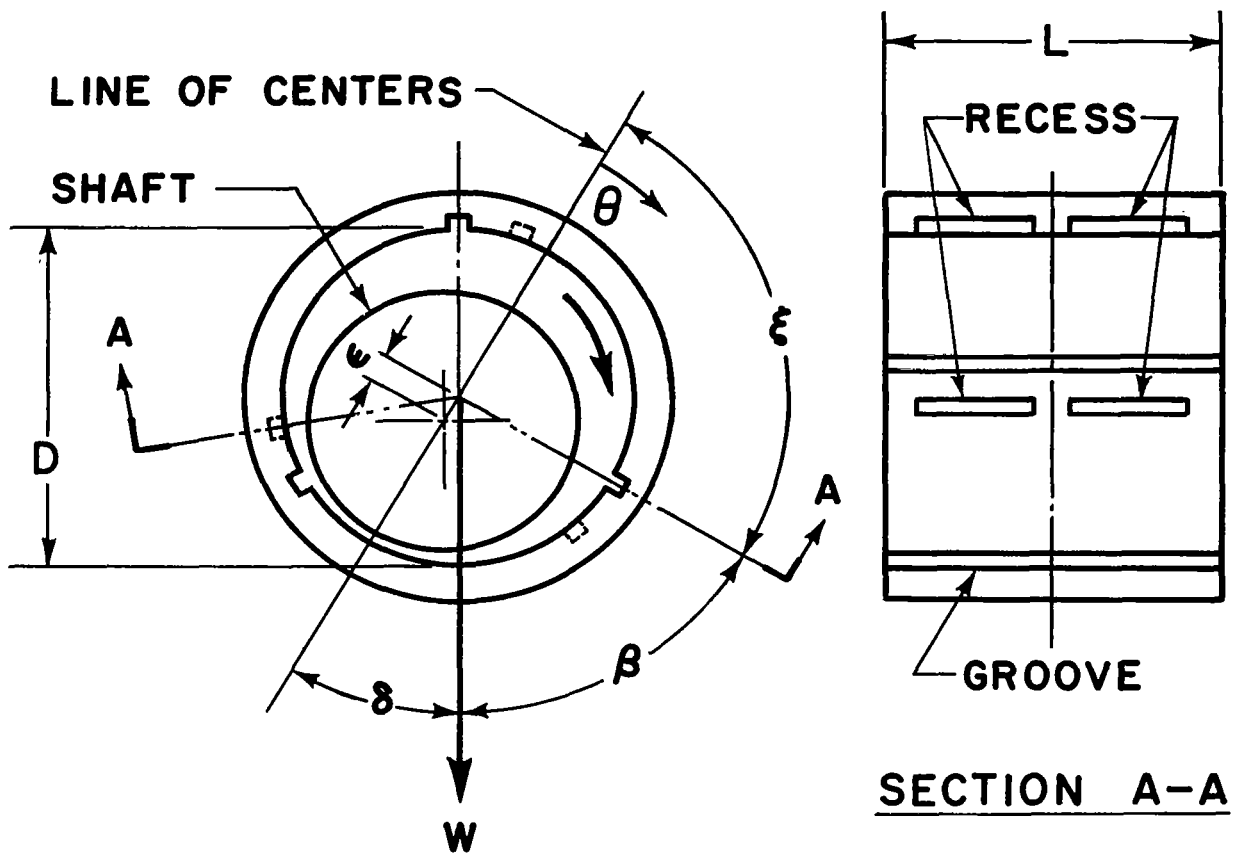
the shaft and bearings; i.e. the equations are applied to a simulated system consisting of a shaft and two bearings. To establish a quasi-steady repetitive cyclic motion of the shaft and bearings at a single operating point involves a large number of repetitive solutions, resulting in a considerable amount of digital computer time. When confronted with determining the effect of the relatively large number of variables such as load, orifice size, eccentricity, speed, etc., which is an ordinary requisite for properly describing performance, use of the dynamic program is currently entirely unfeasible. It is much more efficient to write a separate computer program confined to solving the steady lubrication equations applied to one single bearing. After a bearing configuration is selected on the basis of the steady-state results, the dynamic program can then be utilized to determine stability at only a few operating points at which the stability problem is most pronounced. For this project separate programs have been written, designated "Steady-State Program" and "Time Transient Dynamics Program".

D. Steady-State Analysis

The configuration with appropriate designation of the geometric variables is shown on Figure 2. The steady-state problem is solved when the pressure distribution is such that the Reynolds equation is satisfied at all points in the bearing area, and equality of mass flow through the orifices and bearing lands of each sector exist.

The bearing area is first subdivided into a grid of finite spacing. The film thickness at each grid point is made up of:

- (1) The concentric clearance
- (2) The radial components of displacement of the shaft center
- (3) The radial components due to the shaft angular misalignment



ϵ ANGLE FROM LINE OF CENTERS TO SECTOR I
 β ANGLE BETWEEN LOAD DIRECTION AND SECTOR I
 δ ATTITUDE ANGLE

Figure 2 - Geometric Parameters - Hybrid Journal Bearing

The resulting dimensionless clearance distribution is

$$H = 1 + (x + \eta A_1) \sin \theta + (Y + \eta A_2) \cos \theta \quad (1)$$

where

$$\eta = Z - 1/2 \quad (2)$$

The shaft position is specified externally and the clearance determined at all grid points of a sector from equation (1).

The pressure in the bearing area is governed by the Reynolds equation for isothermal films. In dimensionless form this equation is

$$\frac{\partial}{\partial \theta} \left(PH^3 \frac{\partial P}{\partial \theta} \right) + \frac{R^2}{L^2} \frac{\partial}{\partial \eta} \left(PH^3 \frac{\partial P}{\partial \eta} \right) = \Lambda \frac{\partial PH}{\partial \theta} \quad (3)$$

This equation is transformed so that the dependent variable is $Q(P^2 H^2)$ rather than P . The variable Q is selected because the transformed equation is nearly linear, and the function Q is smooth and therefore well suited to a finite difference scheme. For high values of Λ , the pressure can vary from maximum to ambient in a short distance. On either side of P_{\max} the pressure gradients are large. If P is used as a variable small grid intervals with consequent long running times are required for numerical convergence. The transformed expanded equation is

$$-\frac{1}{2} \frac{\partial H}{\partial \theta} \frac{\partial Q}{\partial \theta} + \frac{H}{2} \frac{\partial^2 Q}{\partial \theta^2} - Q \frac{\partial^2 H}{\partial \theta^2} + \frac{R^2}{L^2} \left[-\frac{1}{2} \frac{\partial H}{\partial \eta} \frac{\partial Q}{\partial \eta} + \frac{H}{2} \frac{\partial^2 Q}{\partial \eta^2} - Q \frac{\partial^2 H}{\partial \eta^2} \right] = \frac{\Lambda}{2\sqrt{Q}} \frac{\partial Q}{\partial \theta} \quad (4)$$

At all edges of each sector the pressure is known to be ambient. Starting from an assumed pressure distribution in the recess and bearing area equation (4) is explicitly iterated until it is satisfied at all interior points exclusive of the recesses. The assumed pressure in the recess must now be adjusted to satisfy equality of mass flow through the orifices and bearing.

The mass flow in the bearing clearance volume is obtained by combining the flow integrals across the separate members of a rectangular path surrounding the recess. The appropriate flow dimensionless equations are:

Flow across a circumferential line

$$f_{L\theta} \frac{12\mu}{K P_a^2 C^3} = \frac{R}{L} \int_{\theta_1}^{\theta_2} \left\{ -\frac{H}{2} \frac{\partial Q}{\partial \eta} + Q \frac{\partial H}{\partial \eta} \right\} d\theta \quad (5)$$

and Flow across an axial line

$$f_{L\eta} \frac{12\mu}{K P_a^2 C^3} = \frac{L}{R} \int_{\eta_1}^{\eta_2} \left\{ -\frac{H}{2} \frac{\partial Q}{\partial \theta} + Q^{1/2} \Lambda + Q \frac{\partial H}{\partial \theta} \right\} d\eta \quad (6)$$

The total non-dimensional flow is described as

$$M_B = \left(\frac{12\mu}{K P_a^2 C^3} \right) f_L \quad (7)$$

The flow through the orifices feeding the recesses is

$$M_o = \frac{N_o A_o C_D P_s G}{\frac{K P_a^2 C^3}{12\mu}} \left\{ \left(\frac{P_r}{P_s} \right)^{2/\gamma} \left[1 - \left(\frac{P_r}{P_s} \right)^{\frac{\gamma-1}{\gamma}} \right] \right\}^{1/2} \quad (8)$$

where

$$G = \sqrt{\frac{2\gamma}{(\gamma-1) R_g T_g}} \quad (9)$$

If the ratio P_r/P_s is found to be less than the critical pressure ratio, P_r/P_s is replaced by $(P_r/P_s)_{crit}$.

where
$$(P_r/P_s)_{\text{crit.}} = \left(\frac{2}{1+\gamma}\right)^{\frac{\gamma}{\gamma-1}} \quad (10)$$

The coefficient of the bracketed term in equation (8) is defined as a non-dimensional orifice flow coefficient (OFC) so that

$$M_o = \text{OFC} \left\{ \left(\frac{P_r}{P_s} \right)^{2/\gamma} \left[1 - \left(\frac{P_r}{P_s} \right)^{\frac{\gamma-1}{\gamma}} \right] \right\}^{1/2} \quad (11)$$

In order to estimate the proper recess pressure that would satisfy the flow equality of bearing and orifice, knowledge of the bearing flow relationship for a purely hydrostatic gas bearing was used. In non-dimensional form this relationship is

$$M_B = \text{BFC} \left[\left(\frac{P_r}{P_s} \right)^2 - \frac{1}{(P_s/P_a)^2} \right] \quad (12)$$

Equating M_o to M_B and rearranging we obtain

$$\left\{ \left(\frac{P_r}{P_s} \right)^{2/\gamma} \left[1 - \left(\frac{P_r}{P_s} \right)^{\frac{\gamma-1}{\gamma}} \right] \right\}^{1/2} - \text{COE} \left[\left(\frac{P_r}{P_s} \right)^2 - \frac{1}{(P_s/P_a)^2} \right] = 0 \quad (13)$$

where

$$\text{COE} = \text{BFC}/\text{OFC} \quad (15)$$

This equation is solved for the new recess pressure numerically by a bi-sectional routine in which successive half intervals not containing the root are eliminated until the root is straddled in an interval of the desired tolerance. Using the new recess pressure, the Reynolds equation is again iterated. The process is repeated until successive recess pressures are identical within an externally specified

tolerance. The identity guarantees satisfaction of both the Reynolds and continuity equations.

The dimensionless load capacities are determined by integration of the pressure over the bearing area.

$$C_T = - \int_{\eta=0}^{\eta=1} \int_{\theta=\xi+(j-1)\alpha}^{\theta=\xi+j\alpha} (P-1) \cos \theta \, d\theta \, d\eta \quad (16)$$

j = bearing sector

$$C_N = - \int_{\eta=0}^{\eta=1} \int_{\theta=\xi+(j-1)\alpha}^{\theta=\xi+j\alpha} (P-1) \sin \theta \, d\theta \, d\eta \quad (17)$$

$$C_L = (C_T^2 + C_N^2)^{1/2} \quad (18)$$

These integrations are conducted for each sector separately and then combined to determine total load magnitude, and its direction relative to the line of centers (attitude angle).

The bearing friction can be evaluated from

$$\frac{M_s}{P_a RCL} = \frac{1}{2} \int_0^1 \int_{\xi+(j-1)\alpha}^{\xi+\alpha} \left(\frac{\partial \sqrt{Q}}{\partial \theta} - P \frac{dH}{d\theta} + \frac{\Lambda}{3H} \right) d\theta \, d\eta \quad (19)$$

In addition to the above parameters it is desirable to know the righting moment capabilities of the bearing. Torques about mutually orthogonal (X-Y) axis were determined from the following equations.

$$\text{TORX} = \frac{M_{xx}}{P_a R_L^2} = \int_{\eta=0}^{\eta=1} \int_{\theta=\xi+(j-1)\alpha}^{\theta=\xi+j\alpha} (P-1) \left(Z-\frac{1}{2}\right) \cos \theta \, d\theta \, d\eta \quad (20)$$

$$\text{TORY} = \frac{M_{yy}}{P_a R_L^2} = \int_{\eta=0}^{\eta=1} \int_{\theta=\xi+(j-1)\alpha}^{\theta=\xi+j\alpha} (P-1) \left(Z-\frac{1}{2}\right) \sin \theta \, d\theta \, d\eta \quad (21)$$

The computer program procedure is summarized as follows:

- (1) Subdivide all bearing areas into a grid of finite spacing
- (2) Assume an initial pressure distribution and generate the clearance distribution from a specified journal position.
- (3) Iterate the Reynolds equation until convergence of the pressure is achieved.
- (4) Equate the mass flow through the bearing to that through the orifice and readjust the recess pressures accordingly.
- (5) Repeat steps (3) and (4) until both the Reynolds and continuity equations are satisfied.
- (6) Calculate forces, flows, friction and torques.
- (7) Change orientation (ξ) and eccentricity (ϵ) sequentially and repeat the entire process.

The program can handle as many as four sectors per bearing. The program will handle one recess per sector or, if multiple recesses are used, it will treat them as if they were short-circuited. For additional righting moment capability it may be desirable to segregate recesses, but for purposes of analysis the mutual interaction of multiple non-short-circuited recesses severely complicates the problem and thus was avoided. The logical flow chart of the computer program executing this procedure is shown on Figure 3.

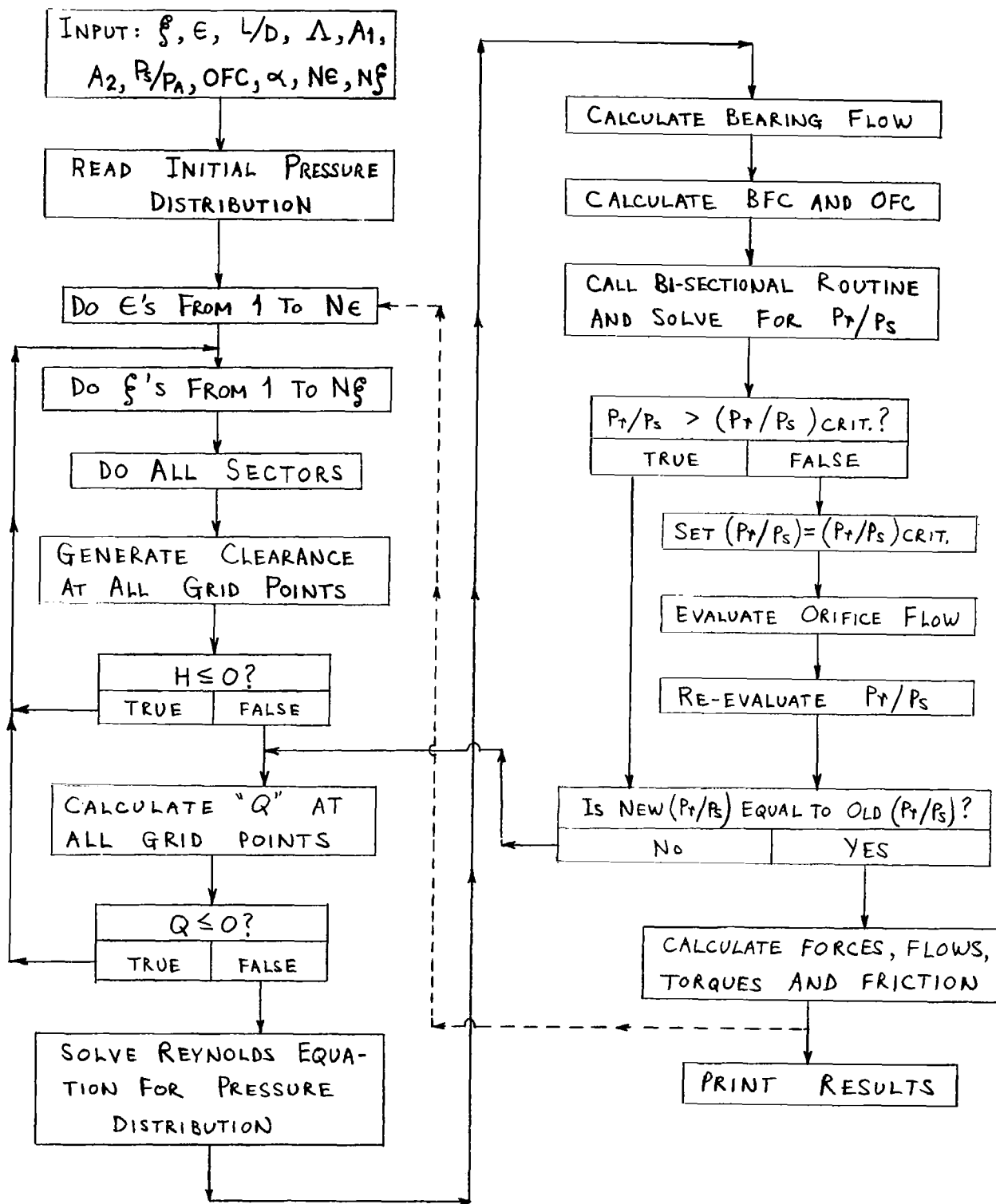


Figure 3 - Conceptual Flow Chart - Steady-State Program

E. Results - Steady-State Analysis

Typical output of the steady-state digital computer program is shown on Figure 4. At the top of the page the important input parameters are listed. The pressure distribution over the entire bearing surface is next displayed; the columns are in the axial direction and the rows are in the circumferential direction. The first and last columns are pressures at the grid points immediately inside the edges. It would have been superfluous to show the edge pressures since they are all ambient. Following the pressure distribution the following are displayed for the combined 3-sector bearing and for each individual sector:

- (1) Dimensionless component loads tangent and normal to the line of centers
- (2) Dimensionless friction moment
- (3) Dimensionless restoring torques about X and Y axis through the center of the bearing
- (4) Dimensionless flows

The recess pressures of each sector, the total combined load, attitude angle, and minimum clearance complete the output.

Preliminary runs were made so that appropriate values of compressibility number Λ , groove orientation ξ , and flow coefficient OFC could be determined.

The effect of load direction with respect to the groove orientation is shown on Figure 5. For practical purposes it is much more convenient to deal with the angle β , defined as the angle between the load vector and the nearest groove, than it is to deal with the angle ξ , which is dependent upon the bearing attitude angle. The optimum load coefficient C_L occurs at a value of $\beta = 63.5^\circ$, with a corresponding attitude angle δ of 41° . It is noted that the minimum attitude angle and maximum load coefficients do not occur at identical values of β . A compromise value of β equal to 60° ($\xi = 90^\circ$) was selected since it

INPUT

CASE 805

LAMBDA = 3.00
A1 = Q.

L/D = 1.000
A2 = Q.

CSI = 90.000
PS/PA = 2.000

EPSILON = 0.600
FLOW COEFF. = 0.5950E 01

		PRESSURE DISTRIBUTION														LEADING EDGE		AXIAL END POINTS WITH AMBIENT PRES- SURE DELETED (BOTH SIDES).	
		AXIAL DIRECTION																	

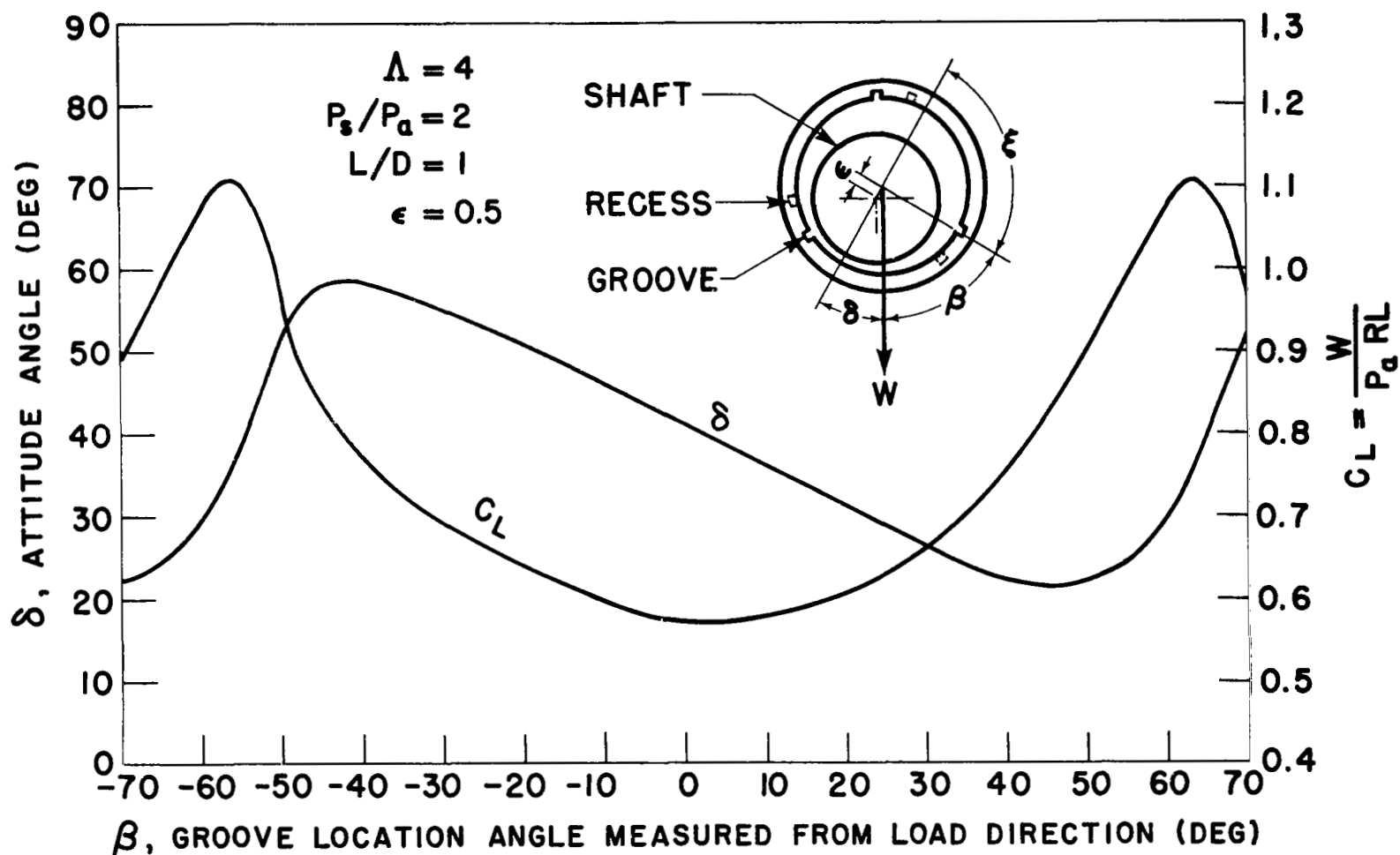


Figure 5 - Attitude Angle and Load Coefficient vs Groove Location Angle - Hybrid Journal Bearing

afforded near optimum values for both lift coefficient and attitude angle. This value of β is also on the left side of the load curve maximum which is in a less precipitous region than what occurs on the right hand side of the peak. It is noted that there is quite a large variation of maximums to minimums for both C_L and δ , which means that precautions should be taken at installation to ensure proper groove orientation.

The effect of the flow coefficient is shown on Figure 6. For any given set of gaseous and geometric conditions variations of the flow coefficient are accomplished by changing the orifice diameter. Over the range of flow coefficient plotted on Figure 6, variations in C_L and δ are slight. This is a rather narrow range however, representing about a 2.5/1 ratio of orifice diameters. In actuality, extension of this range would bring about a sharp drop in C_L and a large increase in δ . For large values of OFC the bearing restriction is very much greater than the orifice restriction so that all recess pressures are equalized and are practically invariant with load or eccentricity. This inability of sector pressures to respond to clearance variations maintains an excessive pre-load on the bearing severely limiting load capacity. On the other end of the spectrum very small orifices essentially eliminate the introduction of external flow so that the bearing capacity results from almost pure hydrodynamic action.

For $\Lambda = 4$, the optimum value of flow coefficient is 30. In order to employ a standard drill size for manufacturing the orifices a flow coefficient of 29.3 was selected. Two 0.021 inch diameter orifices for each sector are incorporated.

Preliminary investigations indicated that a value of $\Lambda = 4$ was necessary for the bearing to carry its maximum load with a minimum clearance of about one mil. The manufactured radial clearance necessary to produce the proper Λ at a shaft speed of 12,000 RPM is 2.03 mils. Figure 7 shows the variation of attitude angle and total load coefficient

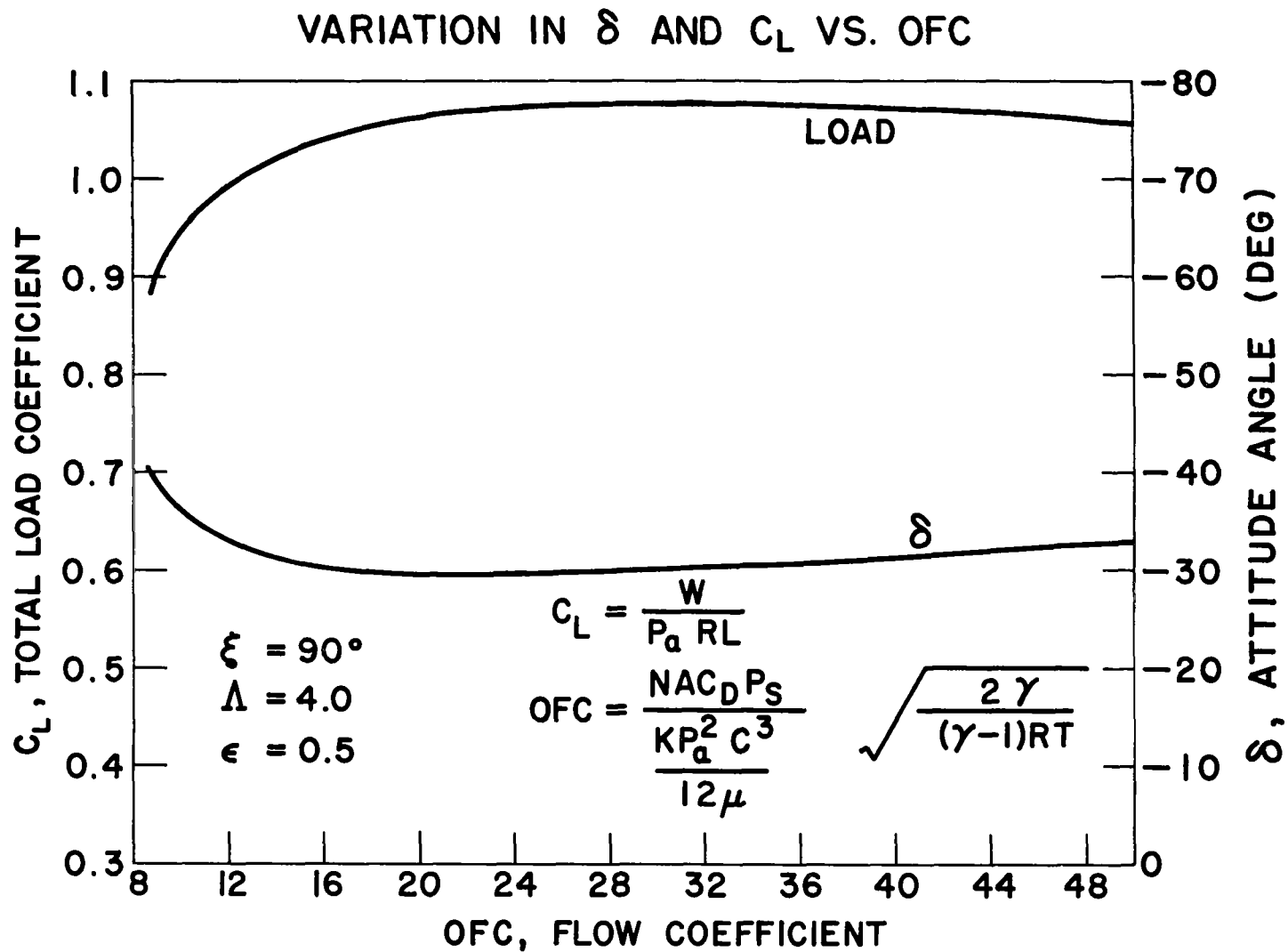


Figure 6 - Attitude Angle and Load Coefficient vs Flow Coefficient - Hybrid Journal Bearing

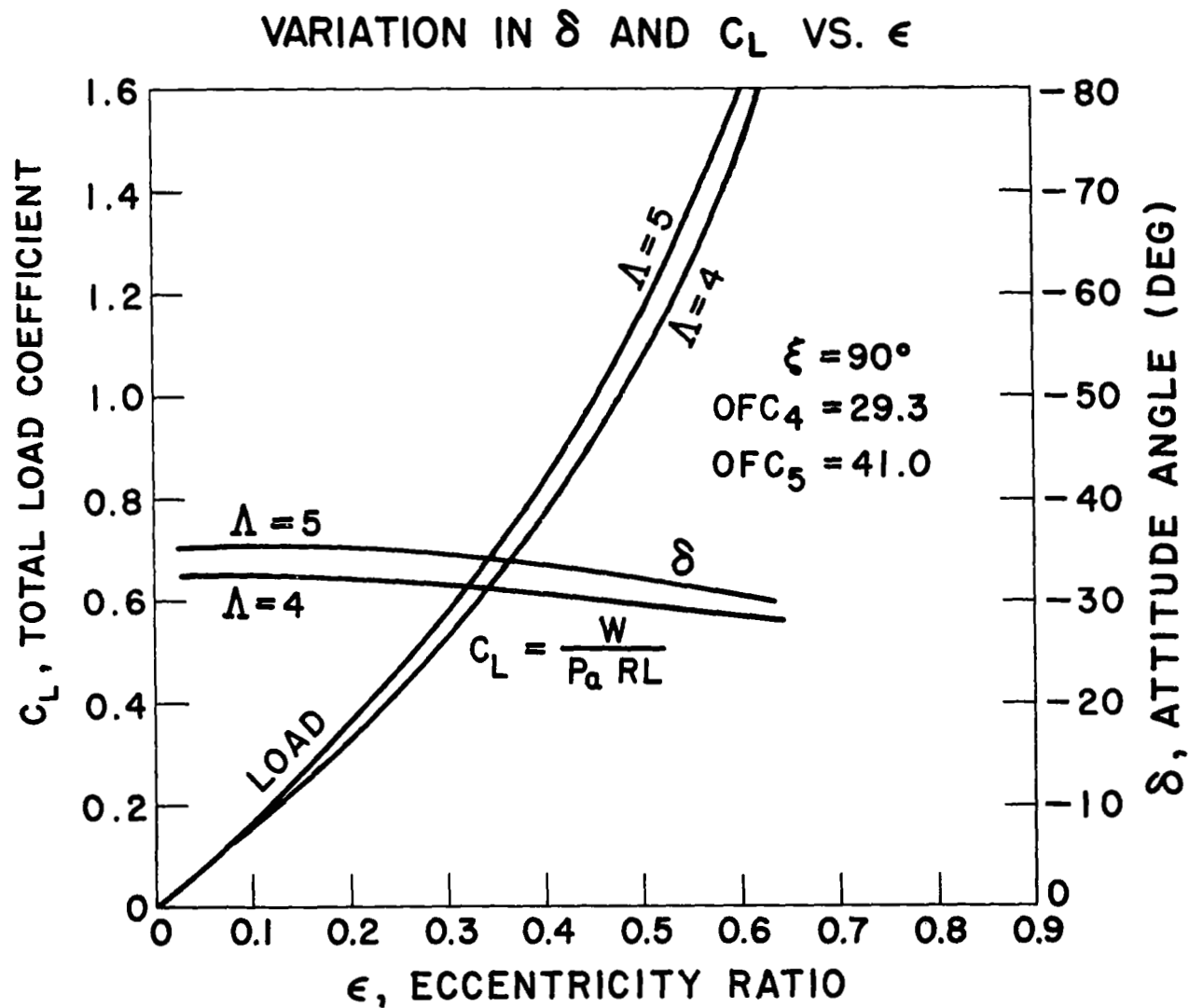


Figure 7 - Attitude Angle and Load Coefficient vs Eccentricity - Hybrid Journal Bearing

vs. eccentricity for values of Λ of 4 and 5. The curve for a Λ of 5 is indicative of what occurs when the bearing radial clearance is reduced by thermal or centrifugal expansions of the shaft. As expected the load is quite responsive to bearing eccentricity; the nearly constant attitude angle is one of the major attributes of the hybrid-slotted bearing.

Figure 8 shows the variation of dimensionless flow vs eccentricity. The flow is rather insensitive to eccentricity because as the loaded side recess pressures increase causing reduced orifice flow, the unloaded side recess pressures decrease causing increased flows with a net result of nearly constant flow.

Figure 9 is a plot of the dimensionless friction moment vs. eccentricity. The viscous friction does not begin to increase substantially until the eccentricity ratio exceeds 0.5. Figure 10 is a curve of the dimensionless recess pressure vs. eccentricity. The two loaded sectors have identical recess pressures. It is noted that by judicious selection of the orifice size there is excellent separation between the loaded and unloaded sector recess pressure at the design load which optimizes the effects of the external pressurization.

Dimensional load and minimum clearance vs. eccentricity, flow vs. eccentricity and friction horsepower vs. eccentricity are displayed on Figures 11, 12 and 13 respectively. A summary of bearing performance is shown on Table I.

All the results obtained thus far have been for bearings in which the journal has not been misaligned. In the actual design there are two recesses per sector, each recess individually fed through an orifice restrictor. This multiple recess configuration enhances the ability of the bearing to produce restoring torques on a misaligned journal. As previously explained, the analysis does not treat segregated recesses; consequently, restoring moments obtained from the analysis are conservative. One computer run was made with a misaligned journal.

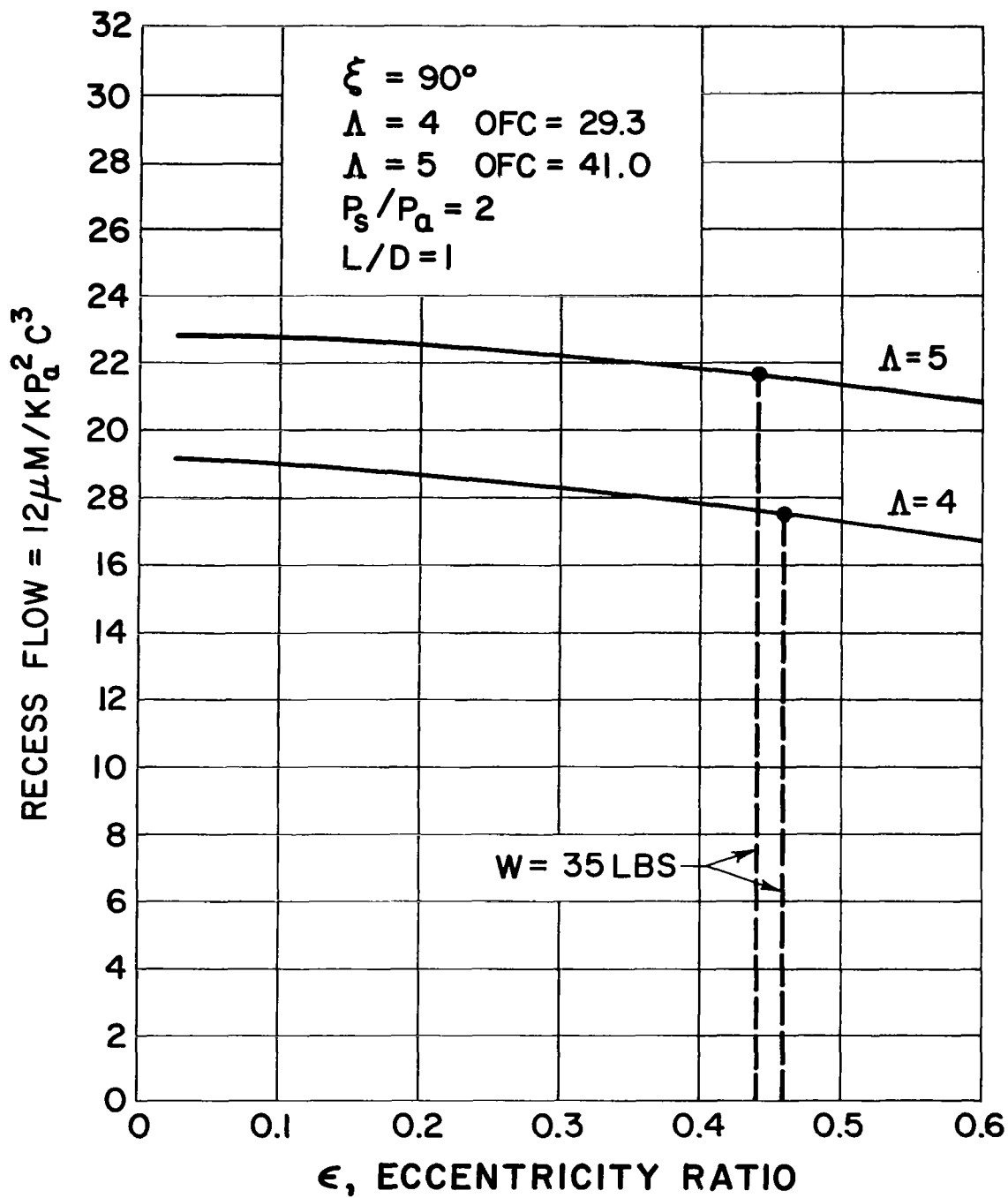


Figure 8 - Dimensionless Flow vs Eccentricity Ratio - Hybrid Journal Bearing

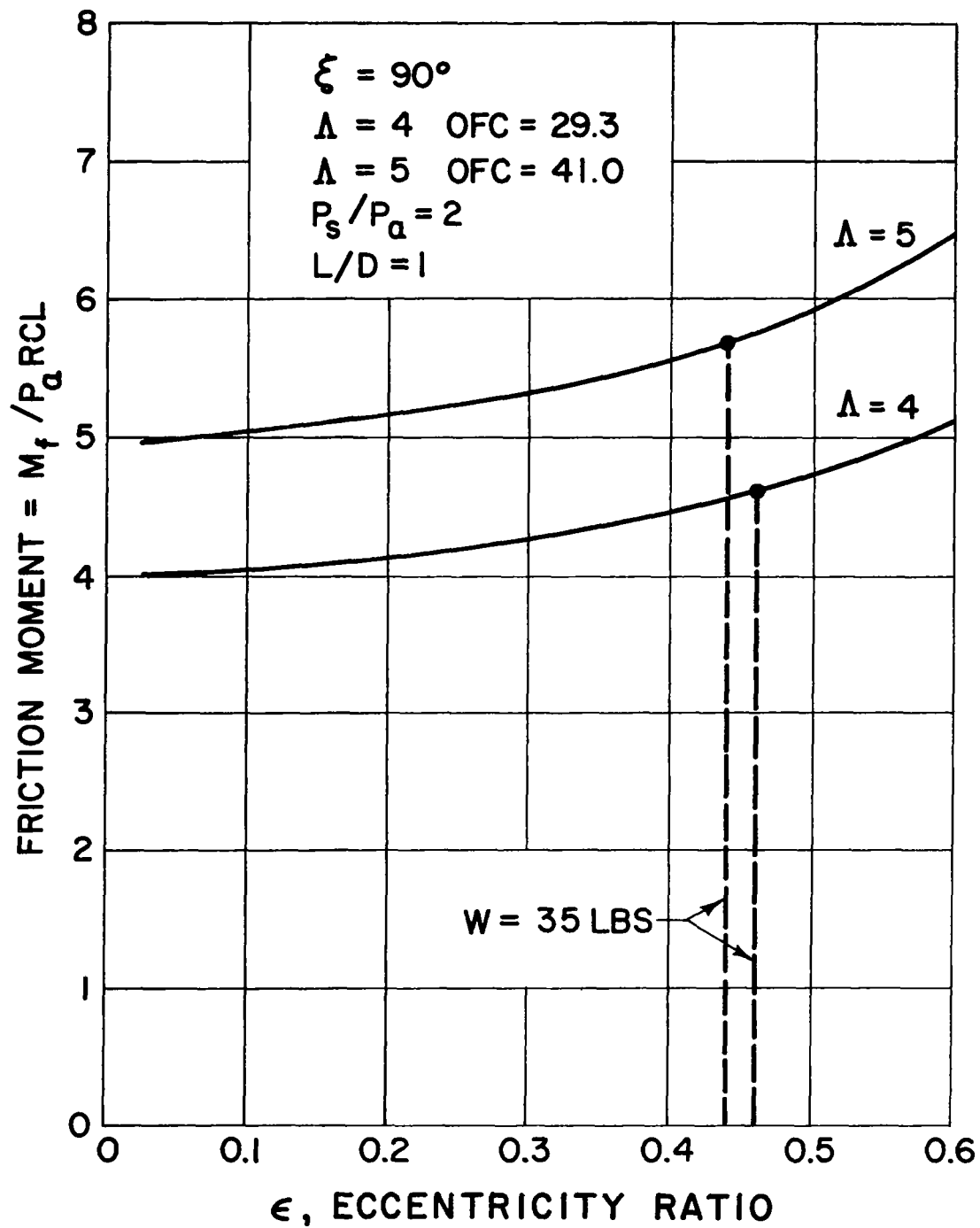


Figure 9 - Dimensionless Friction Moment vs Eccentricity Ratio - Hybrid Journal

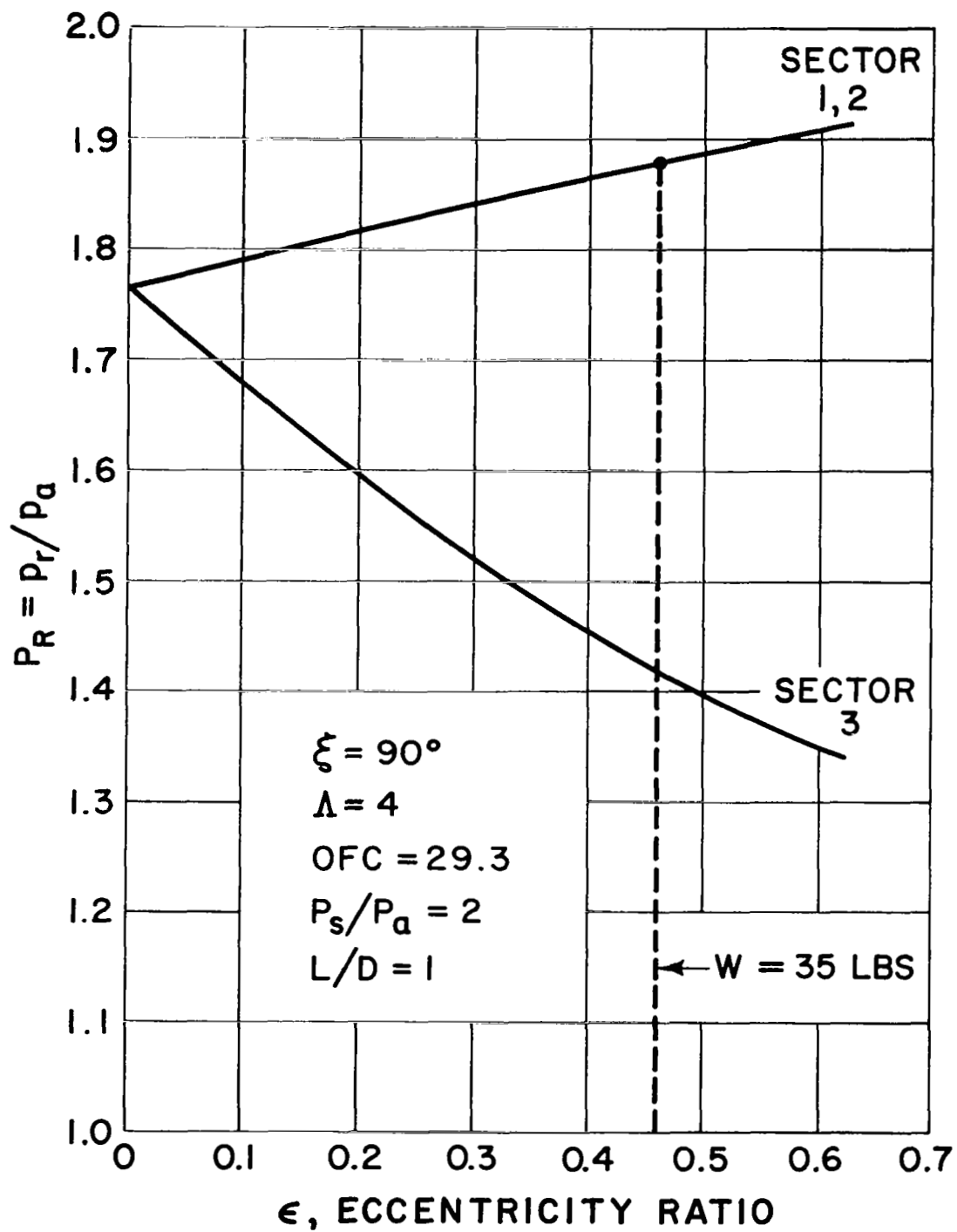


Figure 10 - Dimensionless Recess Pressure vs Eccentricity Ratio - Hybrid Journal Bearing

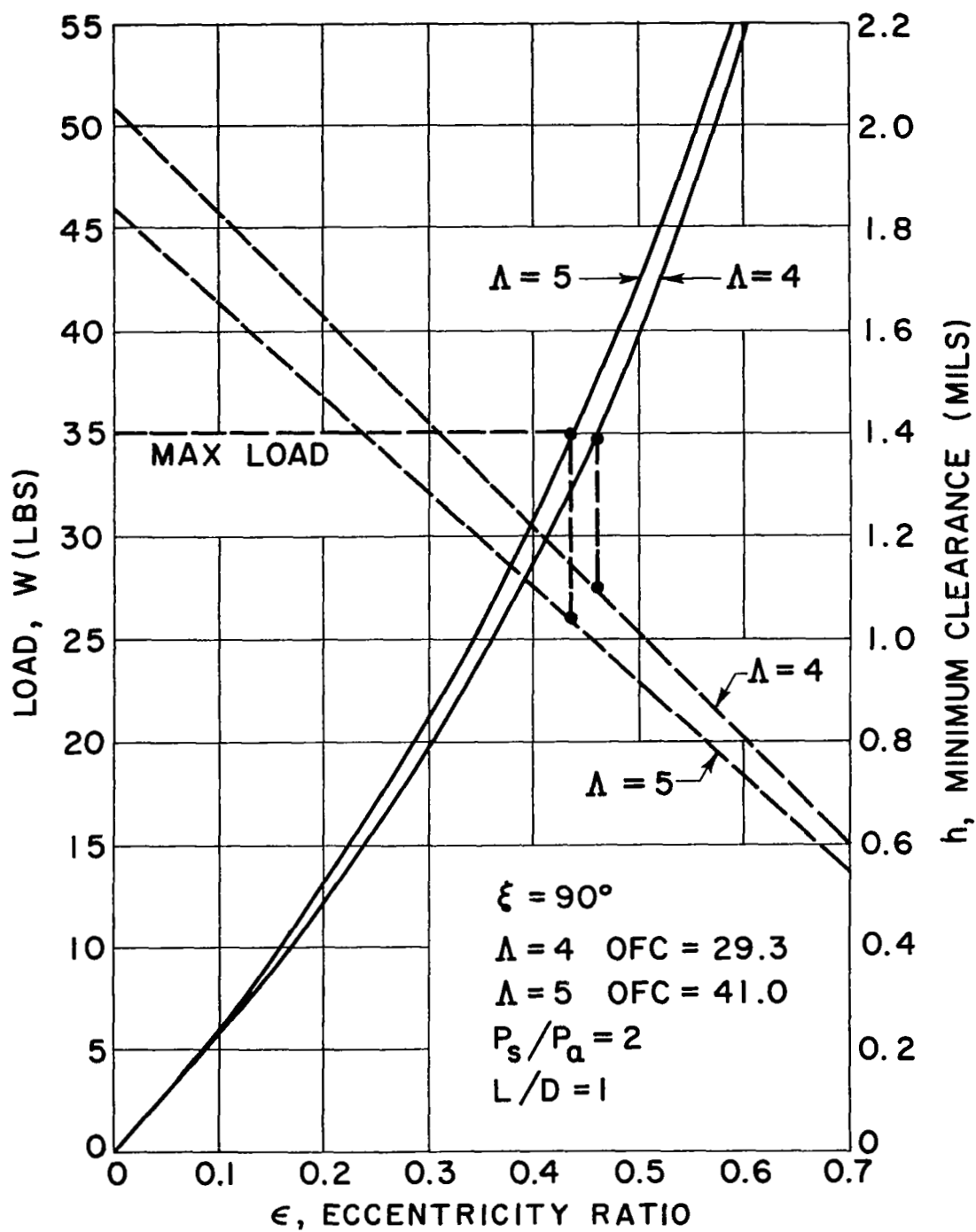


Figure 11 - Load and Minimum Clearance vs Eccentricity Ratio - Hybrid Journal Bearing

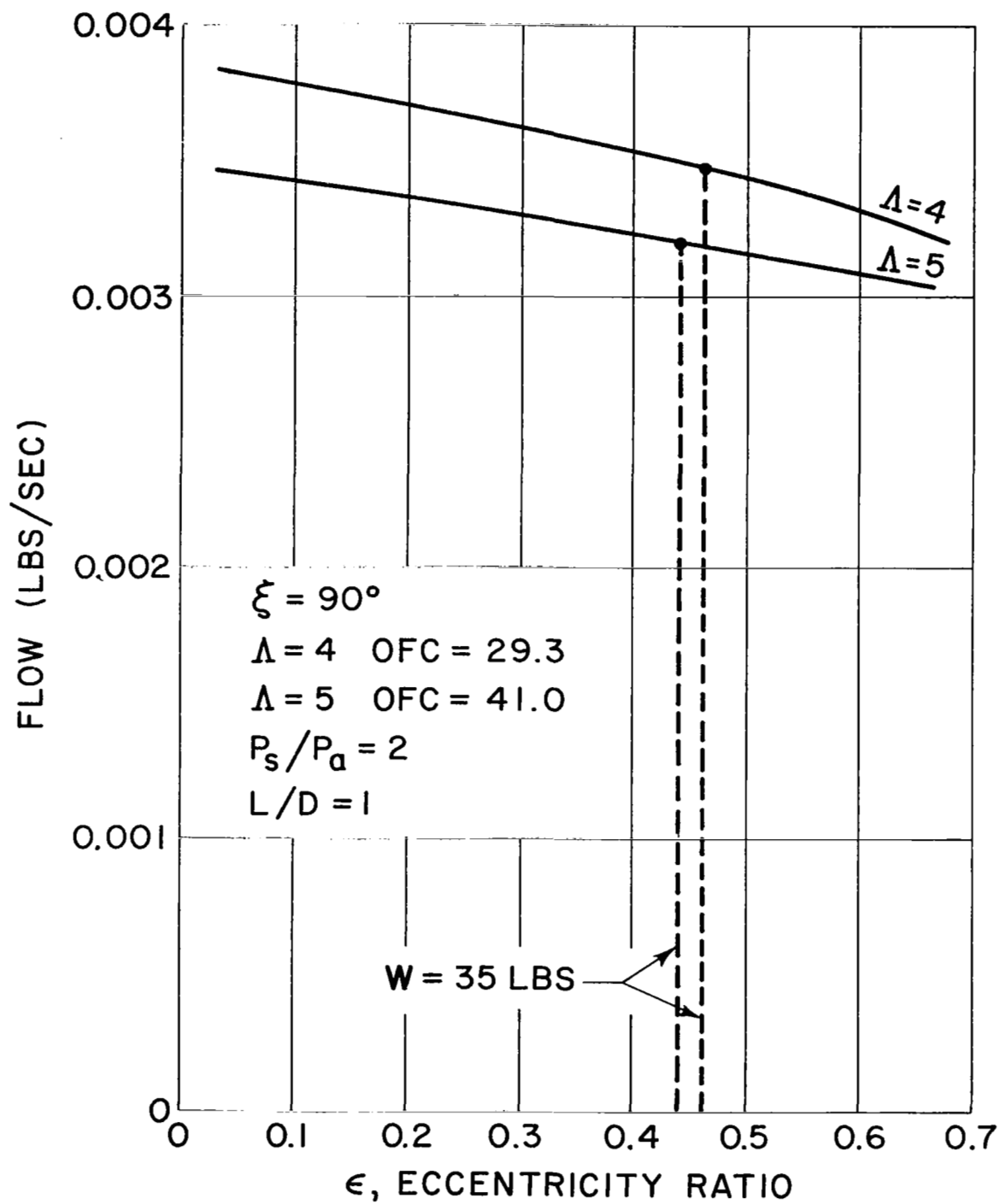


Figure 12 - Flow vs Eccentricity Ratio - Hybrid Journal Bearing

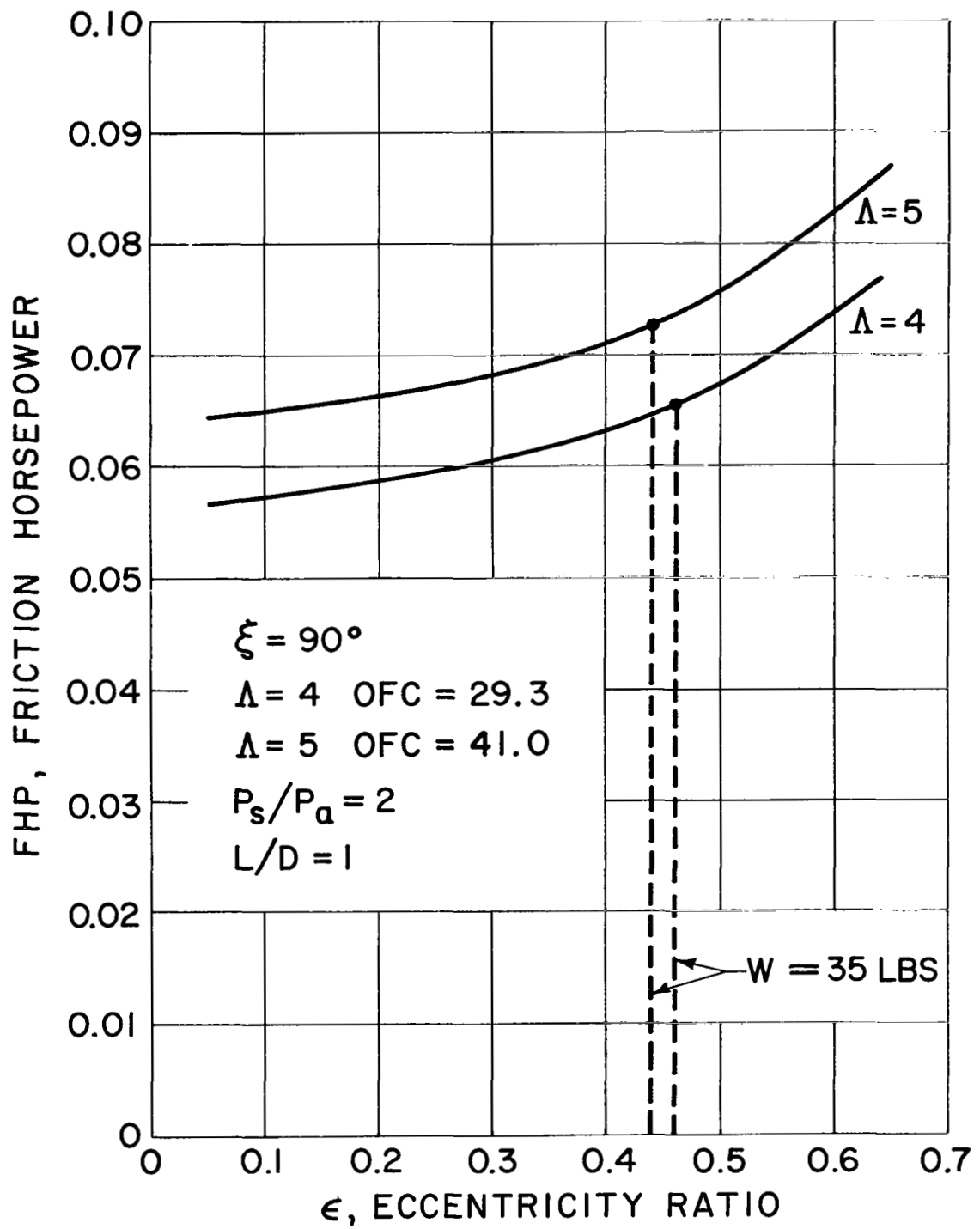


Figure 13 - Friction Horsepower vs Eccentricity Ratio - Hybrid Journal Bearing

With the bearing at an eccentricity of 0.5 in Y direction the shaft was misaligned in the weaker X-Z plane (normal to the eccentricity) so that the dimensionless angular rotation A_1 equaled 0.8. The dimensionless torque produced in this direction by the gas film is equal to 0.0399. This results in a dimensional stiffness of 11,100 in-lbs/rad, less than what is necessary to overcome the resistance of the bearing support structure which has a stiffness of 15,000 to 20,000 in-lbs/rad. However, it is expected that the effect of the segregated recess will offset this deficiency. In addition, the true position of the shaft may not be as described above and can be obtained only by a complete dynamic analysis of the entire system. This has been accomplished and the results described in subsequent sections of this report.

Table I

HYBRID JOURNAL BEARING PERFORMANCE

$\Lambda = 4$, $C = 2.03$ Mils

<u>ϵ</u>	<u>W</u> <u>lbs</u>	<u>FHP</u> <u>HP</u>	<u>f_L</u> <u>lb/sec</u>	<u>δ</u> <u>degrees</u>
0	0	.0565	.00384	-33.00
.1	5.75	.0570	.00378	-32.50
.2	12.00	.0585	.00370	-32.40
.3	19.50	.0605	.00362	-31.70
.4	27.00	.0630	.00352	-30.08
.5	39.50	.0675	.00344	-29.50
.6	56.75	.0740	.00332	-28.50

$\Lambda = 5$, $C = 1.84$ Mils

0	0	.0640	.00348	-35.50
.1	6.00	.0650	.00342	-35.50
.2	13.00	.0665	.00336	-35.20
.3	21.25	.0680	.00330	-34.50
.4	31.00	.0710	.00323	-33.50
.5	42.50	.0760	.00316	-32.50
.6	57.00	.0830	.00308	-30.50

F. Dynamic Analysis

The dynamic behavior of the turbo-alternator unit was analyzed taking into account time transient as well as steady phenomena. The system was represented by a rigid rotor with the same mass, transverse moment of inertia and polar moment of inertia as the real rotor. The unbalance was represented by a mass at a radius R, in the plane of the mass center and two equal masses located equidistant from the plane of the mass center to produce a couple. Consequently the rigid body dynamic characteristics of the shaft were taken into account exactly.

The housing was assumed to be rigid with the exception of the bearing mounts, which were allowed two degrees of freedom each (rotation about two mutually perpendicular axes normal to the main axis). The support reactions to motion in these degrees of freedom were taken as restoring torques about the axes of rotation and directly proportional to the rotations. The constants of proportionality (torsional stiffnesses) can be specified externally.

The system coordinate system is shown on Figure 14. Due to the smallness of the angles of tilt of the rotor and bearings the following equations can be adopted

$$\frac{d^2 X_M}{dT^2} = B \sum_{j=1}^{NB} \sum_{i=1}^{NS} \iint P \sin \theta \, d\theta \, dz + B U_F \cos (2T) \quad (22)$$

$$\frac{d^2 Y_M}{dT^2} = B \sum_{j=1}^{NB} \sum_{i=1}^{NS} \iint P \cos \theta \, d\theta \, dz - B U_F \sin (2T) + B W_y \quad (23)$$

$$\frac{d^2 A_1}{dT^2} = G \frac{dA_2}{dT} + I_s \sum_{j=1}^{NB} \sum_{i=1}^{NS} \iint P (\sin \theta) Z \, d\theta \, dz + I_s U_m \cos (2T) \quad (24)$$

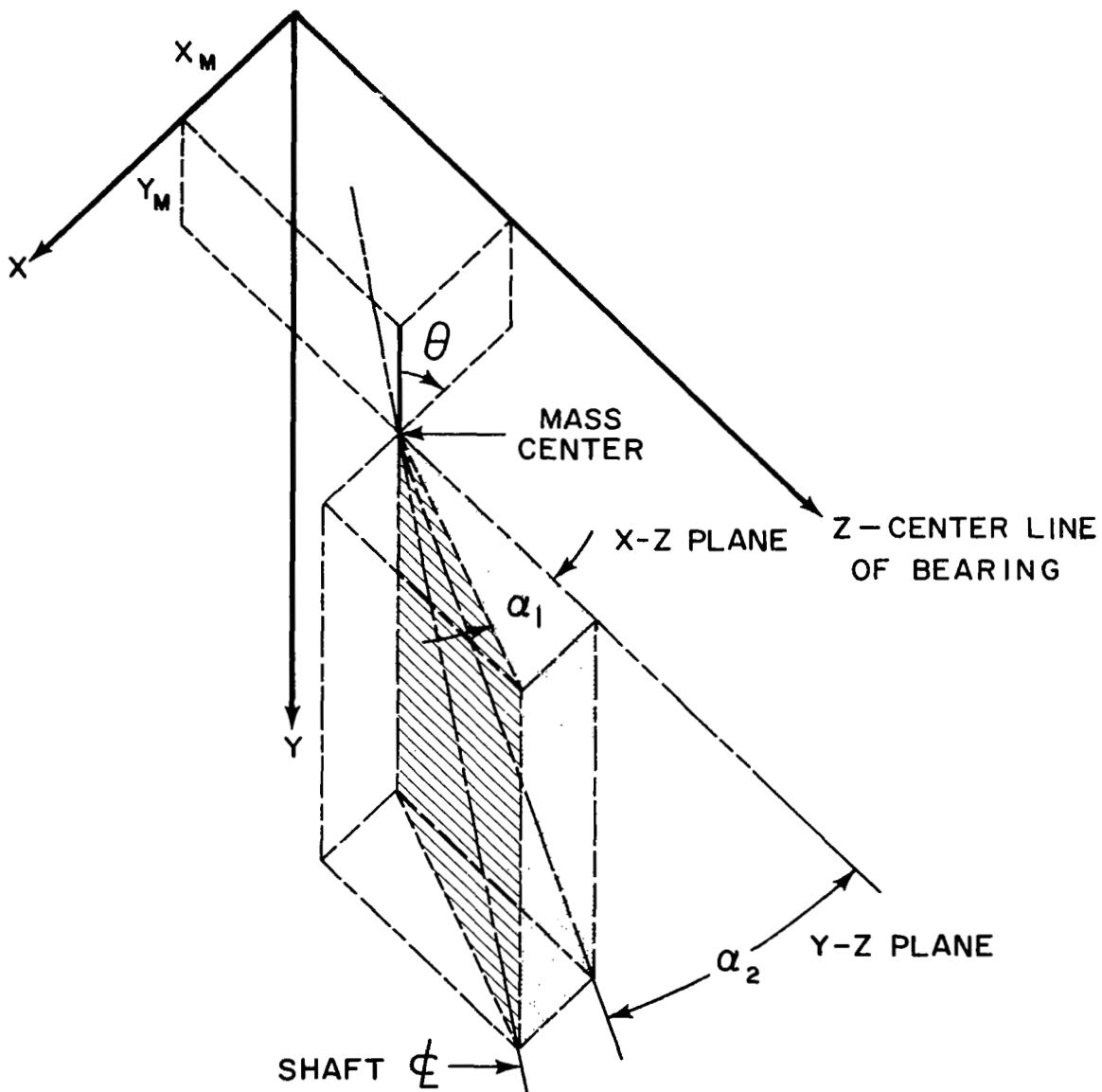


Figure 14 - Coordinate System

$$\frac{d^2 A_2}{dT^2} = -G \frac{dA_1}{dT} + I_s \sum_{j=1}^{NB} \sum_{i=1}^{NS} \iint P(\cos \theta) Z d\theta dz - I_s U_m \sin(2T) \quad (25)$$

$$\frac{d^2 B_{1j}}{dT^2} = I_{Bj} \sum_{i=1}^{NS} \iint P \sin \theta (Z - Z_{Bj}) d\theta dz; j = 1, NB \quad (26)$$

$$\frac{d^2 B_{2j}}{dT^2} = I_{Bj} \sum_{i=1}^{NS} \iint P \cos \theta (Z - Z_{Bj}) d\theta dz; j = 1, NB \quad (27)$$

Note that the first term on the right hand sides of equations (24) and (25) represent the contribution of gyroscopic loads.

The integration of equations (22) through (27) can be carried out numerically once the integrals on their right hand sides are known in time. This involves the solution of the time transient fluid dynamic problem in the recess and feeding element bearing areas.

The pressure in the bearing areas is governed by the purely viscous Reynolds equation for isothermal films since the so called "entrance effects" introducing inertial terms in the momentum equation are minimized by the presence of a small recess. This equation is well known and can be written in dimensionless form

$$\frac{\partial}{\partial \theta} \left(PH^3 \frac{\partial P}{\partial \theta} \right) + \frac{R^2}{L} \frac{\partial}{\partial \eta} \left(PH^3 \frac{\partial P}{\partial \eta} \right) = \Lambda \left(\frac{\partial PH}{\partial \theta} + \frac{\partial PH}{\partial T} \right) \quad (28)$$

The clearance distribution is determined from

$$H = 1 + [X_M(T) + A_1(T) Z - B_{1j}(T) (Z - Z_{Bj})] \sin \theta + [Y_M(T) + A_2(T) Z - B_{2j}(T) (Z - Z_{Bj})] \cos \theta \quad (29)$$

Evidently H in each sector of each bearing is fully specified if the values of the eight dynamic coordinates are known.

Given H from the equations of motion (22) through (27), equation (28) can be handled numerically to establish the transient diffusion of pressure once the boundary conditions are known at each instant of time. At all edges of each sector the pressure is known to be ambient. However, the value of the pressure in the recess is not constant and must be evaluated by means of a mass balance in the recess volume.

The recess mass balance states the fact that the mass content of the recess is altered by mass out-flow into the bearing area and mass in-flow from the restrictor.

$$\frac{d}{dt} (\rho_r V_r) = f_o - f_L \quad (30)$$

The recess gas density can be related to the pressure by the gas equation of state once the process has been established. Also

$$V_r = A_r (d_r + h_r) \quad (31)$$

The mass balance equation can then be rewritten as

$$\frac{A_r}{R^2} \frac{d P_R}{dT} = \frac{F_o - F_L - P_R \frac{d H_r}{dT} \frac{A_r}{R^2}}{D_r + H_r} \quad (32)$$

The differential equation (32) regulates the time transient behavior of the recess pressure; therefore it provides the needed value for the boundary conditions to equation (28). The solution of equation (32) hinges on the evaluation of the dimensionless flow rates F_L and F_o .

Since it is inconvenient and inaccurate to evaluate the mass flow rate in the bearing area on the edge of the recess, another balance equation must be established to relate the flow out of the recess to the flow evaluated out of any closed path encircling the recess

$$f_L = \text{flow rate out of any closed path encircling the recess} + \int_{S_L} \int \frac{\partial p h}{\partial t} ds \quad (33)$$

where S_L is the bearing area enclosed between the recess perimeter and the enclosed path L and ds is an element of bearing area.

Expressing the first term on the right hand side in terms of pressures, clearances and gradients in the bearing film, and making all terms dimensionless,

$$F_L = -\frac{1}{\Lambda} \oint_L PH^3 (\nabla/P) \cdot l \hat{n} dL + \oint_L P \vec{U} \cdot l \hat{n} dL + \int_{S_L} \int \frac{\partial PH}{\partial T} ds \quad (34)$$

where $l \hat{n}$ is tangent to the bearing surface, normal to L and unity in magnitude

\vec{U} is the rotor surface velocity vector

∇/P is the vectorial pressure gradient

The last term of expression (34) is quite important since it represents the change in storage of gas in the clearance space between loop L and the recess perimeter.

The only missing term is now f_o , the flow through the orifice. This term can be easily evaluated as a function of the pressure ratio existing between the supply and recess pressures ($r = P_r/P_s$). In dimensionless form

$$F_o = \pm O_F \left(r^{2/\gamma} \left[1 - r^{\frac{\gamma-1}{\gamma}} \right] \right)^{1/2} \quad (35)$$

For the dynamic situation the possibility of the recess pressure exceeding the supply pressure is not remote. Therefore it may be desirable to insert a check valve in the restrictor line to prevent back flow from the bearing to the supply system. Thus, the various alternatives for F_o become

- (1) for $r > 1$ and a flow check valve in the restrictor line

$$F_o = 0 \quad (36)$$

- (2) for $r > 1$ and no check valve in the restrictor line

$$F_o = -O_F \left[\left(\frac{1}{r} \right)^{2/\gamma} \left(1 - \left(\frac{1}{r} \right)^{\frac{\gamma-1}{\gamma}} \right) \right]^{1/2} \quad (37)$$

provided $\frac{1}{r} > \left(\frac{2}{\gamma + 1} \right)^{\frac{\gamma}{\gamma-1}} = \left(\frac{P_s}{P_r} \right)_{\text{critical}}$

if $\frac{1}{r} \leq \left(\frac{2}{\gamma + 1} \right)^{\frac{\gamma}{\gamma-1}}$ then

$$\frac{1}{r} = \left(\frac{2}{\gamma + 1} \right)^{\frac{\gamma}{\gamma-1}} \quad \text{in equation (37)}$$

- (3) for $r < 1$

F_o is positive in equation (35). If r is less than or equal to the critical pressure ratio, its value equals the critical pressure ratio.

When F_o is introduced in equation (32) at each time instant we have a first order differential equation in the pressure which can be integrated by a Runge-Kutta method.

The problem solution procedure is then the following:

- (1) Subdivide all bearing areas in a grid of finite spacing
- (2) Assume an initial distribution of pressure at all points in the grids and the recesses.
- (3) Evaluate all forces due to pressures and apply them to the dynamic equations to evaluate the value of the position coordinates at the next instant of time.
- (4) Evaluate flow rates out of each recess and through each restrictor element. Use this to estimate the recess pressures at the next time instant.
- (5) Use the Reynolds equation to evaluate the pressure at all points in the grid in the next time instant.

The present conditions can now be used as initial conditions to the next step and the process can be repeated. The logical flow chart of the computer program executing this procedure is shown on Figure 15.

The execution of this program involves amounts of computer time proportional to the number of field grid points. Moreover, critical control over the necessary computer time is exercised by the maximum value of the time steps allowable to insure numerical stability of the integration. The time step (ΔT) required for numerical stability of the computing process is given by the inequality

$$\Delta T \left[\frac{1}{(\Delta \theta)^2} + \frac{R^2}{L^2} \left(\frac{1}{\Delta \eta^2} \right) \right] \leq \frac{\Lambda}{2PH^2} \quad (38)$$

The integration results of greatest interest are the position coordinates for the shaft and bearings, the phase difference between the shaft and the bearing motions and the recess pressures. The position parameters give the motion amplitude, mode, and frequency while the recess pressures indicate the effectiveness of the recesses in damping out the whirl motion and contributing to the load-carrying capacity of the bearing.

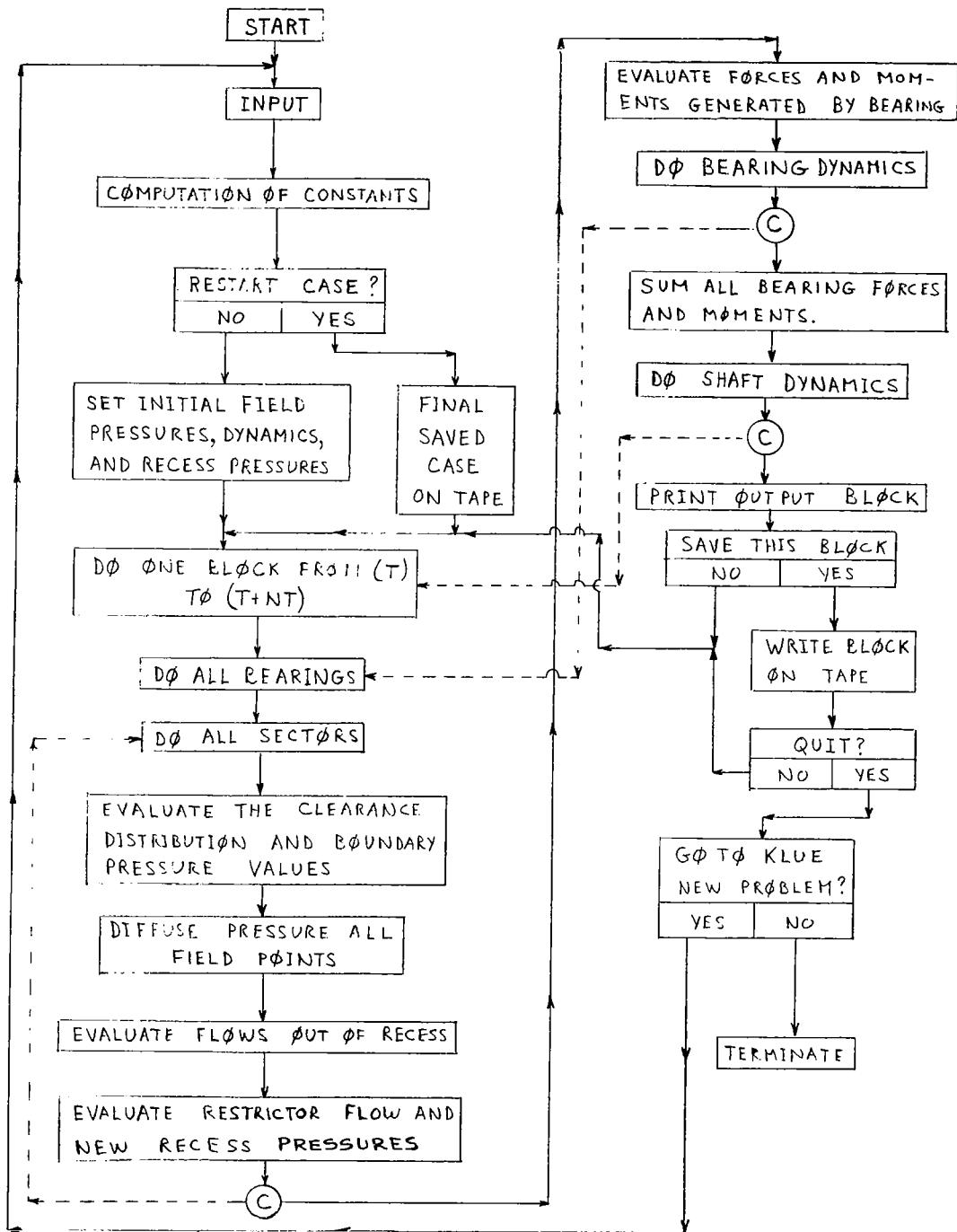


Figure 15 - Flow Chart - Dynamics Program

A valid check of the accuracy of the orbit program can be obtained by letting a stable case run until equilibrium is reached. At that point the time averaged position parameters and the pressure distributions should coincide with those predicted by the steady-state calculations.

Prior to running the program a decision is made to stop the program at some point, print out the data and plot the results. The computer program has been written so that it is possible to continue a case from the point at which it was previously terminated. The ability of the program to save the necessary information to continue a particular case has proved extremely valuable in minimizing the total amount of computer time necessary to complete a case.

G. Results - Dynamic Analysis

Some typical computer outputs of the time transient program are shown on Figures 16 and 17. For each time step all recess pressures, shaft forces and moments, X and Y displacements, angular displacements of the shaft, and angular displacements of the bearings are produced. From this output an orbit plot of the center of mass of the shaft can be obtained (a plot of X_m vs Y_m). Such a curve is shown on Figure 18 for the shaft running vertically at the overspeed condition at 14,400 RPM. The shaft was initially displaced in the Y direction an eccentricity of 0.15, held for approximately 1/2 shaft revolution to allow the recess pressures to dissipate, and then released.

An excellent check on the correctness of the dynamics program was available by comparing recess pressures just prior to release with those determined by the steady-state program with identical journal positions, supply pressure, and Λ . This steady-state case was run and the following are the comparative results

$$\epsilon = 0.15$$

$$N = 14,400 \text{ RPM}$$

$$P_s = 13.8 \text{ psia}$$

$$P_a = 6 \text{ psia}$$

STEP	RPR(1)	RPR(2)	RPR(3)	RPR(4)	RPR(5)	RPR(6)	RPR(7)	RPR(8)	X-FORCE	Y-FORCE	A1-MOMENT	A2-MOMENT
1551	1.8837	2.0389	1.7524	-0.0000	1.8511	2.0549	1.7696	-0.0000	-0.2255E-00	-0.4932E-00	0.1601E-00	0.2694E-01
1552	1.8828	2.0393	1.7571	-0.0000	1.8501	2.0553	1.7695	-0.0000	-0.2284E-00	-0.4922E-00	0.1608E-00	0.2519E-01
1553	1.8819	2.0397	1.7532	-0.0000	1.8491	2.0556	1.7708	-0.0000	-0.2314E-00	-0.4911E-00	0.1614E-00	0.2357E-01
1554	1.8810	2.0400	1.7581	-0.0000	1.8481	2.0559	1.7707	-0.0000	-0.2344E-00	-0.4901E-00	0.1620E-00	0.2169E-01
1555	1.8801	2.0403	1.7539	-0.0000	1.8471	2.0562	1.7721	-0.0000	-0.2374E-00	-0.4890E-00	0.1625E-00	0.1994E-01
1556	1.8792	2.0407	1.7591	-0.0000	1.8461	2.0566	1.7720	-0.0000	-0.2404E-00	-0.4880E-00	0.1631E-00	0.1793E-01
1557	1.8783	2.0410	1.7547	-0.0000	1.8450	2.0569	1.7733	-0.0000	-0.2434E-00	-0.4870E-00	0.1636E-00	0.1607E-01
1558	1.8774	2.0414	1.7601	-0.0000	1.8440	2.0572	1.7732	-0.0000	-0.2464E-00	-0.4861E-00	0.1640E-00	0.1394E-01
1559	1.8765	2.0417	1.7554	-0.0000	1.8430	2.0575	1.7746	-0.0000	-0.2495E-00	-0.4850E-00	0.1645E-00	0.1200E-01
1560	1.8756	2.0420	1.7610	-0.0000	1.8420	2.0578	1.7745	-0.0000	-0.2525E-00	-0.4841E-00	0.1649E-00	0.9799E-02
1561	1.8747	2.0423	1.7562	-0.0000	1.8410	2.0581	1.7759	-0.0000	-0.2556E-00	-0.4831E-00	0.1653E-00	0.7796E-02
1562	1.8738	2.0427	1.7618	-0.0000	1.8400	2.0584	1.7758	-0.0000	-0.2586E-00	-0.4821E-00	0.1657E-00	0.5559E-02
1563	1.8729	2.0430	1.7569	-0.0000	1.8390	2.0587	1.7772	-0.0000	-0.2617E-00	-0.4811E-00	0.1661E-00	0.3536E-02
1564	1.8720	2.0433	1.7625	-0.0000	1.8380	2.0590	1.7771	-0.0000	-0.2648E-00	-0.4801E-00	0.1665E-00	0.1300E-02
1565	1.8711	2.0436	1.7576	-0.0000	1.8370	2.0592	1.7786	-0.0000	-0.2678E-00	-0.4790E-00	0.1669E-00	-0.7054E-03
1566	1.8702	2.0439	1.7631	-0.0000	1.8360	2.0595	1.7784	-0.0000	-0.2709E-00	-0.4779E-00	0.1673E-00	-0.2903E-02
1567	1.8693	2.0442	1.7584	-0.0000	1.8350	2.0598	1.7799	-0.0000	-0.2740E-00	-0.4768E-00	0.1676E-00	-0.4857E-02
1568	1.8684	2.0445	1.7637	-0.0000	1.8340	2.0600	1.7798	-0.0000	-0.2770E-00	-0.4757E-00	0.1680E-00	-0.6983E-02
1569	1.8675	2.0448	1.7591	-0.0000	1.8330	2.0603	1.7813	-0.0000	-0.2801E-00	-0.4745E-00	0.1683E-00	-0.8857E-02
1570	1.8666	2.0451	1.7643	-0.0000	1.8320	2.0606	1.7812	-0.0000	-0.2831E-00	-0.4733E-00	0.1687E-00	-0.1089E-01
1571	1.8658	2.0454	1.7598	-0.0000	1.8310	2.0608	1.7826	-0.0000	-0.2862E-00	-0.4720E-00	0.1691E-00	-0.1266E-01
1572	1.8649	2.0456	1.7648	-0.0000	1.8300	2.0611	1.7825	-0.0000	-0.2892E-00	-0.4707E-00	0.1695E-00	-0.1458E-01
1573	1.8640	2.0459	1.7606	-0.0000	1.8290	2.0613	1.7840	-0.0000	-0.2922E-00	-0.4693E-00	0.1699E-00	-0.1624E-01
1574	1.8631	2.0462	1.7654	-0.0000	1.8280	2.0615	1.7840	-0.0000	-0.2953E-00	-0.4679E-00	0.1703E-00	-0.1804E-01
1575	1.8622	2.0465	1.7614	-0.0000	1.8270	2.0618	1.7854	-0.0000	-0.2983E-00	-0.4664E-00	0.1708E-00	-0.1959E-01
1576	1.8613	2.0467	1.7659	-0.0000	1.8260	2.0620	1.7854	-0.0000	-0.3013E-00	-0.4649E-00	0.1712E-00	-0.2127E-01
1577	1.8604	2.0470	1.7622	-0.0000	1.8250	2.0622	1.7868	-0.0000	-0.3042E-00	-0.4633E-00	0.1717E-00	-0.2271E-01
1578	1.8595	2.0472	1.7665	-0.0000	1.8240	2.0624	1.7868	-0.0000	-0.3072E-00	-0.4617E-00	0.1721E-00	-0.2426E-01
1579	1.8586	2.0475	1.7631	-0.0000	1.8230	2.0627	1.7883	-0.0000	-0.3102E-00	-0.4601E-00	0.1726E-00	-0.2560E-01
1580	1.8577	2.0478	1.7672	-0.0000	1.8220	2.0629	1.7883	-0.0000	-0.3131E-00	-0.4584E-00	0.1731E-00	-0.2705E-01
1581	1.8569	2.0480	1.7640	-0.0000	1.8210	2.0631	1.7897	-0.0000	-0.3160E-00	-0.4566E-00	0.1736E-00	-0.2829E-01
1582	1.8560	2.0482	1.7679	-0.0000	1.8200	2.0633	1.7898	-0.0000	-0.3190E-00	-0.4549E-00	0.1742E-00	-0.2963E-01
1583	1.8551	2.0485	1.7650	-0.0000	1.8190	2.0635	1.7912	-0.0000	-0.3219E-00	-0.4530E-00	0.1747E-00	-0.3079E-01
1584	1.8542	2.0487	1.7687	-0.0000	1.8180	2.0637	1.7913	-0.0000	-0.3248E-00	-0.4512E-00	0.1753E-00	-0.3205E-01
1585	1.8533	2.0489	1.7660	-0.0000	1.8170	2.0638	1.7927	-0.0000	-0.3276E-00	-0.4493E-00	0.1758E-00	-0.3313E-01
1586	1.8524	2.0492	1.7695	-0.0000	1.8161	2.0640	1.7928	-0.0000	-0.3305E-00	-0.4474E-00	0.1764E-00	-0.3431E-01
1587	1.8516	2.0494	1.7671	-0.0000	1.8151	2.0642	1.7942	-0.0000	-0.3334E-00	-0.4454E-00	0.1770E-00	-0.3533E-01
1588	1.8507	2.0496	1.7704	-0.0000	1.8141	2.0644	1.7943	-0.0000	-0.3362E-00	-0.4434E-00	0.1776E-00	-0.3644E-01
1589	1.8498	2.0498	1.7683	-0.0000	1.8131	2.0646	1.7957	-0.0000	-0.3390E-00	-0.4413E-00	0.1782E-00	-0.3740E-01
1590	1.8489	2.0500	1.7714	-0.0000	1.8121	2.0647	1.7959	-0.0000	-0.3419E-00	-0.4393E-00	0.1789E-00	-0.3845E-01
1591	1.8480	2.0503	1.7695	-0.0000	1.8111	2.0649	1.7972	-0.0000	-0.3447E-00	-0.4372E-00	0.1795E-00	-0.3937E-01
1592	1.8472	2.0505	1.7724	-0.0000	1.8102	2.0650	1.7974	-0.0000	-0.3475E-00	-0.4350E-00	0.1801E-00	-0.4037E-01
1593	1.8463	2.0507	1.7707	-0.0000	1.8092	2.0652	1.7987	-0.0000	-0.3502E-00	-0.4329E-00	0.1808E-00	-0.4125E-01
1594	1.8454	2.0509	1.7735	-0.0000	1.8082	2.0653	1.7990	-0.0000	-0.3530E-00	-0.4307E-00	0.1815E-00	-0.4221E-01
1595	1.8446	2.0511	1.7720	-0.0000	1.8073	2.0655	1.8003	-0.0000	-0.3558E-00	-0.4285E-00	0.1821E-00	-0.4306E-01
1596	1.8437	2.0512	1.7746	-0.0000	1.8063	2.0656	1.8006	-0.0000	-0.3585E-00	-0.4262E-00	0.1828E-00	-0.4399E-01
1597	1.8428	2.0514	1.7734	-0.0000	1.8053	2.0657	1.8019	-0.0000	-0.3613E-00	-0.4240E-00	0.1835E-00	-0.4481E-01
1598	1.8419	2.0516	1.7758	-0.0000	1.8044	2.0659	1.8023	-0.0000	-0.3640E-00	-0.4217E-00	0.1842E-00	-0.4571E-01
1599	1.8411	2.0518	1.7748	-0.0000	1.8034	2.0660	1.8035	-0.0000	-0.3667E-00	-0.4194E-00	0.1849E-00	-0.4651E-01
1600	1.8402	2.0520	1.7771	-0.0000	1.8024	2.0661	1.8039	-0.0000	-0.3694E-00	-0.4170E-00	0.1856E-00	-0.4738E-01

Figure 16 - Dynamic Program Computer Output I - Hybrid Journal Bearings

CASE NUMBER 10

	XM	YM	A1	A2	B1(1)	B2(1)	B1(2)	B2(2)
1601	0.136229	0.102679	-0.007305	0.005235	-0.007708	0.003528	-0.007746	0.003518
1602	0.136882	0.101948	-0.007312	0.005273	-0.007700	0.003573	-0.007739	0.003562
1603	0.137531	0.101214	-0.007320	0.005310	-0.007692	0.003618	-0.007731	0.003605
1604	0.138177	0.100477	-0.007327	0.005348	-0.007684	0.003662	-0.007724	0.003649
1605	0.138820	0.099737	-0.007334	0.005386	-0.007675	0.003707	-0.007716	0.003693
1606	0.139459	0.098994	-0.007341	0.005424	-0.007666	0.003751	-0.007707	0.003736
1607	0.140095	0.098248	-0.007348	0.005462	-0.007657	0.003795	-0.007699	0.003779
1608	0.140728	0.097499	-0.007354	0.005500	-0.007647	0.003839	-0.007690	0.003822
1609	0.141357	0.096747	-0.007360	0.005539	-0.007637	0.003883	-0.007681	0.003865
1610	0.141982	0.095992	-0.007366	0.005577	-0.007627	0.003927	-0.007671	0.003908
1611	0.142604	0.095234	-0.007372	0.005616	-0.007617	0.003971	-0.007662	0.003951
1612	0.143223	0.094473	-0.007378	0.005655	-0.007606	0.004014	-0.007652	0.003994
1613	0.143838	0.093709	-0.007383	0.005694	-0.007596	0.004058	-0.007642	0.004036
1614	0.144449	0.092942	-0.007388	0.005734	-0.007585	0.004101	-0.007631	0.004078
1615	0.145057	0.092172	-0.007393	0.005773	-0.007573	0.004144	-0.007621	0.004120
1616	0.145661	0.091400	-0.007397	0.005813	-0.007562	0.004187	-0.007610	0.004162
1617	0.146262	0.090625	-0.007401	0.005853	-0.007550	0.004230	-0.007599	0.004204
1618	0.146859	0.089846	-0.007405	0.005893	-0.007538	0.004273	-0.007587	0.004246
1619	0.147453	0.089066	-0.007409	0.005933	-0.007525	0.004315	-0.007575	0.004288
1620	0.148043	0.088282	-0.007412	0.005973	-0.007513	0.004358	-0.007564	0.004329
1621	0.148629	0.087496	-0.007416	0.006013	-0.007500	0.004400	-0.007551	0.004370
1622	0.149211	0.086706	-0.007418	0.006054	-0.007487	0.004442	-0.007539	0.004411
1623	0.149790	0.085915	-0.007421	0.006095	-0.007473	0.004484	-0.007526	0.004452
1624	0.150365	0.085120	-0.007423	0.006136	-0.007460	0.004526	-0.007513	0.004493
1625	0.150937	0.084323	-0.007425	0.006177	-0.007446	0.004568	-0.007500	0.004534
1626	0.151505	0.083524	-0.007427	0.006218	-0.007432	0.004609	-0.007487	0.004575
1627	0.152069	0.082721	-0.007428	0.006259	-0.007417	0.004650	-0.007473	0.004615
1628	0.152629	0.081917	-0.007429	0.006301	-0.007403	0.004692	-0.007460	0.004655
1629	0.153185	0.081109	-0.007430	0.006342	-0.007388	0.004733	-0.007445	0.004695
1630	0.153738	0.080299	-0.007431	0.006384	-0.007373	0.004774	-0.007431	0.004735
1631	0.154287	0.079487	-0.007431	0.006426	-0.007358	0.004814	-0.007417	0.004775
1632	0.154832	0.078672	-0.007430	0.006468	-0.007342	0.004855	-0.007402	0.004814
1633	0.155373	0.077855	-0.007430	0.006510	-0.007327	0.004895	-0.007387	0.004854
1634	0.155910	0.077035	-0.007429	0.006553	-0.007311	0.004936	-0.007371	0.004893
1635	0.156443	0.076213	-0.007428	0.006595	-0.007294	0.004976	-0.007356	0.004932
1636	0.156973	0.075389	-0.007426	0.006638	-0.007278	0.005015	-0.007340	0.004971
1637	0.157499	0.074562	-0.007424	0.006681	-0.007261	0.005055	-0.007324	0.005010
1638	0.158020	0.073733	-0.007422	0.006723	-0.007244	0.005095	-0.007308	0.005048
1639	0.158538	0.072901	-0.007420	0.006766	-0.007227	0.005134	-0.007292	0.005087
1640	0.159052	0.072068	-0.007417	0.006810	-0.007210	0.005173	-0.007275	0.005125
1641	0.159562	0.071232	-0.007413	0.006853	-0.007192	0.005212	-0.007258	0.005163
1642	0.160068	0.070393	-0.007410	0.006896	-0.007175	0.005251	-0.007241	0.005201
1643	0.160570	0.069553	-0.007406	0.006940	-0.007157	0.005290	-0.007224	0.005238
1644	0.161068	0.068710	-0.007401	0.006983	-0.007138	0.005328	-0.007206	0.005276
1645	0.161562	0.067865	-0.007396	0.007027	-0.007120	0.005367	-0.007189	0.005313
1646	0.162052	0.067018	-0.007391	0.007071	-0.007101	0.005405	-0.007171	0.005350
1647	0.162538	0.066169	-0.007386	0.007115	-0.007082	0.005443	-0.007153	0.005387
1648	0.163020	0.065318	-0.007380	0.007159	-0.007063	0.005481	-0.007134	0.005424
1649	0.163498	0.064465	-0.007373	0.007203	-0.007044	0.005518	-0.007116	0.005461
1650	0.163971	0.063610	-0.007366	0.007248	-0.007024	0.005556	-0.007097	0.005497

Figure 17 - Dynamic Program Computer Output II - Hybrid Journal Bearings

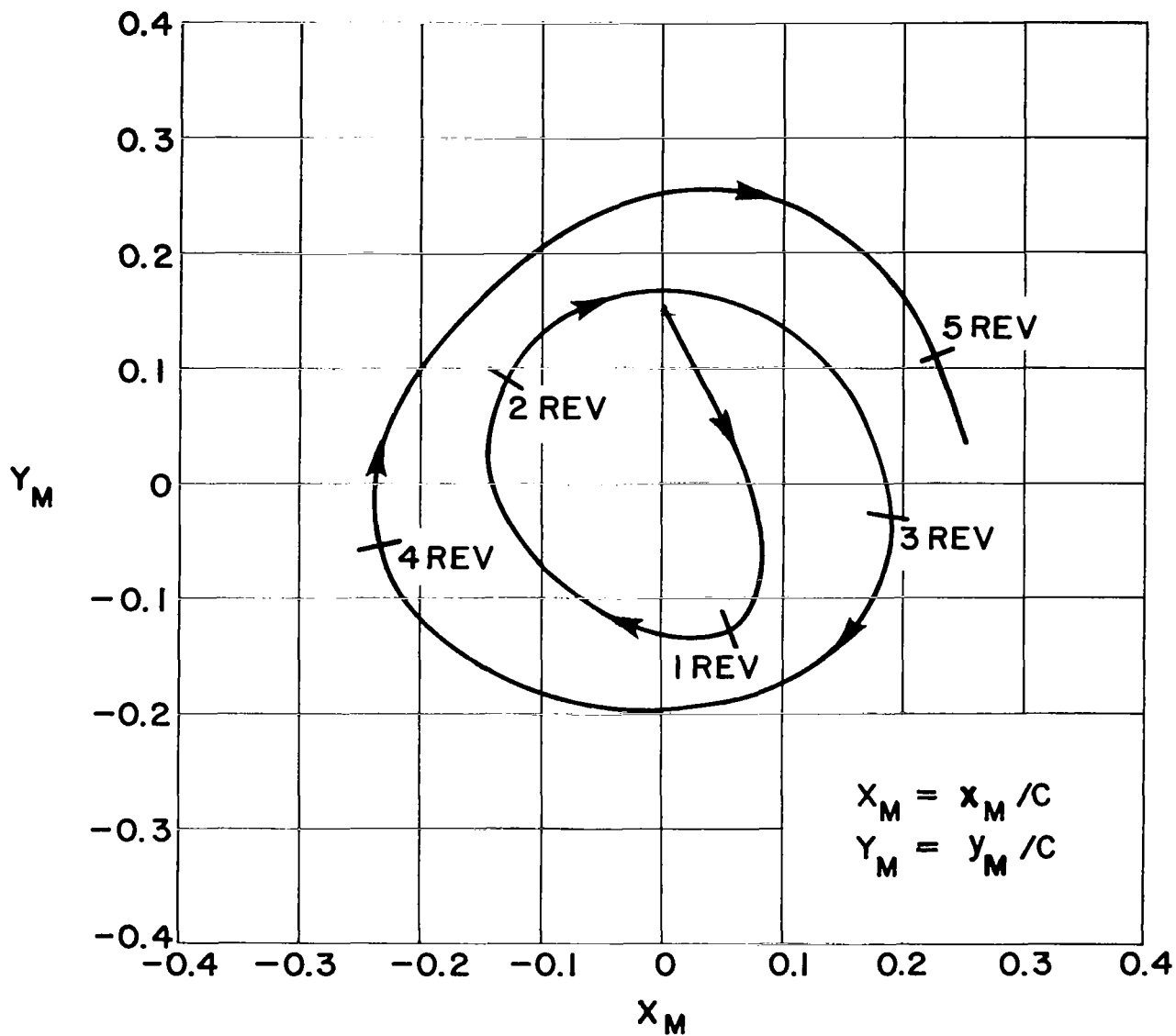


Figure 18 - Orbit of Shaft Mass Center - Hybrid Journal Bearings

<u>Sector</u>	<u>Recess Pressures</u>	
	<u>Steady-State</u>	<u>Dynamic</u>
1	1.950	1.963
2	1.957	1.972
3	1.732	1.742

The agreement is excellent considering that one method is an "equilibrium" solution while the other is obtained from a diffusion process.

After release the orbit is continually expanding but at a reduced rate as time progresses. Stability is questionable, but the indication of settling into a constant orbit diameter is encouraging, and with possibly slight modification stable operation could result. A typical alteration to improve stability would be to unbalance orifice sizes, so as to cause a deliberate eccentricity in the zero "G" condition.

An interesting comparison of shaft orbits is shown on Figure 19. The large orbit is representative of a bearing that does not have external pressurization. This bearing failed by physical contact between the journal and bearing after approximately three shaft revolutions and a little over one precession orbit had been completed.

Figure 20 is a plot of X_M and Y_M vs. shaft revolutions. Figure 20a shows variation in shaft force vs. shaft revolutions. Figures 21 and 22 show the relative angular deflection between the shaft and bearing shell in the X-Z and X-Y planes. The large increase occurring at about the 5th shaft revolution represents opposite phase motions of the shaft and shell. It is anticipated that the bearing will shortly change directions and begin to align itself with the shaft. Again, the true effect of segregated recesses and also the added restoring torques on the shaft from the thrust bearing which are not included in the dynamic analysis will limit the magnitude of the angular deviation. Figures 23 and 24 show the absolute rather than the relative magnitude of the angular deviations and are included primarily to supply

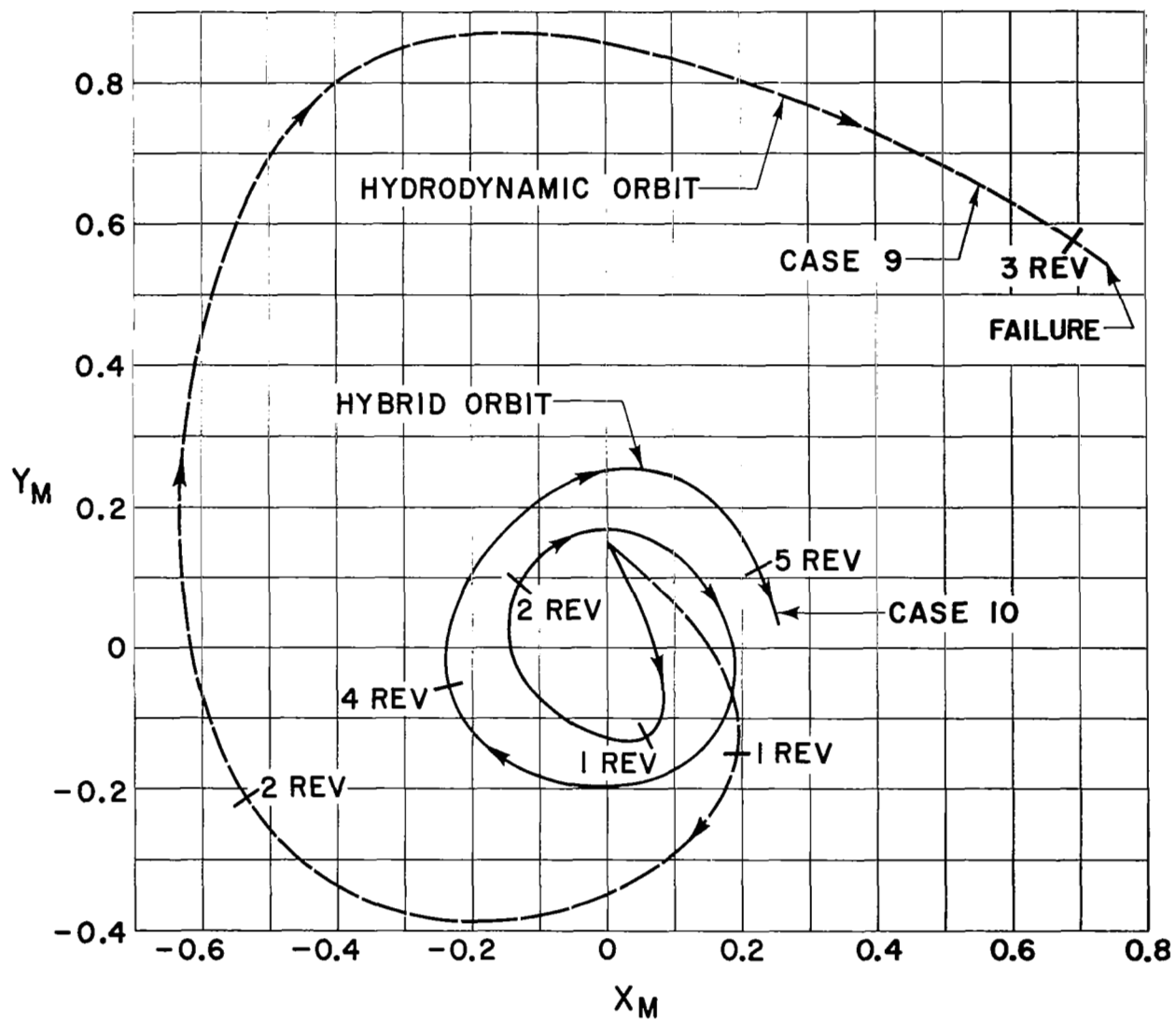


Figure 19 - Orbit of Shaft Mass Center - Hydrodynamic and Hybrid Journal Bearings

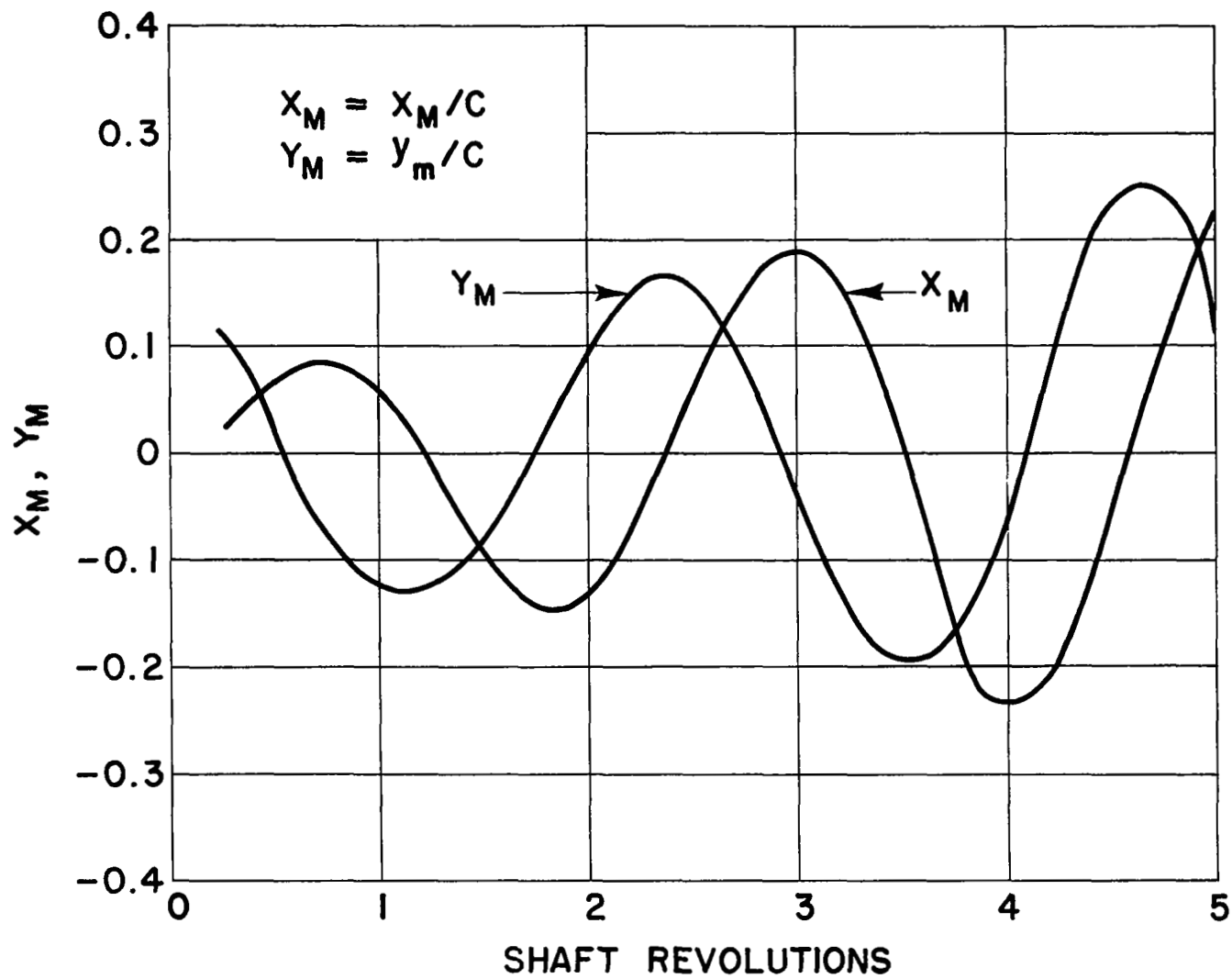


Figure 20 - X and Y Displacement of Mass Center vs Shaft Revolutions
Hybrid Journal Bearings

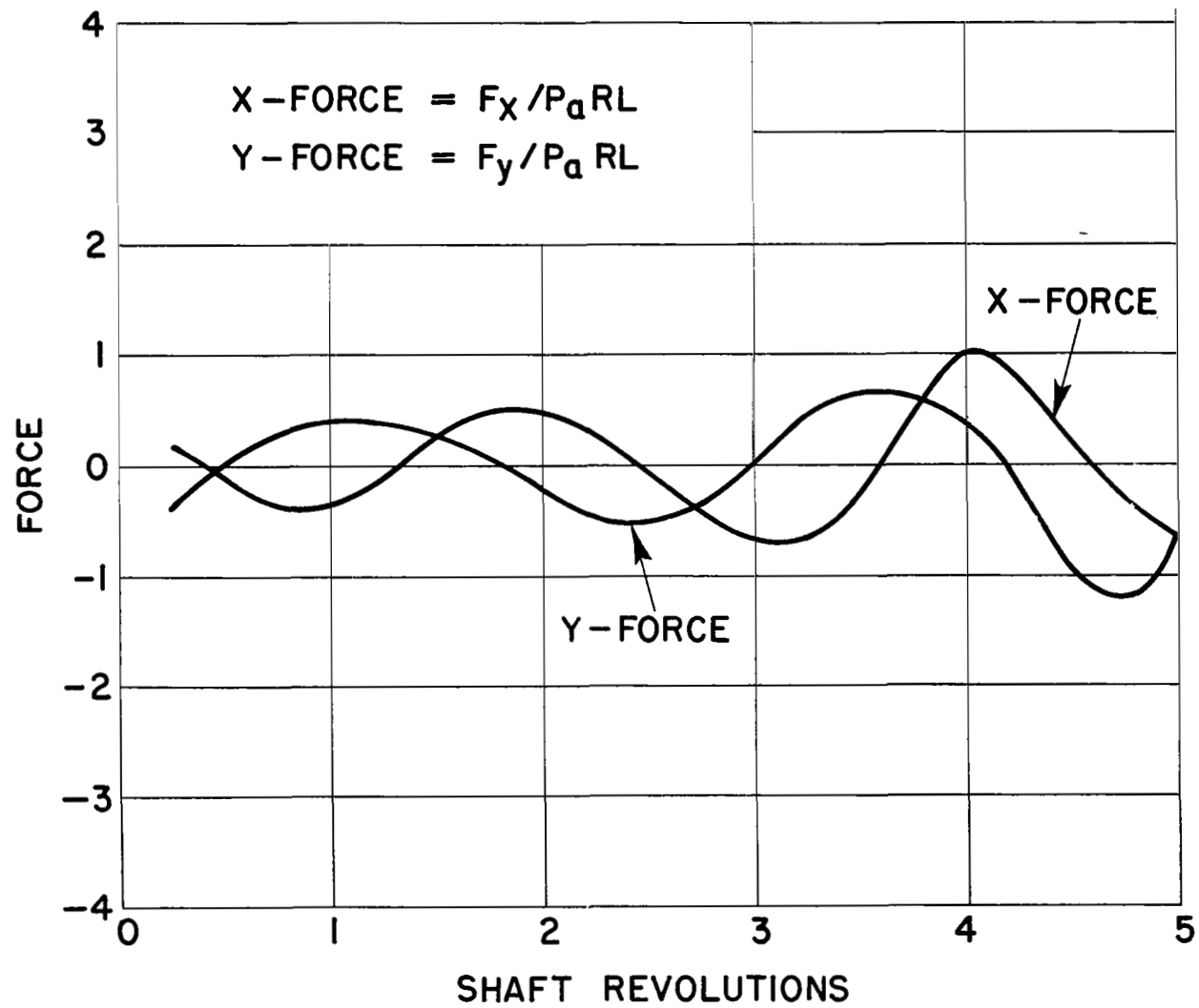


Figure 20a - X and Y Forces vs Shaft Revolutions - Hybrid Journal Bearings

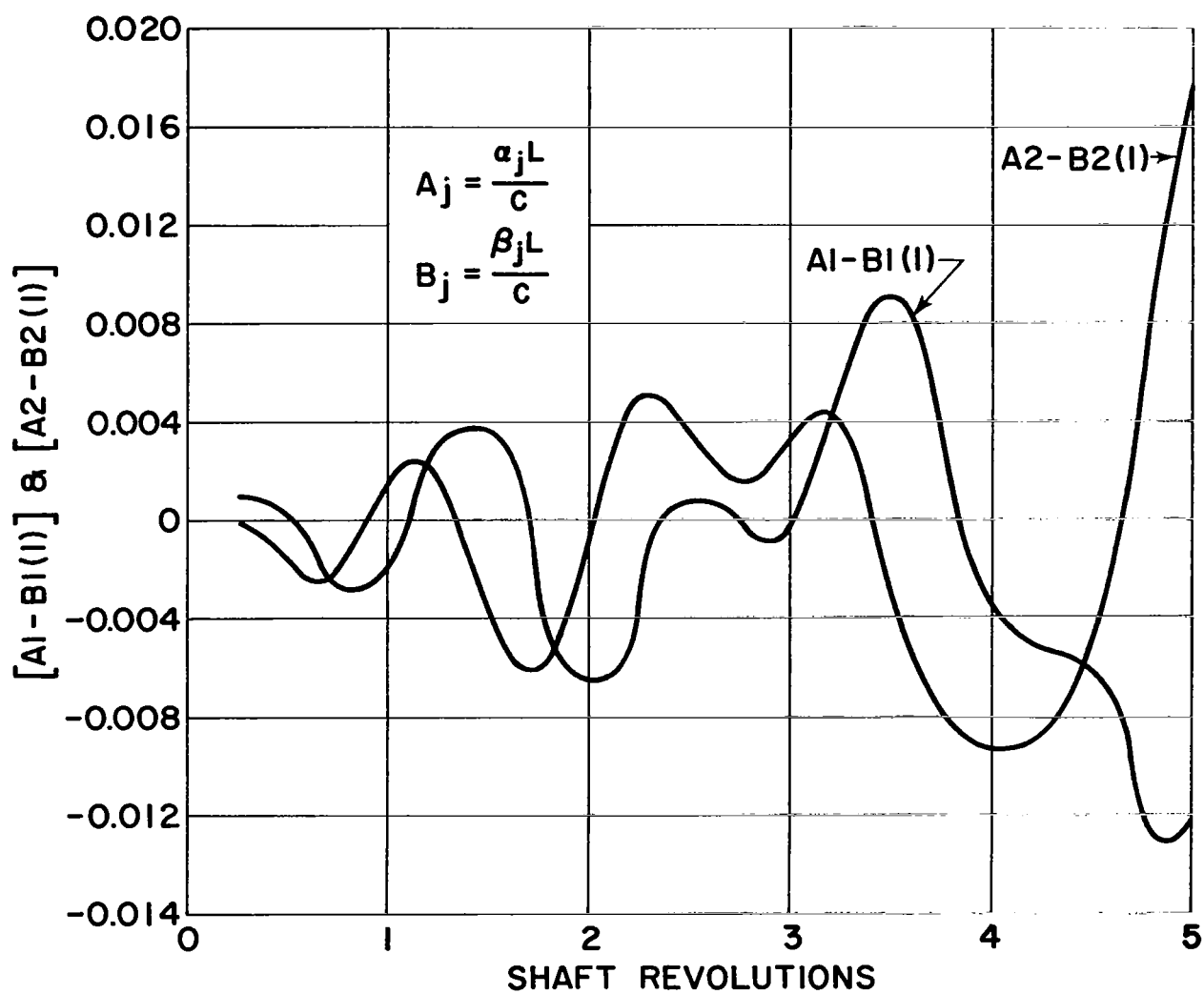


Figure 21 - Relative Angular Displacement Between Shaft and Bearing 1 vs Shaft Revolutions - Hybrid Journal Bearings

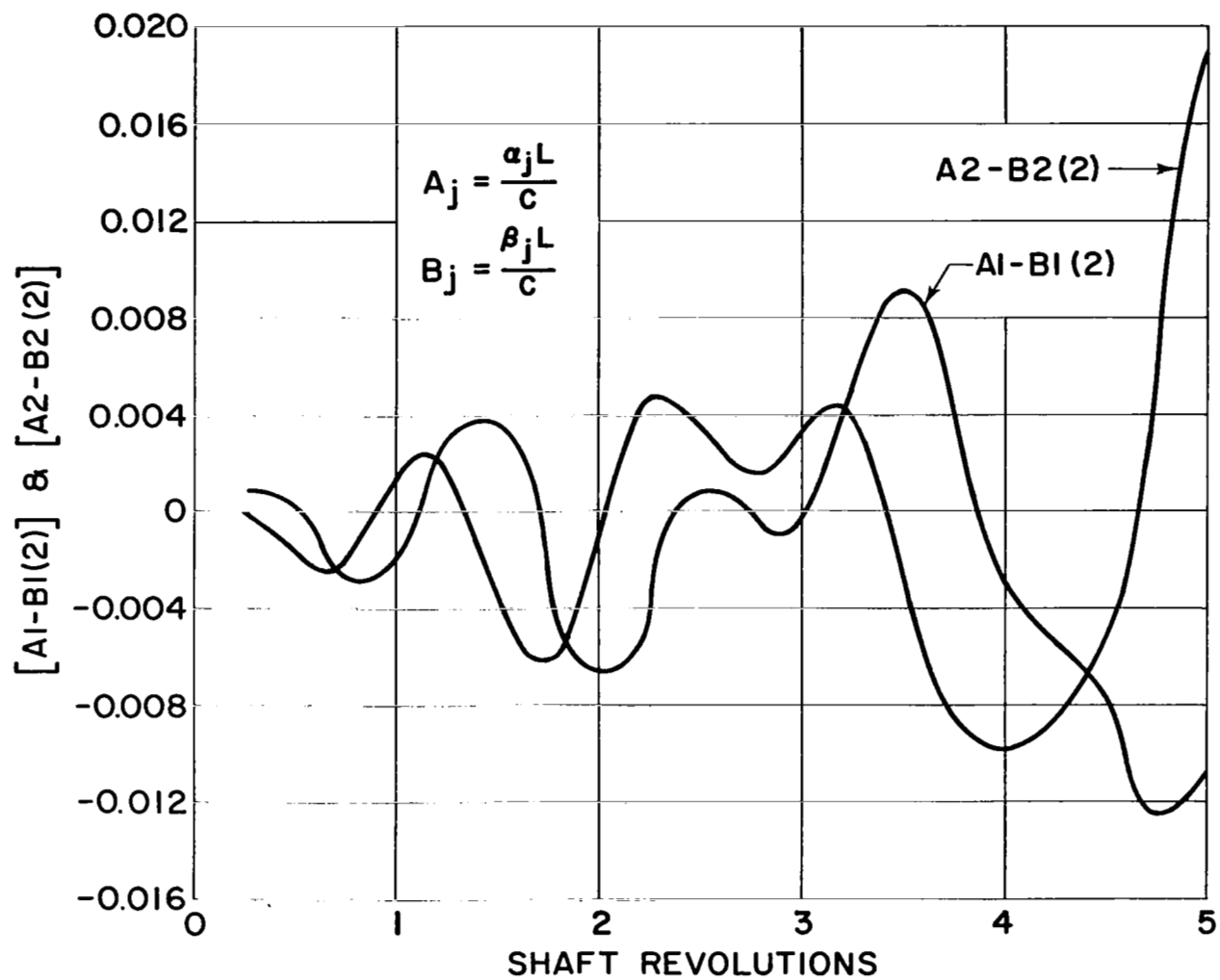


Figure 22 - Relative Angular Displacement Between Shaft and Bearing 2
vs Shaft Revolutions - Hybrid Journal Bearings

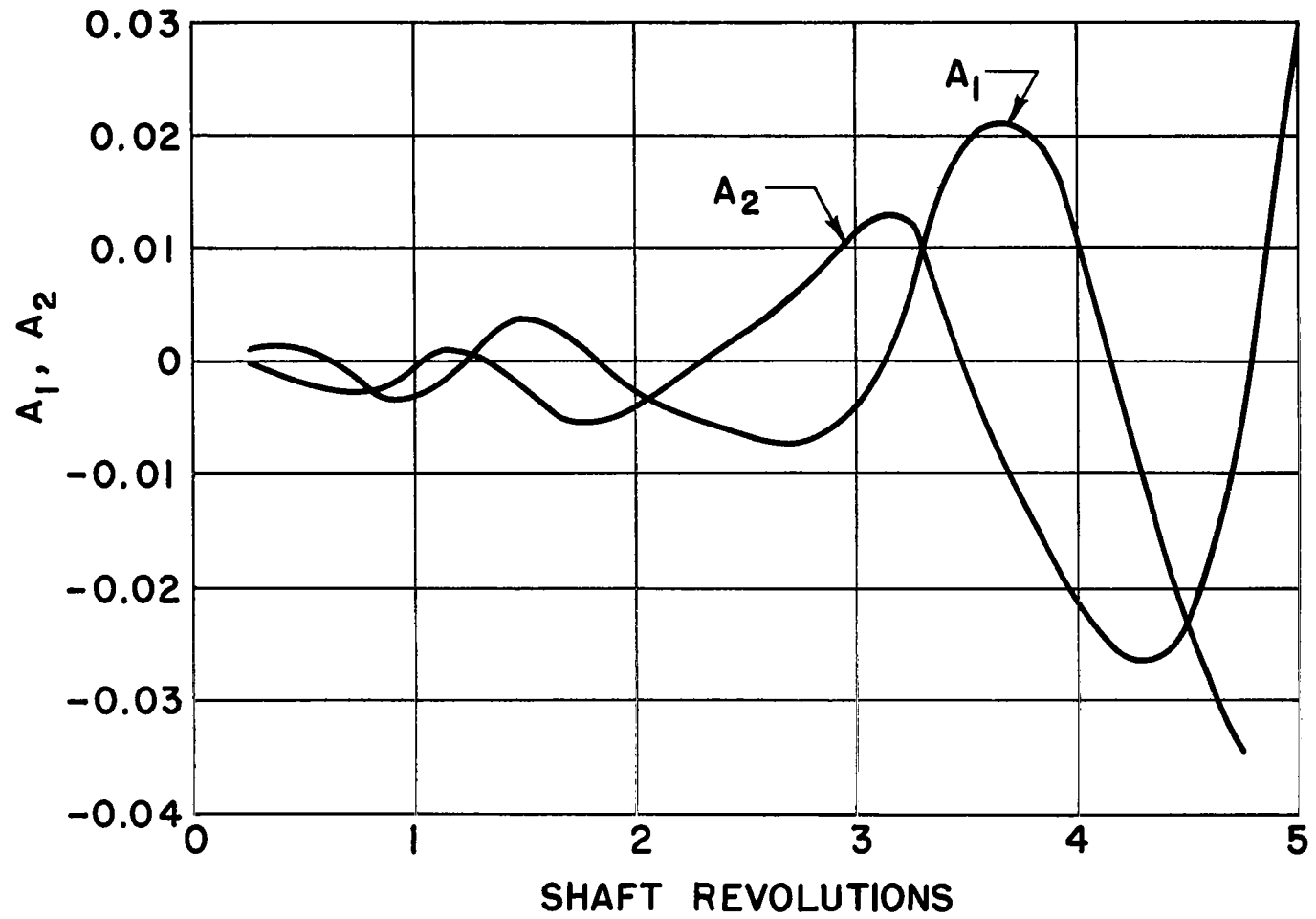


Figure 23 - Shaft Angular Displacements vs Shaft Revolutions

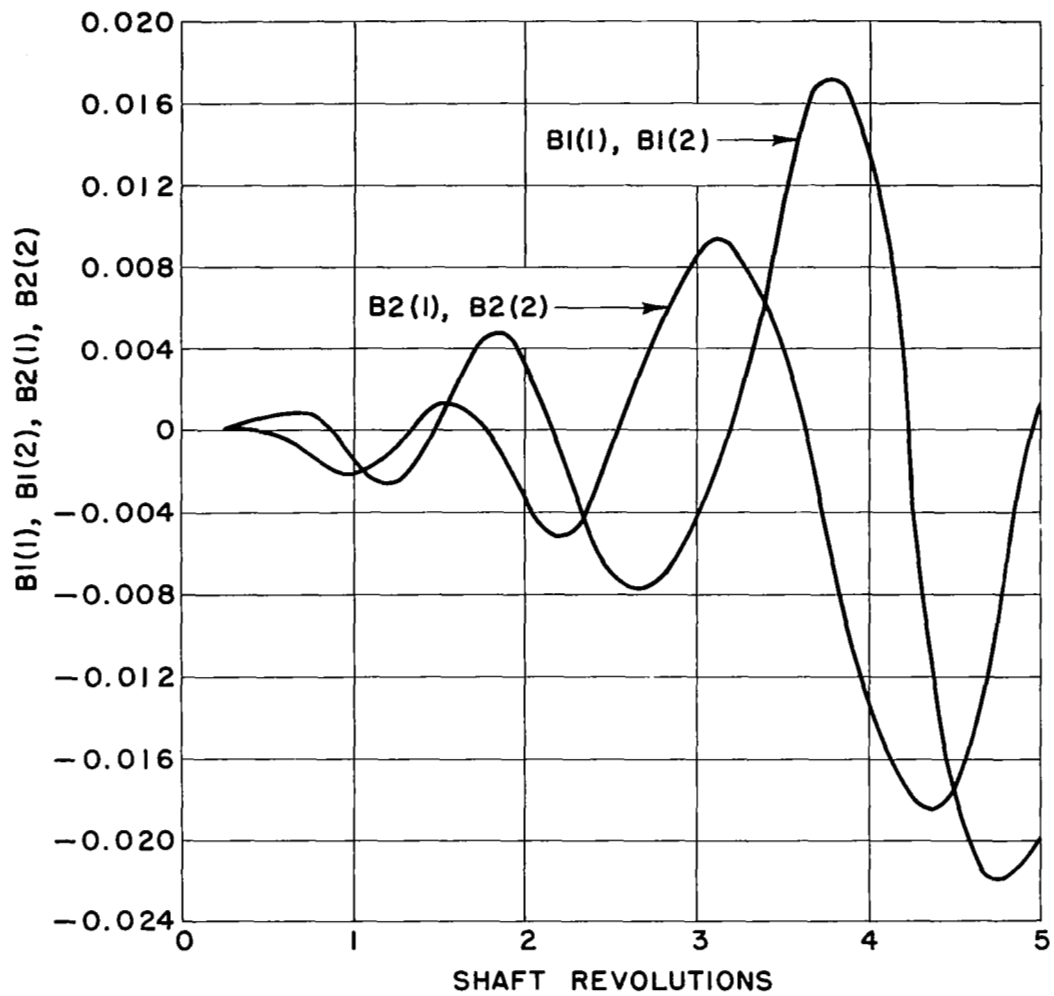


Figure 24 - Bearing Angular Displacements vs Shaft Revolutions

data that can be used to compare with test results, since the instrumentation installation is designed to measure the motions of the bearing and shaft separately.

H. Rigid Rotor Dynamics

The time transient dynamics program is an extremely powerful tool for determining shaft and bearing motions at a particular operating condition. Its use is limited however, because of long running time. Other means must be used to determine for example, critical shaft speed or other dynamic properties that require results over a wide spectrum of operating conditions. To investigate dynamic properties over a wide range of speed an available rigid rotor dynamics program was utilized.

This lumped parameter program considers a rigid rotor supported by springs at two ends. The spring constant is chosen so that it approximates the film stiffness of the bearing. It also takes into consideration damping and unbalances. The motion of the rotor has four degrees of freedom; -- the motion of the center of mass of rotor in the X, and Y directions and the rotation of shaft in the X-Y and Y-Z planes. To describe this motion, a set of four second order ordinary differential equations is derived. The solution of this set of equations has been programed for an IBM 7094 computer. It gives a complete description of the rotor motion over a wide range of running speed, and indicates the critical speed region and approximate threshold. Being an approximate treatment this program is used primarily to indicate the range where the accurate orbital program should be used to investigate the behavior of the bearing system.

The lumped parameter program has been run for the bearing operating in the horizontal orientation. The results are shown on Figure 25 and are summarized on Table II.

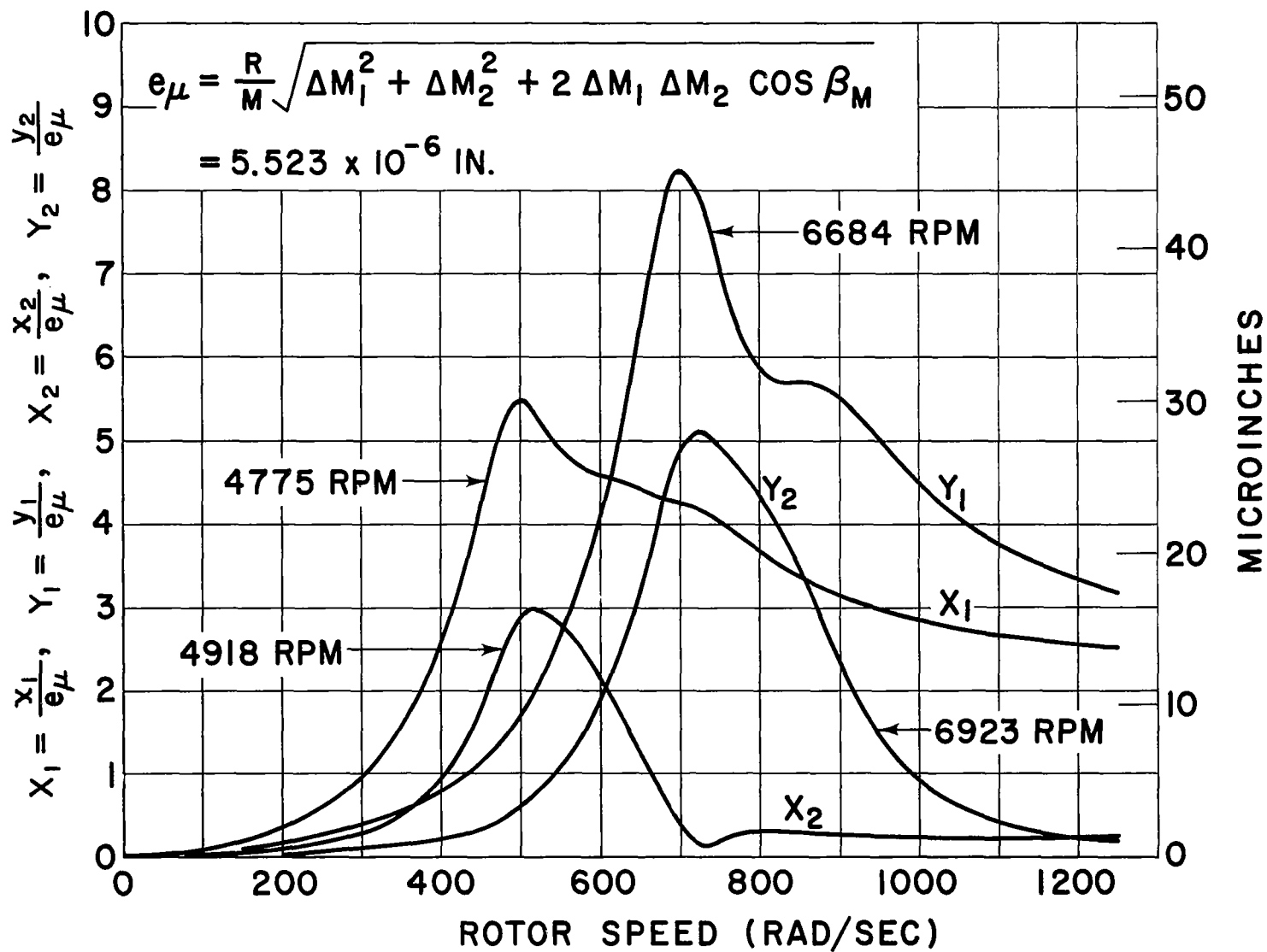


Figure 25 - Rigid Rotor Analysis - Amplitude vs Shaft Speed

Table II

RPM	Mode	RPM	Mode
$\omega_{x1}^{(1)} = 4775$	96% Conical	$\omega_{x2}^{(1)} = 6685$	86% Conical
$\omega_{y1}^{(1)} = 6684$	98% Conical	$\omega_{y2}^{(1)} = 8165$	74% Conical
$\omega_{x1}^{(2)} = 4918$	93% Conical	$\omega_{x2}^{(2)} = 7640$	98% Conical
$\omega_{y1}^{(2)} = 6923$	97% Conical		

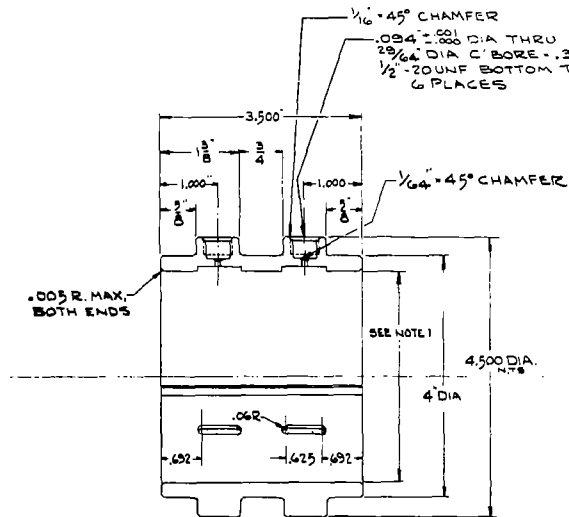
Unbalance = 0.005 in.-oz in plane of turbine
 Maximum amplitude = 50 microinches and is associated with $\omega_{y1}^{(1)}$
 $\omega_{y1}^{(1)}$ = First rigid body critical resonance in Y direction for bearing (1) (Typical)

I. Mechanical Design

The mechanical design of the hybrid journal bearing is shown on Figure 26. Mass and inertia of the bearing are minimized as much as possible to permit angular compliance between the bearing and shaft. A conically shaped sheet metal diaphragm is attached to the bearing as a supporting structure. The diaphragm has very small resistance to torques about the X and Y axis and essentially provides a self-aligning support. The bearing was designed to permit ready removal of the orifice restrictors for changing orifices during the testing phase of the program. The bearing material is AMS 6440 (52100) hardened to 50-60 Rc. In addition to being a good stable material, its expansion coefficient is compatible with the shaft material and anticipated thermal gradients, so that during normal operation the bearing clearance will remain essentially constant.

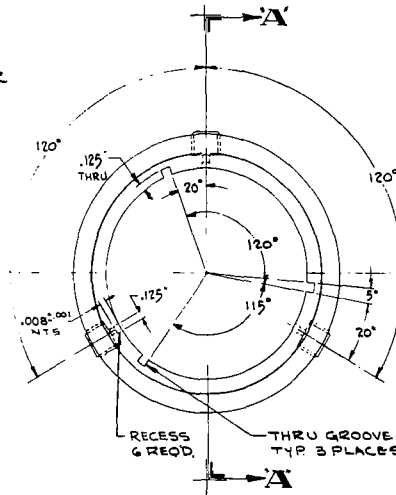
J. Conclusions and Recommendations

1. From the steady-state point of view the journal bearing performs exceptionally well; the only dubious area is the quantitative restoring or aligning torques provided by the segregated recesses in each sector



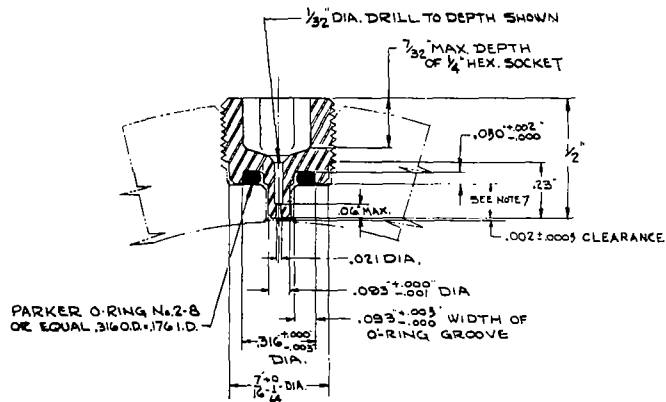
SECTION A-A

WITH ORIFICE RESTRICTOR REMOVED



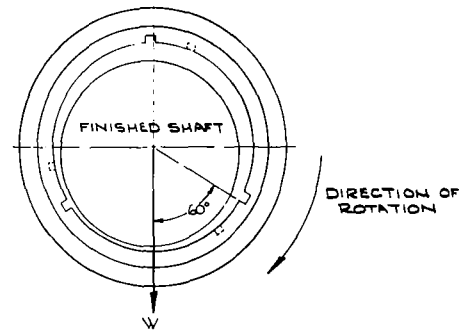
NOTES:

1. FINISH INSIDE DIAMETER (3.5" NOMINAL) TO PROVIDE RADIAL CLEARANCE OF $.002 \pm .0005$ WITH FINISHED SHAFT.
2. INSTALLED BEARING ASSEMBLY IS TO BE BALANCED TO PROVIDE MINIMUM STATIC MOMENT ON SELF-ALIGNING SUPPORT STRUCTURE. BALANCING SHOULD BE ACCOMPLISHED WITH FEED LINE ACTIVATED.
3. PROVIDE .005" BREAK ON RECESS AND GROOVE EDGES
4. MATERIAL - CHROMIUM STEEL AMS 6440 (SAE 52100) STABILIZE AND HARDEN TO ROCKWELL 'C' 50-60
5. FOR OPTIMUM LOAD CAPACITY, ORIENTATION OF GROOVES WITH LOAD DIRECTION IS TO BE AS INDICATED IN LOADING ORIENTATION DIAGRAM.
6. BEARING SUPPORT AND MOUNTING STRUCTURE TO BE SUPPLIED BY P.W.
7. THIS DIMENSION TO BE HELD SO CLEARANCE BETWEEN BOTTOM OF RESTRICTOR AND TOP OF RECESS IS $.002 \pm .0005$



ORIFICE RESTRICTOR DETAIL

CAN BE MADE FROM $\frac{1}{2}$ " 20 UNF $\times \frac{3}{8}$ " LG
 HALF DOG SOC. SET SCREW
 SCALE - 4 TIMES ACTUAL SIZE (6 REQ'D)



LOADING ORIENTATION

SEE NOTE 5

Figure 26 - Mechanical Design - Hybrid Journal Bearing

2. The stability of the system is marginal when the alternator is in the vertical orientation running at the overspeed condition. Improvement upon what the analytical results presently indicate may be realized because of the additional aligning torques provided by the segregated recesses and by the thrust bearing; the contribution of these effects was not included in the analytical investigations.

3. It is recommended that the present program be extended to determine the effect of pre-loading schemes that would enhance stability (e.g. the effect of unbalancing orifices on the system stability should be established).

4. The frequency and amplitude of the gas film forces, determined from the dynamics program, should be applied as a forcing function to the governing vibration equation of the alignment cone so that precautions can be taken to prevent structural resonance of the cone.

5. It is recommended that a simple test program be initiated to validate the steady-state and time transient dynamic programs, since testing in the dynamic simulator is a complex procedure and is not likely to occur for some months.

6. As a longer range recommendation analytical techniques that would allow segregation of recesses in one sector should be investigated and carried through if feasible. An implicit method of recent origin shows promise in this direction.

7. It is recommended that check valves be inserted in the lines feeding the orifice restrictions to each recess. This will prevent backflow and loss of load capacity, in dynamic situations, when recess pressure exceeds supply pressure. Each check valve should be located as close as possible to the recess in order to minimize compressibility effects of the fluid between the recess and the check valve.

8. The present design calls for a support structure stiffness of 15,000 to 20,000 in-lb/rad. It is recommended that the effects of varying this stiffness be determined by a number of dynamic computer program runs in which the stiffness parameter is varied over a suitable range. The effects may also be determined empirically by first experimenting with a stiff structure and subsequently reducing its thickness to increase flexibility.

III. THRUST BEARING

Configuration

The thrust bearing configuration selected for analysis and design is shown diagrammatically on Figure 27. It consists of a dead-ended, spiral-groove, hydrodynamic bearing surrounded by an inherently compensated hydrostatic bearing. The primary reasons why this type of bearing was selected are:

- (1) The dead-ended spiral groove bearing produces maximum hydrodynamic load capacity per unit of available thrust area.
- (2) Location of the supply gas at the outer perimeter of the hydrodynamic bearing feeds the natural inward pumping tendency of the spiral groove bearing, and also provides maximum hydrostatic load capacity.
- (3) The design optimizes righting moment capability from hydrostatic action.

A typical pressure distribution for the hybrid bearing is shown on Figure 27, and gives an indication of increase in load capacity obtained from the external pressurization effect.

In addition to the main thrust bearing, a reaction or bumper bearing is required for start-up and shut-down conditions. The reaction bearing is shown on Figure 28. It is basically an annular configuration with a row of supply holes located around the mid-circumference. No provisions were made for this bearing to produce any hydrodynamic thrust. When the alternator is running all aerodynamic thrust is toward the main bearing, and the various orientations of the alternator are such that gravity loading is never directed toward the reaction bearing. During start-up, in the horizontal orientation, the reaction bearing will be required to take the pre-load from the main bearing until the aerodynamic load builds up sufficiently to ensure that all loading is directed toward the main bearing. It is also possible at start-up for the turbine to produce a momentary aerodynamic thrust load in a direction opposite to that of normal operation so that an additional function of the reaction bearing is to accept this load.

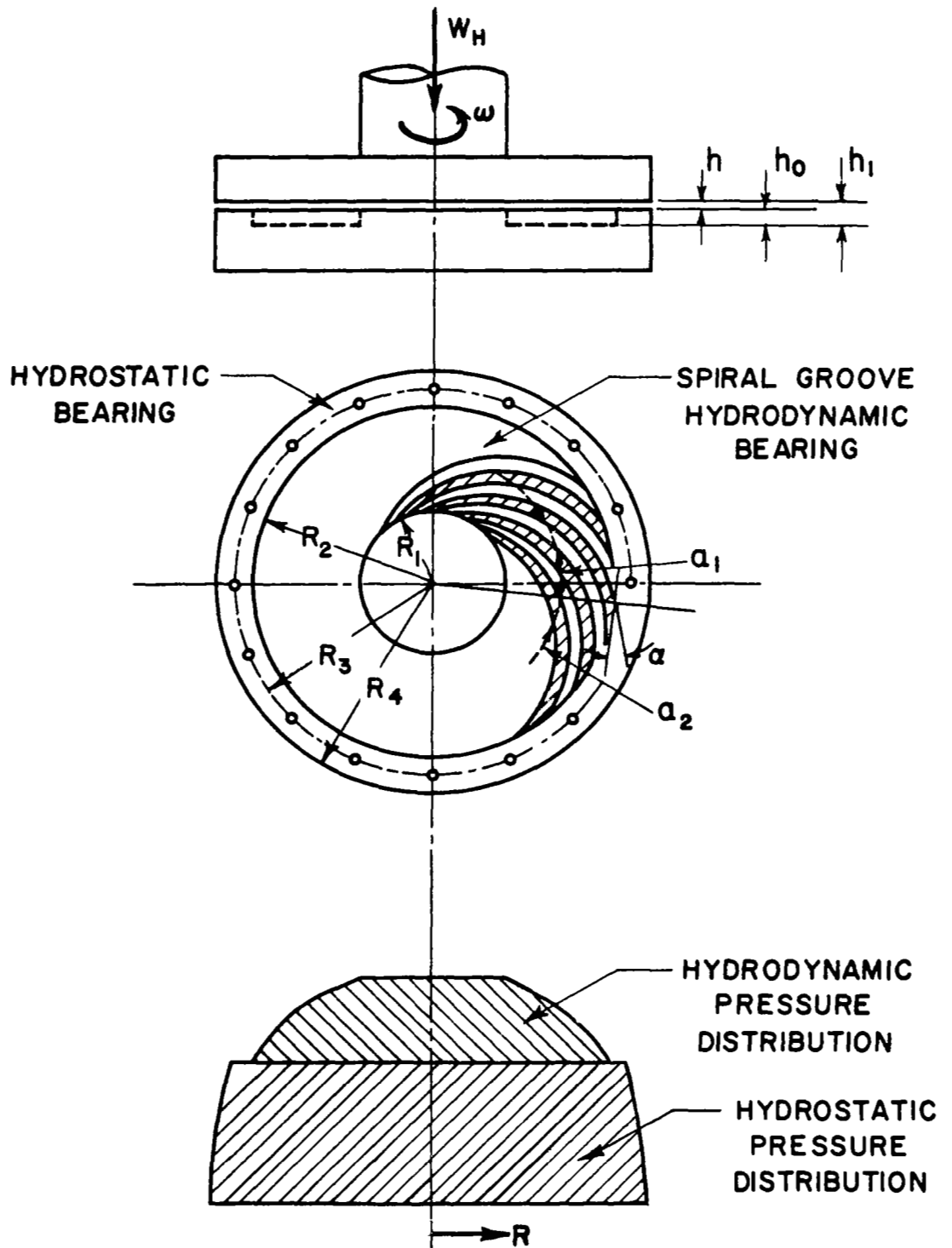
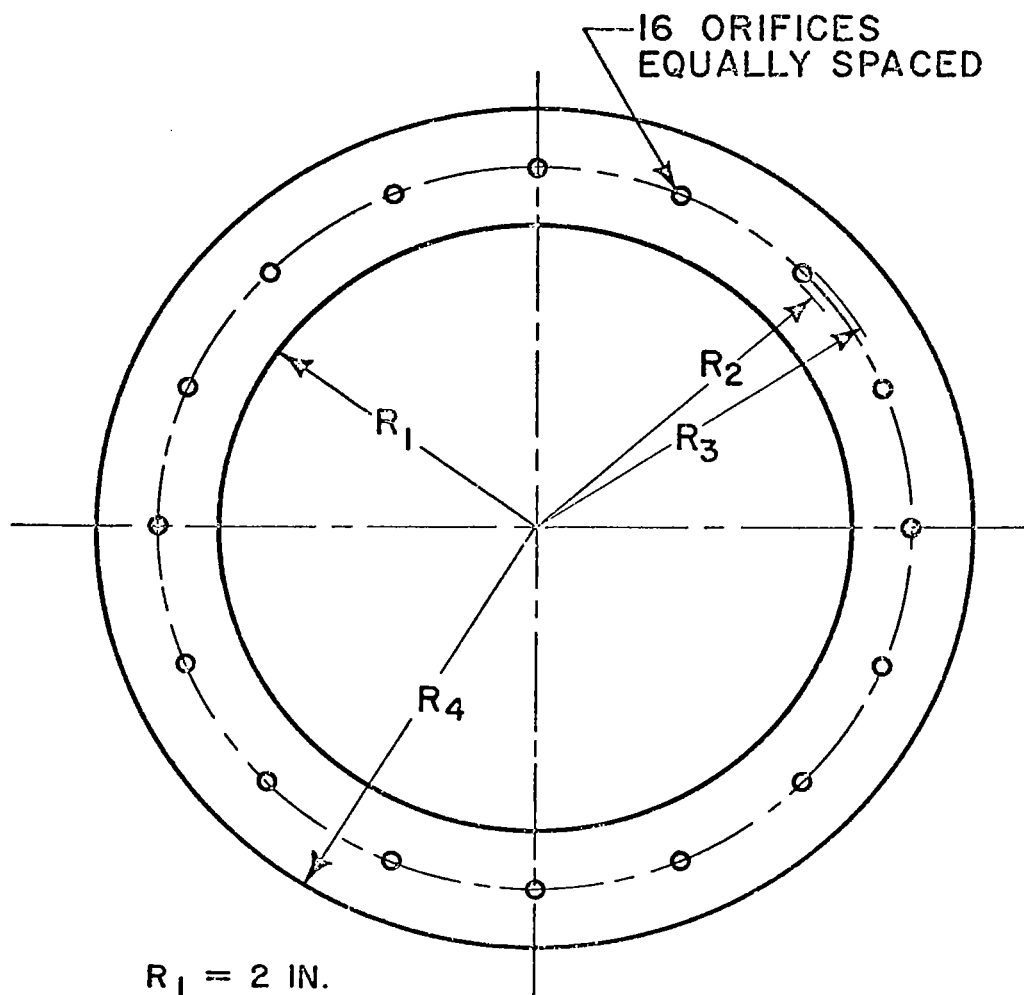


Figure 27 - Hybrid Thrust Bearing



$$R_1 = 2 \text{ IN.}$$

$$R_2 = 2.735 \text{ IN.}$$

$$R_3 = 2.766 \text{ IN.}$$

$$R_4 = 3 \text{ IN.}$$

$$D_0 = 0.031 \text{ IN.}$$

Figure 28 - Reaction Thrust Bearing

B. Specifications and Performance Requirements*

The following specifications were used for performing the analysis.

- (1) Lubricant - argon gas
- (2) Operating Temperature, $T = 300^{\circ}\text{F}$
- (3) Shaft speed, $N = 12,000 \text{ RPM}$
- (4) Supply Pressure, $P_s = 12 \text{ psia}$ (operating at speed)
 $P_s = 0\text{-}100 \text{ psia}$ (lift off and shut down)
- (5) Ambient pressure, $P_a = 6 \text{ psia}$
- (6) Aerodynamic load 30 lbs
- (7) Gravity load 56 lbs
- (8) Total load 86 lbs
- (9) Gas viscosity - $4.3 \times 10^{-9} \text{ lb-sec/in}^2$
- (10) Bearing diameter $D = 6 \text{ in}$
- (11) Maximum total clearance of both main thrust and reaction bearing = 10 mils.

The target performance requirements are

- (1) Minimum operating clearance - 1.5 mils
- (2) Maximum allowable flow = .006 lb/sec
(1% of compressor flow)
- (3) Minimum orifice diameter $D_o = .015 \text{ in}$
- (4) Maximum Friction Loss 0.1 HP

C. Analytical Approach

The general approach used for determining the performance of the hybrid thrust bearing was to superimpose hydrostatic and hydrodynamic effects. If a sufficient number of orifices are incorporated the orifice circle can be considered as a line source of pressure, so that

* Subsequent to completion of the analysis design changes required that heavier loads be carried by the Thrust Bearing. This resulted in considerable modification to the original design. The final design and performance form appendix B of this report.

the hydrostatic pressure inside the orifice circle is essentially constant. The hydrostatic pressure then essentially raises the ambient pressure level of the spiral groove bearing and the hydrodynamic pressure generation is directly cumulative to this increased level. The basic relationships for determining performance of the hydrodynamic bearing were extracted from Reference 1.

For the thrust bearing the problem of stability is concerned with a phenomenon known as "pneumatic hammer". It is common in externally pressurized bearings containing recesses. Characteristic of this type of instability is a violent chattering of the opposed bearing surfaces which, if not checked, can cause loss of film thickness.

The approach to the instability problem is that described by L. Licht in References 2 and 3. In this theory deviations from the equilibrium conditions are expressed in terms of lumped parameters. The pressure distribution is assumed to vary quasi-statically so that the effect of the frequency of vibration is ignored. Also, the pressure profile is assumed to be known. In general, this simplified theory will permit reasonable approximations regarding stability, and comparisons between theory and experiments indicate that conservative results can be anticipated.

D. Main Hybrid Bearing - Steady-State and Stability Analysis

The externally pressurized bearing was treated as a bearing with a constant pressure distribution in the region interior to the orifice circle. As explained in the previous section, this is a reasonable assumption if the orifices are located in close proximity to one another. The fact that a low supply pressure to ambient pressure ratio exists, enables the computations to be simplified. Under these conditions the shape of the hydrostatic pressure distribution curve can be reasonably predicted. The pressure profile will vary as the ratio of recess pressure to ambient pressure (P_r/P_a) varies. This ratio changes in accordance with the load applied to the bearing. For low values of

P_r/P_a compressibility affects are minimal and the shape of the pressure distribution approximates that of the incompressible case (a convex shape between the orifice circle and outer perimeter). As the ratio increases, the pressure variation between the orifice circle and the outer perimeter becomes linear. And a further increase causes the pressure profile to become concave in shape. From data indicated in Reference 4 it was reasonable to assume an incompressible pressure distribution for $P_r/P_a < 1.8$ and a linear pressure distribution for $P_r/P_a > 1.8$. When the pressure distribution is known the effective area of the externally pressurized bearing can readily be determined.

$$A = \frac{\pi}{3} R_3^2 \left[\left(\frac{R_4}{R_3} \right)^2 + \left(\frac{R_4}{R_3} \right) + 1 \right] \quad (39)$$

for $P_r/P_a > 1.8$ (linear profile)

$$A = \frac{\pi}{2} \frac{(R_4^2 - R_3^2)}{\ln (R_4/R_3)} \quad (40)$$

for $P_r/P_a \leq 1.8$ (incompressible profile)

Equation (39) is obtained from transforming the effective area equation of Reference 2. Equation (40) is derived in Reference 5. When the effective area is known the contribution to load-carrying capacity of the externally pressurized bearing can be determined from

$$W_{EP} = (P_r - P_a) A \quad (41)$$

The bearing flow is determined solely from the external pressurization, since the net flow of the dead-ended spiral groove bearing is zero. When recess and supply pressures are known the bearing flow is determined from the orifice equation.

$$Q_o = N_o C_D A_o \sqrt{\frac{2\gamma}{(\gamma-1) R_g T_g}} P_s \left\{ \left(\frac{P_r}{P_s} \right)^{2/\gamma} \left[1 - \left(\frac{P_r}{P_s} \right)^{\frac{\gamma-1}{\gamma}} \right] \right\}^{1/2} \quad (42)$$

when $(P_r/P_s) \leq$ the critical pressure ratio where

$$(P_r/P_s)_{\text{crit}} = \left(\frac{2}{1 + \gamma} \right)^{\frac{\gamma}{\gamma-1}} \quad (43)$$

the flow is choked and the quantity of flow is determined by replacing (P_r/P_s) in (42) by $(P_r/P_s)_{\text{crit}}$.

The orifice area depends upon the type of compensation desired. If the orifice feeds directly into the clearance region (no recess) and the diameter of the orifice is large compared to the clearance, inherent compensation results. The effective orifice area is then the surface area of the cylinder formed in the clearance region of diameter equal to that of the orifice and height equal to the clearance.

$$A_o = \pi D_o h \quad (44)$$

The flow through the orifice now becomes a function of the downstream pressure and the clearance (for constant supply pressure). For a bearing in which the orifices feed into recesses, the flow is a function of the downstream pressure only. The recessed bearing has greater load capacity and stiffness than an inherently compensated (IC) bearing, but the recessed bearing is very sensitive to instability, while the IC bearing is stable over a wider range of conditions.

The bearing clearance can be determined by equating the flow through the bearing to the flow through the orifices. A specified relationship exists between the flow through an incompressible fluid hydrostatic bearing and a compressible fluid hydrostatic bearing

that is a function of the recess pressure, ambient pressure, gas constant, and absolute temperature. This relationship can be obtained by comparing the electric analog flow equations for the two fluids. From Loeb's work as described in Reference 6 the volume flow of an incompressible fluid can be put in the form

$$V_B = \frac{(P_r - P_a) h^3 r}{12\mu R} \quad (45)$$

From Reference 7 Licht showed that the mass flow of a compressible fluid is

$$Q_B = \frac{h P_a^2 \left[\left(\frac{P_r}{P_a} \right)^2 - 1 \right]}{24\mu \left(\frac{R}{r} \right) R_g T_g} \quad (46)$$

Thus for identical model configurations

$$Q_B = \frac{V_B P_a}{2 R_g T_g} \left[\left(\frac{P_r}{P_a} \right) + 1 \right] \quad (47)$$

Consequently by knowing the flow for the incompressible configuration, it is a simple matter to obtain the mass flow for the compressible case. There are many configurations for which flows of incompressible fluids have been obtained (see Ref. 8). Thus this relationship is extremely valuable.

For the central recess hydrostatic bearing configuration, V_B has been derived in Reference 5.

$$V_B = \frac{\pi h^3 (P_r - P_a)}{6\mu \ln (R_4/R_3)} \quad (48)$$

Substituting (48) into (47)

$$Q_B = \frac{\pi h^3 P_a^2 \left[\left(\frac{P_r}{P_a} \right)^2 - 1 \right]}{12 \mu R_g T_g \ln (R_4/R_3)} \quad (49)$$

The clearance is determined by equating expressions (42) and (49) using $\pi D_o h$ as the orifice area. The result is

$$h = \left\{ \frac{12 \mu R_g T_g \ln (R_4/R_3) N_o C_D D_o \sqrt{\frac{2\gamma}{(\gamma-1) R_g T_g}} P_s \left\{ \left(\frac{P_r}{P_s} \right)^{2/\gamma} \left[1 - \left(\frac{P_r}{P_s} \right)^{\frac{\gamma-1}{\gamma}} \right] \right\}^{1/2}}{P_a^2 \left[\left(\frac{P_r}{P_a} \right)^2 - 1 \right]} \right\}^{1/2} \quad (50)$$

All parameters of equation (50) are known so that h can be obtained. Once h is known the mass flow can be obtained from either of equations (42) or (49). The next step in the analysis is to incorporate the hydrodynamic effects of the spiral groove bearing.

Muijdermann (Ref. 1) develops the geometric criteria in order to optimize the bearing for load carrying capacity. The values applied to the alternator thrust bearing are as follows:

no. of grooves,	$k = 15$
radius/ratio,	$\lambda = 0.4$
groove angle,	$\alpha_{\max} = 12.4^\circ$
compression ratio,	$\delta_{\max} = 0.32$
ridge/groove ratio,	$\gamma_{\max} = 1.16$
load factor,	$C_L = \frac{W_{SG} h^2}{\mu \omega R_2^4} = 0.383$

The subscript max means that the value of the parameter is the value that will yield maximum load carrying capacity. The parameters k , λ , α_{\max} , γ_{\max} are the geometric variables that can be fixed by manufacture of the bearing. Both the compression ratio and load factor depend upon the bearing operating clearance. Figure 29 (extracted from Reference 1) shows the relationship between load factor C_L and compression ratio δ . For ease of computer calculations the curve was approximated by a series of straight lines as shown on the figure. The load factor approximated as straight lines has the following relationships

$$C_L = 1.267 \delta \quad \delta \leq 0.3 \quad (51)$$

$$C_L = 0.06 \quad \delta > 2.4 \quad (52)$$

$$C_L = .16 - .0714 (\delta - 1) \quad 1 < \delta \leq 2.4 \quad (53)$$

$$C_L = 0.38 - 0.315 (\delta - 0.3) \quad 0.3 < \delta \leq 1.0 \quad (54)$$

The hydrodynamic load carrying capacity is then

$$W_{SG} = \frac{C_L \mu R_2^4 \omega}{h^2} \quad (55)$$

The total load capacity is obtained by adding the external pressure and hydrodynamic load capacities.

$$W_H = W_{SG} + W_{EP} \quad (56)$$

All steady-state performance parameters can now be determined; it remains to check stability.

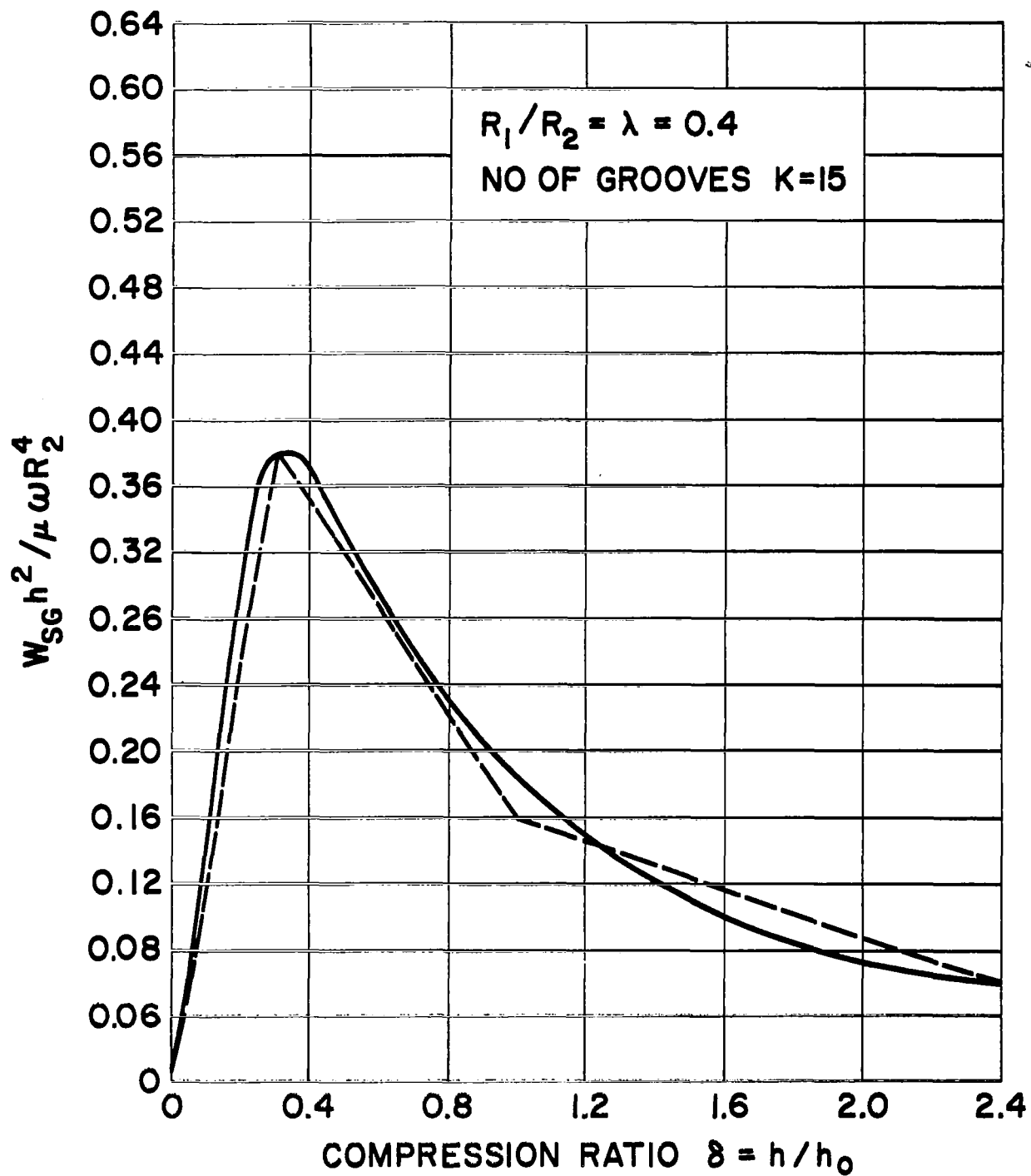


Figure 29 - Load Factor vs Compression Ratio - Spiral Groove Thrust Bearing

The equation of motion for the bearing is

$$m\ddot{h} = p'A \quad (57)$$

The conservation of mass states that the time rate of change of the bearing gas content equals the difference between inflow and outflow. Corresponding to the time rates of small deviations from the equilibrium position the following equations are obtained

$$q_{in} = \left(\frac{\partial Q_{in}}{\partial P} \right) p' + \left(\frac{\partial Q_{in}}{\partial h} \right) h' \quad (58)$$

Similarly,

$$q_{out} = \left(\frac{\partial Q_{out}}{\partial P} \right) p' + \left(\frac{\partial Q_{out}}{\partial h} \right) h' \quad (59)$$

$$q_{in} - q_{out} = \left(\frac{\partial Q_{in}}{\partial P} - \frac{\partial Q_{out}}{\partial P} \right) p' + \left(\frac{\partial Q_{in}}{\partial h} - \frac{\partial Q_{out}}{\partial h} \right) h' \quad (60)$$

The mass content contained within the bearing has been derived in Reference 2 and is

$$M = \frac{1}{R_g T_g} [h P_r A + \Delta P_r \pi R_3^2 + h P_a (\pi R_4^2 - A)] \quad (61)$$

The rate of change of mass within the bearing is

$$\dot{M} = \left(\frac{\partial M}{\partial P} \right) \dot{p}' + \left(\frac{\partial M}{\partial h} \right) \dot{h}' \quad (62)$$

Equating (60) to (62) we obtain

$$\left(\frac{\partial Q_{in}}{\partial P} - \frac{\partial Q_{out}}{\partial P} \right) p' + \left(\frac{\partial Q_{in}}{\partial h} - \frac{\partial Q_{out}}{\partial h} \right) h' = \left(\frac{\partial M}{\partial P} \right) \dot{p}' + \left(\frac{\partial M}{\partial h} \right) \dot{h}' \quad (63)$$

From (57)

$$p' = \frac{m \ddot{h}'}{A} \quad (64)$$

$$\dot{p}' = \frac{m \dddot{h}'}{A} \quad (65)$$

Eliminating p' and \dot{p}' from (63) by substitution of (64) and (65) we obtain

$$\ddot{h}' + \frac{\left(\frac{\partial Q_{out}}{\partial P} - \frac{\partial Q_{in}}{\partial P} \right) \ddot{h}'}{\frac{\partial M}{\partial P}} + \frac{\left(\frac{\partial M}{\partial h} \right) \frac{A}{m} \dot{h}'}{\frac{\partial M}{\partial P}} + \frac{\frac{A}{m} \left(\frac{\partial Q_{out}}{\partial h} - \frac{\partial Q_{in}}{\partial h} \right)}{\frac{\partial M}{\partial P}} h' = 0 \quad (66)$$

let

$C_2 = \text{coefficient of } \ddot{h}'$

$C_1 = \text{coefficient of } \dot{h}'$

$C_0 = \text{coefficient of } h'$

Equation (66) thus becomes

$$\ddot{h}' + C_2 \ddot{h}' + C_1 \dot{h}' + C_0 h' = 0 \quad (67)$$

In accordance with Routh's criteria (see Ref. 10) the condition for stability is that all coefficients are positive and that

$$C_2 C_1 > C_0 \quad (68)$$

Substitution of the values of the coefficients leads to the inequality

$$\frac{\frac{\partial M}{\partial P}}{\frac{\partial M}{\partial h}} \Leftarrow \frac{\frac{\partial Q_{out}}{\partial P} - \frac{\partial Q_{in}}{\partial P}}{\frac{\partial Q_{out}}{\partial h} - \frac{\partial Q_{in}}{\partial h}} \quad (69)$$

where

$$\frac{\partial M}{\partial P} = \frac{Ah + h A_o}{R_g T_g} \quad (70)$$

$$\frac{\partial M}{\partial h} = \frac{A (P_{rh} - P_a) + A_p P_a}{R_g T_g} \quad (71)$$

$$\frac{\partial Q_{out}}{\partial P} = \frac{2\pi h^3 P_r}{12\mu R_g T_g \ln(R_4/R_3)} = \frac{2 P_r Q}{(P_r^2 - P_a^2)} \quad (72)$$

$$- \frac{\partial Q_{in}}{\partial P} = \frac{Q \left[\left(\frac{\gamma+1}{\gamma} \right) (P_r/P_s)^{\frac{\gamma-1}{\gamma}} - \frac{2}{\gamma} \right]}{2 P_r \left(1 - (P_r/P_s)^{\frac{\gamma-1}{\gamma}} \right)} \quad (73)$$

$$\text{If } \left(\frac{P_r}{P_s} \right) < (P_r/P_s)_{crit.}, - \frac{\partial Q_{in}}{\partial P} = 0.0 \quad (74)$$

$$\frac{\partial Q_{out}}{\partial h} = 3Q/h \quad (75)$$

$$\frac{\partial Q_{in}}{\partial h} = Q/h \quad (76)$$

In order to solve expeditiously a number of problems with variations in the variables, a computer program was written. A flow chart of the computer program is shown on Figure 30. By applying a given load to the externally pressurized bearing it is possible to determine all the steady-state performance parameters and determine whether the bearing is stable. In lieu of determining whether the inequality (69) was true or false, the ratios were equated and the groove depth at which the instability is initiated was determined.

E. Bi-Directional Pair Steady-State and Stability Analysis

The same general concepts used on the main thrust bearing can be used for analyzing the bi-directional pair used at start-up and shutdown, with some additional complications. The reaction bearing geometry is shown on Figure 28. For purposes of analysis the downstream orifice pressure was considered to exist inside an annulus whose width equals the orifice diameter. A schematic representation of the bi-directional pair is shown on Figure 31. The method of solution is as follows: (subscript 1 refers to the reaction bearing and subscript 2 refers to the main bearing).

Assume a given load is applied to bearing 1; then

$$P_{r1} = \frac{W_1}{A_1} + P_a \quad (77)$$

where

$$A_1 = \pi/2 \left[\frac{R_4^2 - R_3^2}{\ln(R_4/R_3)} - \frac{R_2^2 - R_1^2}{\ln(R_2/R_1)} \right] \quad (78)$$

See Reference (11)

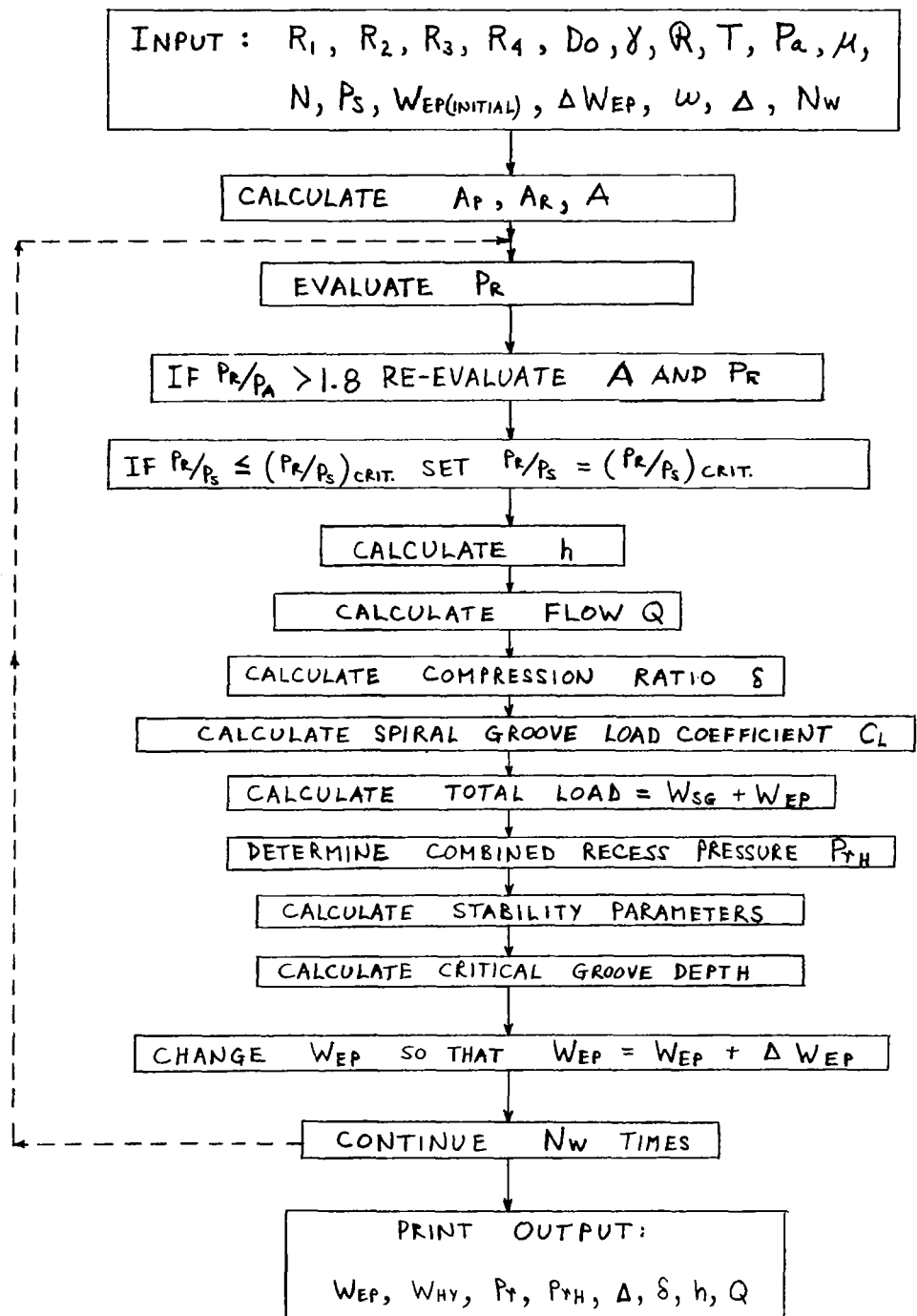


Figure 30 - Flow Chart - Main Hybrid Thrust Bearing

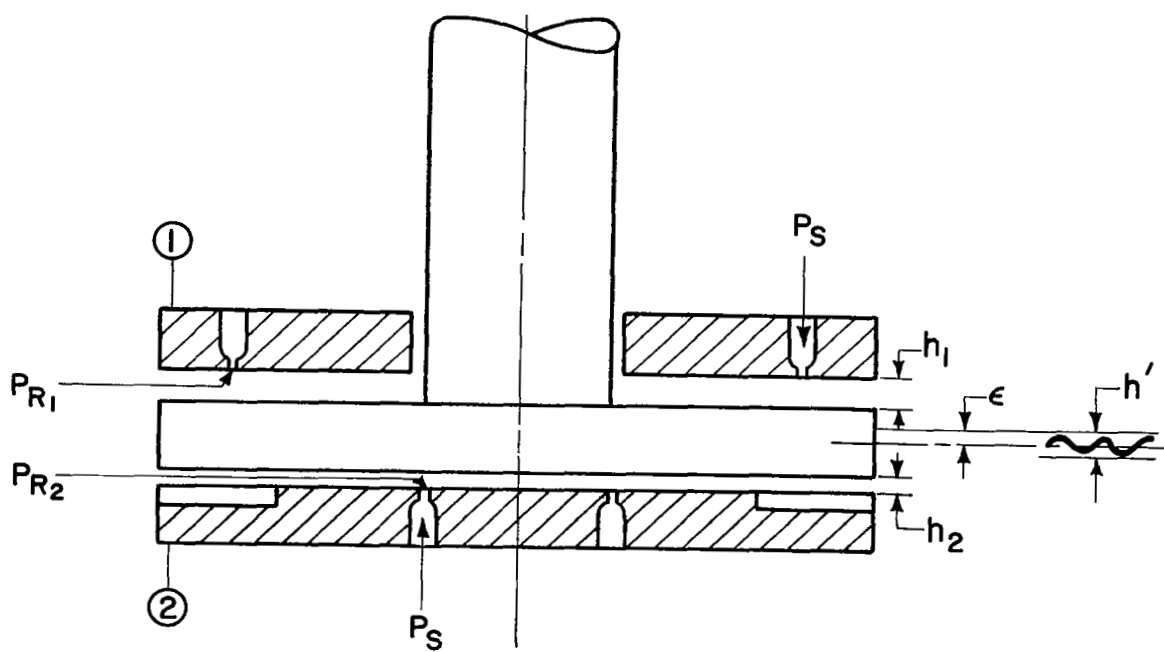


Figure 31 - Bi-Directional Pair - Schematic

for $P_{r1}/P_a < 1.8$ (incompressible pressure distribution)

$$A_1 = \pi \left[R_4^2 - R_1^2 - \frac{(R_2^3 + 2 R_1^3 - 3 R_2 R_1^2)}{3 (R_2 - R_1)} - \frac{(R_3^3 + 2 R_4^3 - 3 R_3 R_4^2)}{3 (R_4 - R_3)} \right] \quad (79)$$

for $P_{r1}/P_a > 1.8$ (linear pressure distribution; derivation similar to that in ref. 2)

The bearing mass flow is given by

$$Q_{B1} = \frac{h_1^3 P_a^2}{R_g T_g} \left[\frac{P_{r1}^2}{P_a^2} - 1 \right] \frac{\pi}{12\mu} \left[\frac{1}{\ln(R_4/R_3)} + \frac{1}{\ln(R_2/R_1)} \right] \quad (80)$$

[from ref. (11) and equation (47)].

This flow is equated to the flow through the orifices in order to determine the reaction bearing clearance. The resulting equation is

$$h_i = \left\{ \frac{12\mu R_g T_g N_{ol} D_{ol} C_D \sqrt{\frac{2\gamma}{(\gamma-1) R_g T_g}} P_s \left\{ \left(\frac{P_{r1}}{P_s} \right)^{2/\gamma} \left[1 - \left(\frac{P_{r1}}{P_s} \right)^{\gamma-1/\gamma} \right] \right\}^{1/2}}{(P_{r1}^2 - P_a^2) \left(\frac{1}{\ln(R_4/R_3)} + \frac{1}{\ln(R_2/R_1)} \right)} \right\}^{\frac{1}{2}}$$

where $P_{r1}/P_s = (P_r/P_s)_{crit}$ for $P_{r1}/P_s < (P_r/P_s)_{crit}$

Once the clearance has been calculated the mass flow is found from the orifice equation. All performance parameters at the particular load in question have now been determined for the reaction bearing (Bearing 1).

The clearance of the main bearing is constrained by the requirement that the total axial clearance must remain constant. Thus

$$h_2 = H_T - h_1 \quad (82)$$

To determine the recess pressure due to the external pressurization of the main bearing we again equate the flows through the orifices to the flow through the bearing.

$$\frac{P_a^2 \pi h_2^3 \left[\frac{P_{r2}^2}{P_a^2} - 1 \right]}{12\mu R_g T_g \ln(R_4/R_3)} = N_{o2} A_{o2} C_D P_s \left\{ \left(\frac{P_{r2}}{P_s} \right)^{2/\gamma} \left[1 - \left(\frac{P_{r2}}{P_s} \right)^{\frac{\gamma-1}{\gamma}} \right] \right\}^{1/2} \quad (83)$$

Determining the recess pressure from this equality requires numerical methods. The particular technique used to solve this equation was the bi-sectional routine as described in Section II of this report dealing with the journal bearing analysis. The roots of the transcendental equation in P_{r2}/P_s lie between 0 and 1. The bi-sectional routine essentially eliminates successive half intervals, concentrating on the particular half interval for which the function at the left and right extremities have opposite signs. After a number of repetitions the root is located to an accuracy dependent upon the number of intervals halved.

If $(P_{r2}/P_s) < (P_r/P_s)_{crit}$ the flow is determined from the orifice equation using $(P_r/P_s)_{crit}$ for (P_{r2}/P_s) . Then the recess pressure must be recalculated to ensure equality of mass flows through the orifices and bearing.

$$P_{r2} = \left\{ P_a^2 + \frac{Q_{o2} R_g T_g 12\mu \ln(R_4/R_3)}{h_2^3 \pi} \right\}^{1/2} \quad (84)$$

$$\text{for } P_{r2}/P_s \leq \left(\frac{P_r}{P_s} \right)_{crit}$$

If $P_{r2}/P_s > (P_r/P_s)_{crit}$ the flow is determined from the orifice equation without change in the recess pressure obtained from the bi-sectional routine.

The total flow of both bearings is

$$Q_T = Q_{o1} + Q_{o2} \quad (85)$$

The load capacity of the main bearing from the external pressurization is

$$W_{EP} = (P_{r2} - P_a) A_2 \quad (86)$$

where the proper equation for A_2 is determined by the ratio P_{r2}/P_a . The hydrodynamic load carrying capacity of the spiral groove bearing is determined in the identical manner as described under the Main Thrust Bearing Analysis. Superimposing hydrostatic and hydrodynamic effects allows the total load W_H on the main bearing to be determined. The net load on the bi-directional pair is the difference in load of the two separate bearings.

$$W_T = W_{EP1} - W_H \quad (87)$$

A negative number indicates that the load is directed toward the main bearing. A positive number indicates that the load is directed toward the reaction bearing.

The procedure for determining stability characteristics is described in Reference 3. The equation of motion for the shaft is

$$m\ddot{h}' = p_1' A_1 - p_2' A_2 \quad (88)$$

From mass continuity the net gas inflow equals the net rate of change of mass inside the clearance regions.

For bearing 1

$$\left(\frac{\partial Q_{in(1)}}{\partial P_{r1}} - \frac{\partial Q_{out(1)}}{\partial P_{r1}} \right) \dot{p}_1' + \left(\frac{\partial Q_{in(1)}}{\partial h_1} - \frac{\partial Q_{out(1)}}{\partial h_1} \right) \dot{h}_1' = \frac{\partial M(1)}{\partial h} \dot{h}_1' + \frac{\partial M(2)}{\partial P_r} \dot{p}_1' \quad (89)$$

For bearing 2

$$\left(\frac{\partial Q_{in(2)}}{\partial P_{r2}} - \frac{\partial Q_{out(2)}}{\partial P_{r2}} \right) \dot{p}_2' + \left(\frac{\partial Q_{in(2)}}{\partial h_2} - \frac{\partial Q_{out(2)}}{\partial h_2} \right) \dot{h}_2' = \frac{\partial M(2)}{\partial h} \dot{h}_2' + \frac{\partial M(2)}{\partial P_r} \dot{p}_2' \quad (90)$$

h_2 can be eliminated by noting that

$$h' = h_1' = -h_2'$$

For the purpose of simplifying the notation the partial derivatives are designated as follows:

$$\begin{aligned} \lambda_1 &= \frac{\partial M}{\partial h} & \lambda_3 &= -\frac{\partial Q_{in}}{\partial P_r} & \lambda_5 &= \frac{\partial Q_{out}}{\partial P_r} \\ \lambda_2 &= \frac{\partial M}{\partial P_r} & \lambda_4 &= \left(\frac{\partial Q_{out}}{\partial h} - \frac{\partial Q_{in}}{\partial h} \right) \end{aligned}$$

inserting these symbols and applying the Laplace transformation to equations (88), (89) and (90) we obtain

$$\bar{h} = \frac{1}{ms^2} (\bar{p}_1 A_1 - \bar{p}_2 A_2) \quad (91)$$

$$-(\lambda_3 + \lambda_5)_1 \bar{p}_1 - (\lambda_4)_1 \bar{h} = (\lambda_1 s)_1 \bar{h} + (\lambda_2 s)_1 \bar{p}_1 \quad (92)$$

$$(\lambda_3 + \lambda_5)_2 \bar{p}_2 + (\lambda_4)_2 \bar{h} = -(\lambda_1 s)_2 \bar{h} + (\lambda_2 s)_1 \bar{p}_2 \quad (93)$$

where the bar symbol denotes the transformed quantity. Substituting (91) into (92) and (93) and rearranging we obtain

$$\left[\frac{ms^2 (\lambda_3 + \lambda_5 + s \lambda_2)_1}{A_1 (\lambda_4 + s \lambda_1)_1} + 1 \right] \bar{p}_1 A_1 - \bar{p}_2 A_2 = 0 \quad (94)$$

$$- \bar{p}_1 A_1 + \left[\frac{ms^2 (\lambda_3 + \lambda_5 + s \lambda_2)_2}{A_1 (\lambda_4 + s \lambda_1)_2} \right] \bar{p}_2 A_2 = 0 \quad (95)$$

In order for a solution to exist the determinant of the coefficients must vanish. Expansion of the determinant yields the characteristic equation whose roots determine the stability threshold.

The characteristic equation is

$$s^4 + \Lambda_3 s^3 + \Lambda_2 s^2 + \Lambda_1 s + \Lambda_0 = 0 \quad (96)$$

where

$$\Lambda_3 = \frac{(\lambda_3 + \lambda_5)_1 (\lambda_2)_2 + (\lambda_2)_1 (\lambda_3 + \lambda_5)_2}{(\lambda_2)_1 (\lambda_2)_2} \quad (97)$$

$$\Lambda_2 = \frac{(\lambda_3 + \lambda_5)_1 (\lambda_3 + \lambda_5)_2 + \frac{A_2}{m} (\lambda_2)_1 (\lambda_1)_2 + \frac{A_1}{m} (\lambda_2)_2 (\lambda_1)_1}{(\lambda_2)_1 (\lambda_2)_2} \quad (98)$$

$$\Lambda_1 = \left\{ \frac{A_2}{m} [(\lambda_3 + \lambda_5)_1 (\lambda_1)_2 + (\lambda_2)_1 (\lambda_4)_2] + \frac{A_1}{m} [(\lambda_3 + \lambda_5)_2 (\lambda_1)_1 + (\lambda_2)_2 (\lambda_4)_1] \right\} \frac{1}{(\lambda_2)_1 (\lambda_2)_2} \quad (99)$$

$$\Lambda_o = \frac{\frac{A_2}{m} (\lambda_3 + \lambda_5)_1 (\lambda_4)_2 + \frac{A_1}{m} (\lambda_3 + \lambda_5)_2 (\lambda_4)_1}{(\lambda_2)_1 (\lambda_2)_2} \quad (100)$$

The stability criteria is (see Reference 3)

(a) All coefficients $\Lambda > 0$

(b) $\Lambda_1 \Lambda_2 \Lambda_3 > \Lambda_1^2 + \Lambda_3^2 \Lambda_o$

It is quite obvious from the development of the governing equations and the methods of solution that hand computation for even a single applied load to a particular geometry is a tedious task. Consequently a digital computer program was developed and utilized for determining performance parameters and stability information. A conceptual flow chart of the program is included herein as Figure 32.

F. Determination of Viscous Friction Losses

Three separate areas contribute to the frictional drag of the thrust bearing. The first is the circular area contained inside R_1 , the second is the annular area containing the spiral grooves, and the last is the annular rim area where the feed orifices are located.

For the ungrooved areas the viscous shear stresses are defined as

$$dF = \mu A \frac{dv}{dh} \quad (101)$$

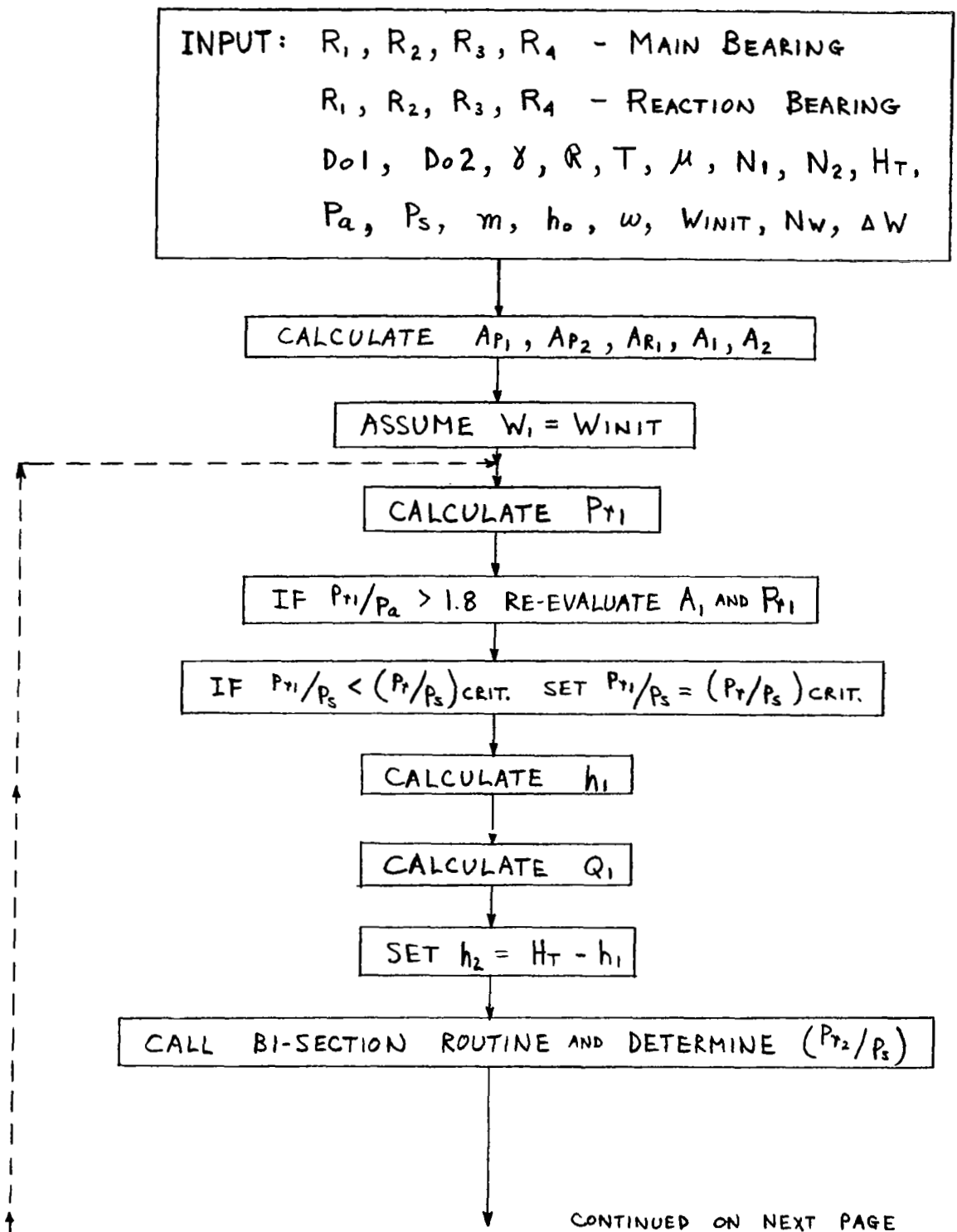


Figure 32 - Flow Chart - Bi-Directional Opposed Thrust Pair

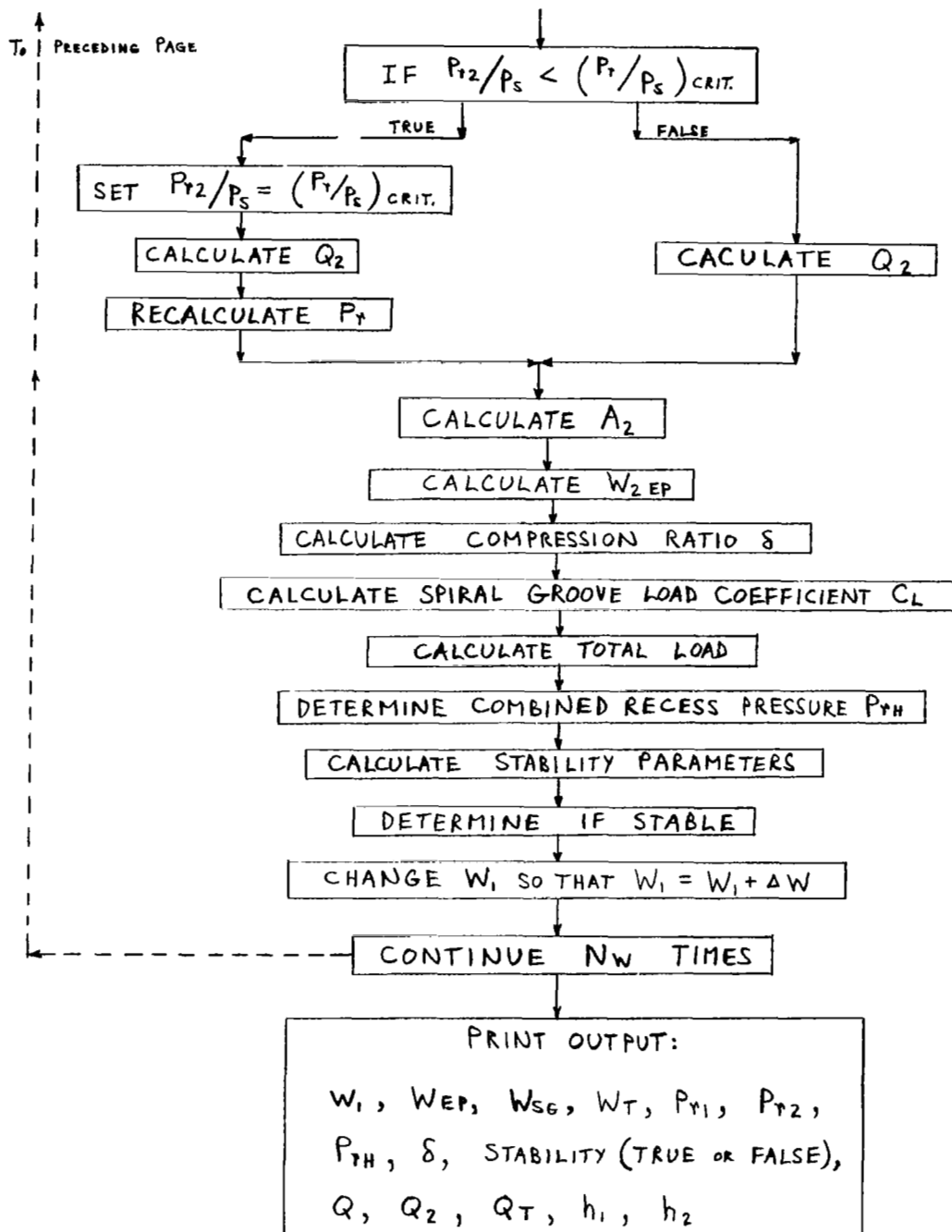


Figure 32A - Flow Chart - Bi-Directional Opposed Thrust Pair

Considering a differential annulus

$$dF = \frac{2\pi\mu\omega r^2}{h} dr \quad (102)$$

The friction moment is thus

$$dT_f = \frac{2\pi\mu\omega r^3}{h} dr \quad (103)$$

Integrating, we obtain the total friction moment

$$T_f = \int_{R_{in}}^{R_{out}} \frac{2\pi\mu\omega r^3}{h} dr = \frac{\pi}{2h} \mu\omega (R_{out}^4 - R_{in}^4) \quad (104)$$

Converting to horsepower we obtain

$$HP = \frac{15\mu\omega^2 (R_{out}^4 - R_{in}^4)}{63,000 h} \quad (105)$$

This equation is applicable to both ungrooved areas of the hybrid bearing.

The friction moment contribution of the spiral groove area can be found by employing the following equation as derived in Reference 1.

$$(T_f)_{SG} = \frac{\pi\mu\omega R_2^4}{2h} (1 - \lambda^4) G_2 \quad (106)$$

G_2 is a function of α , δ and γ related to the geometry of the spiral groove bearings. A curve of G_2 vs clearance is shown on Figure 33.

The friction horsepower contribution is

$$(HP)_{SG} = (T_f)_{SG} N/63,000 \quad (107)$$

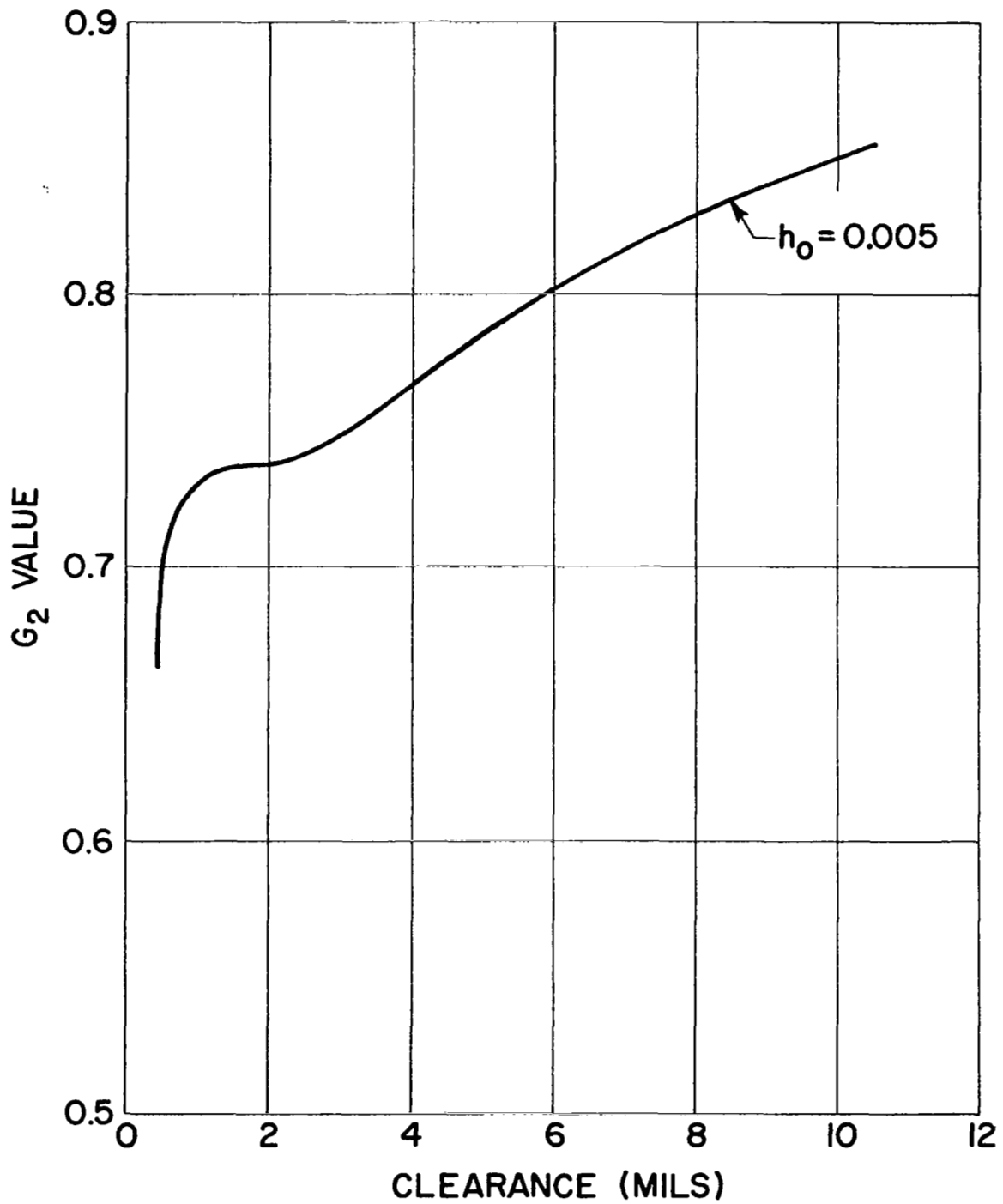


Figure 33 - Friction Factor vs Clearance - Spiral Groove Bearing

The total viscous horsepower is the sum of the horsepowers of the three individual areas.

G. Determination of Bearing Righting Moment Capability

To approximate the righting moment capability of the thrust bearing the orifices were considered as springs and the spring constant determined from the axial stiffness of the externally pressurized bearing. To that an estimate of the hydrodynamic effect was added. This was accomplished by subdividing the bearing into springs located at the mid radius of the hydrodynamic bearing (see Fig. 34). For the externally pressurized bearing

$$K_{EP} = \frac{S_{EP}}{N_o} \quad (108)$$

$$\begin{aligned} K_{TEP} = \frac{M_{xx}}{\psi} \Big|_{EP} &= 4 K_{EP} R_3^2 \left[\sin^2 \theta_1 + \sin^2 \theta_2 + \sin^2 \theta_3 + \sin^2 \theta_4 \right] = \\ &= 3.78 S_{EP} \end{aligned} \quad (109)$$

For the Spiral Groove Bearing

$$\begin{aligned} K_{TSG} = \frac{M_{xx}}{\psi} \Big|_{SG} &= \frac{S_{SG} R_2^2}{8} \left[\sin^2 \theta_1 + \sin^2 \theta_2 + \sin^2 \theta_3 + \sin^2 \theta_4 \right] = \\ &= 0.781 S_{SG} \end{aligned} \quad (110)$$

Total tilting stiffness of fluid film

$$K_T = K_{TEP} + K_{TSG} \quad (111)$$

H. Synchronous Vibrations of Thrust Bearing

Because the rotating collar cannot be aligned exactly perpendicular to the axis of rotation, there will be an angular swashing

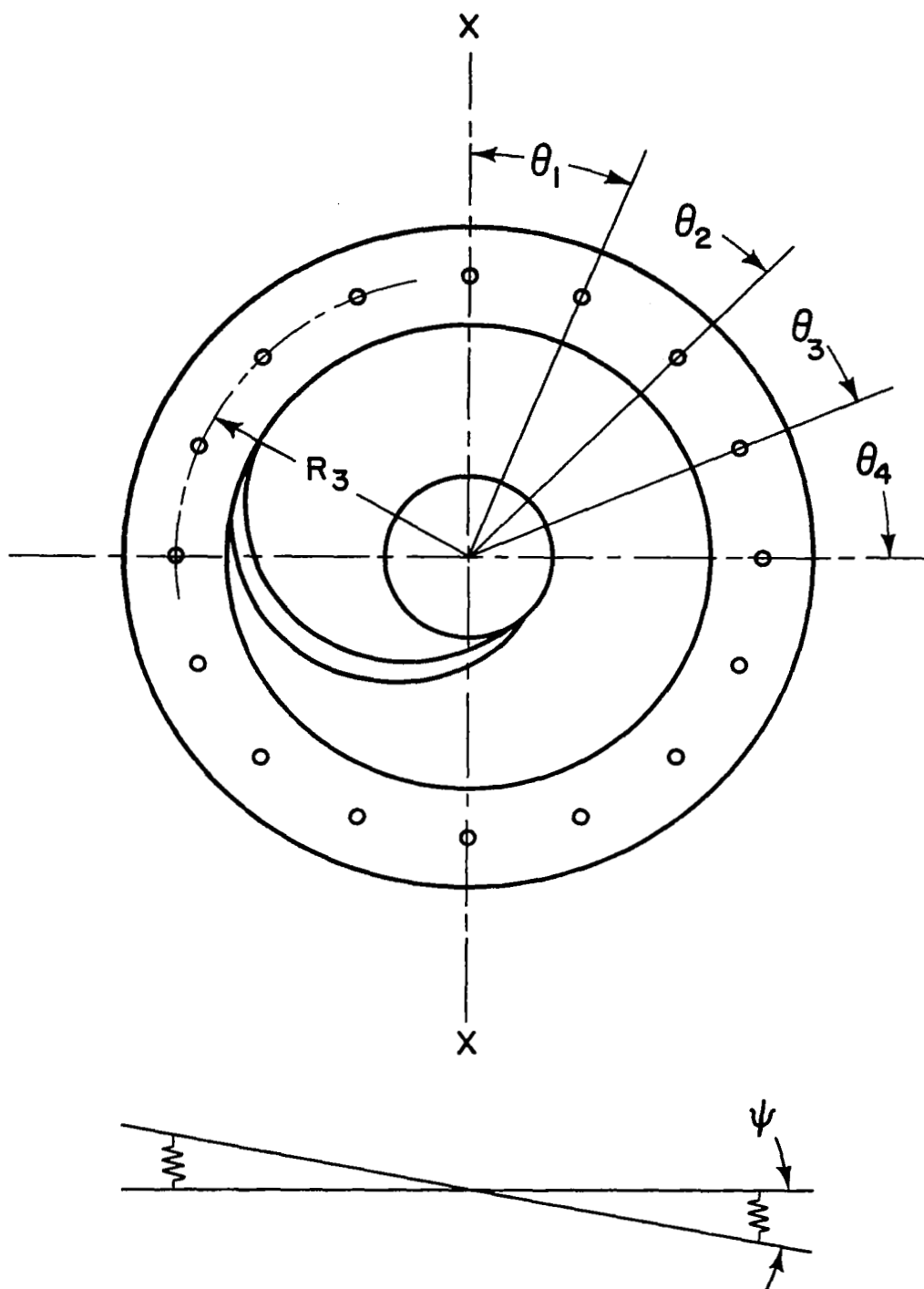


Figure 34 - Restoring Moment - geometric parameters

of the collar as it rotates. This produces a forcing function on the stationary collar and causes it to vibrate. This type of vibration has been analyzed by Whitley and Williams as described in Reference 9, and forms the basis of the analytical description following.

Referring to Figure 35, the rotating plate swashes through an angle $\epsilon_0 \sin \omega t$ in the plane of the paper and $\epsilon_0 \cos \omega t$ in the plane perpendicular to the paper. (ϵ_0 is the total angular swash and ω is the speed of the rotating plate)

$$\epsilon_1 = \epsilon_0 \sin \omega t \text{ (plane of paper)} \quad (112)$$

$$\epsilon_2 = \epsilon_0 \cos \omega t \text{ (plane perpendicular to paper)} \quad (113)$$

Because of this motion the stationary plate will move through angles ξ and ζ according to the equations of motion

$$\left. \begin{aligned} I_T \ddot{\xi} &= -K_T (\xi - \epsilon_0 \sin \omega t) \\ I_T \ddot{\zeta} &= -K_T (\zeta - \epsilon_0 \cos \omega t) \end{aligned} \right\} * \quad (114)$$

$$(115)$$

The steady-state solutions are

$$\xi = \epsilon_0 \frac{\omega_c^2}{\omega_c^2 - \omega^2} \sin \omega t \quad (116)$$

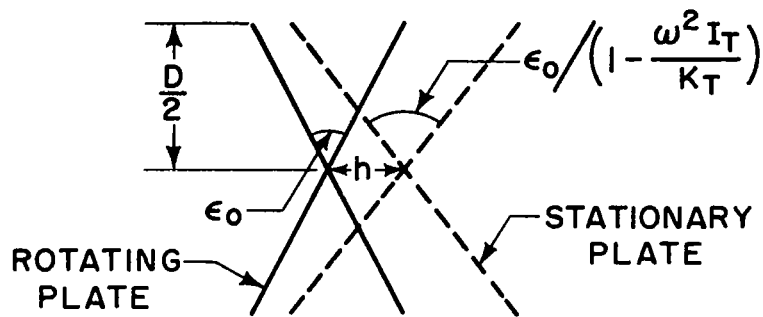
$$\zeta = \epsilon_0 \frac{\omega_c^2}{\omega_c^2 - \omega^2} \cos \omega t \quad (117)$$

for $\omega < \omega_c$ the stationary plate swashes in phase with the rotating plate but through a larger amplitude.

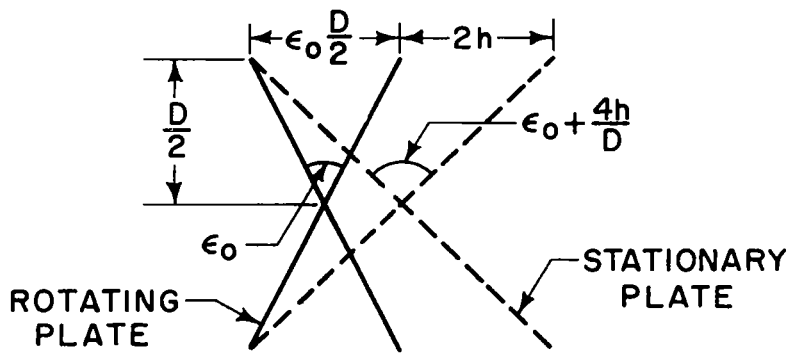
The amplitude of the relative swash ϵ is given by

$$\epsilon = \xi - \epsilon_0 \sin \omega t = \epsilon_0 \sin \omega t \left(\frac{\omega_c^2}{\omega_c^2 - \omega^2} \right) \quad (118)$$

* K_T in equations (114 and (115) include stiffness of the structure.



(a) NORMAL RUNNING



(b) RUBBING

Figure 35 - Synchronous Vibration of Thrust Bearing

therefore the maximum amplitude of the differential swash ϵ between the plates is given by

$$\epsilon_{\max} = \epsilon_o \left(\frac{\omega^2}{\omega_c^2 - \omega^2} \right) \quad (119)$$

From the previous equation the maximum angular displacement of the stationary plate is

$$\xi_{\max} = \frac{\epsilon_o \omega_c^2}{\omega_c^2 - \omega^2} = \frac{\epsilon_o}{1 - \omega^2 I/K_T} \quad (120)$$

At contact conditions the total displacement of the rotating plate equals $\frac{\epsilon_o D}{2}$. The total displacement of the stationary plate is

$2 \frac{\epsilon_o D}{4} + h$. Dividing by $D/2$ gives the total angle at the stationary plate and it equals

$$\xi_{\text{rubbing}} = \epsilon_o + 4h/D \quad (121)$$

This shows that the maximum differential swash that the plates can sustain without rubbing is $4h/D$.

I Thermal Distortion

The analytical model for the thermal distortion problem is shown on Figure 36.

From similar triangles

$$\frac{\Delta L}{a} = \frac{R_4}{R'} \quad (122)$$

but

$$\Delta L = \alpha' R_4 \Delta T \quad (123)$$

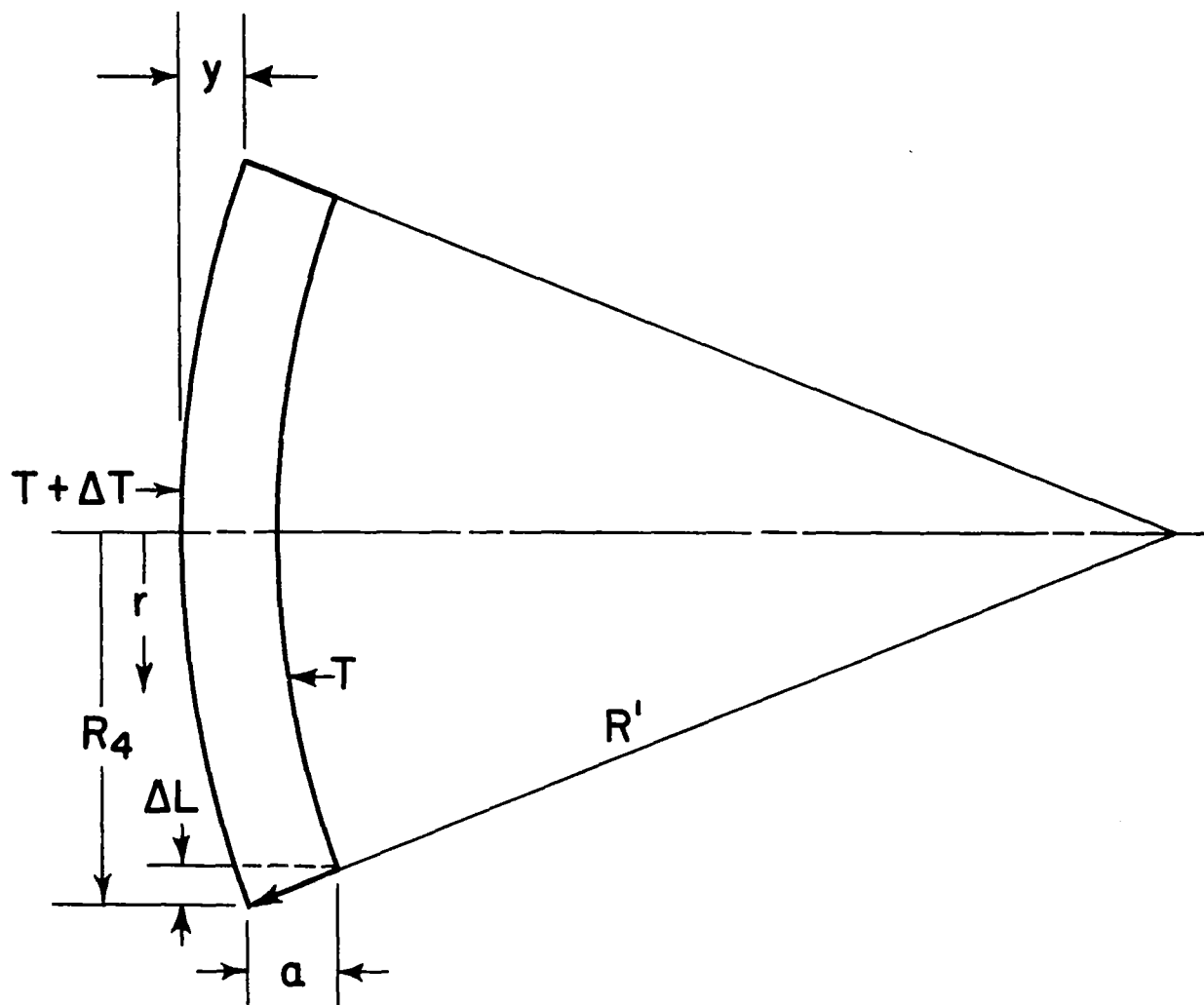


Figure 36 - Thermal Distortion - Analytical Model

and
$$\Delta T = Fa/K \quad (124)$$

Substituting (124) into (123)

$$\Delta L = \alpha' R_4 Fa/K \quad (125)$$

Substituting (125) into (122) we obtain

$$\frac{1}{R'} = \frac{\Delta L}{R_4 a} = \frac{\alpha' F}{K} \quad (126)$$

For small curvatures the reciprocal of the radius of curvature can be approximated by

$$\frac{d^2 y}{dr^2} = \frac{1}{R'} = \frac{\alpha' F}{K} \quad (127)$$

The heat generation F is a result of viscous friction, and is proportional to the square of the radius.

$$F = K_1 r^2 \quad (128)$$

The total power generation is

$$P = \int_0^{R_4} 2\pi F r \, dr = 2\pi K_1 \int_0^{R_4} r^3 \, dr = \frac{\pi K_1 R_4^4}{2} \quad (129)$$

Therefore the constant K_1 is

$$K_1 = \frac{2P}{\pi R_4^4} \quad (130)$$

Substituting into (128) we obtain

$$F = \frac{2Pr^2}{\pi R_4^4} \quad (131)$$

Now going back to (127)

$$\frac{d^2y}{dr^2} = \frac{2\alpha' Pr^2}{K \pi R_4^4} \quad (132)$$

The boundary conditions for this differential equation is

$$\frac{dy}{dr} = 0 \quad \text{at} \quad r = 0 \quad (133)$$

$$y = 0 \quad \text{at} \quad r = 0 \quad (134)$$

The solution of (132) becomes

$$y = \frac{P\alpha r^4}{6K\pi R_4^4} \quad (135)$$

with y_{\max} occurring at $r = R_4$

therefore The ~~Maximum~~ thermal distortion

$$y_{\max} = \frac{P\alpha' R_4^4}{6K\pi} \quad (136)$$

J. Main Thrust Bearing - Analytical Results

The initial consideration in the design of the hybrid bearing was to determine the spiral groove depth that would cause the bearing to operate at a maximum clearance when subjected to a particular load. Two loads pertinent to bearing operation occur at two different operating conditions. The first is with the shaft operating in a vertical attitude and the machine oriented with the turbine end up. The total thrust load on the bearing then consists of both the gravity load and the aerodynamic load, producing a total of 86 pounds. This particular orientation corresponds to the attitude of the package when attached to a launch vehicle ready for liftoff. The second important position of the machinery would be for a zero gravity attitude which pertains to space operation. Then, the only load on the thrust bearing would be to aerodynamic forces which has been specified as a total of 30 pounds. Thus, determination of the optimum spiral groove depths were limited to the 30 and 86 pound cases.

From Figure 29 it is apparent that maximum clearance for any load will occur when the compression ratio, δ , is equal to 0.4 (0.4 is actually to the right of the peak of the load factor optimum. This value was selected however, because it is on the less precipitous side of the peak and variations will not cause as pronounced effects as would be the case if we operated at the peak or on the left side of the peak). The main bearing computer program was run for spiral groove depths varying between 0.005 in. and 0.0095 in. The variation in groove depths with compression ratio, δ , for the two particular loads in question are shown on Figure 37 and 38. The curves shown are for each of two different orifice diameters 0.020 and 0.031 in. The 0.020 orifice size represents what is considered a practical minimum value and the 0.031 size is one that is relatively free of clogging and contamination and is quite practical in all respects provided flow values do not become excessive. The number of orifices is 16 for both cases. There is a possibility that the number of orifices may have to be increased to produce good agreement with the theoretical predictions. It would be desirable to produce a bearing of similar configurations but with 24 orifices of 0.020 in. diameter. Comparative testing would then demonstrate the effect of the orifice spacing. The optimum groove depths are as follows:

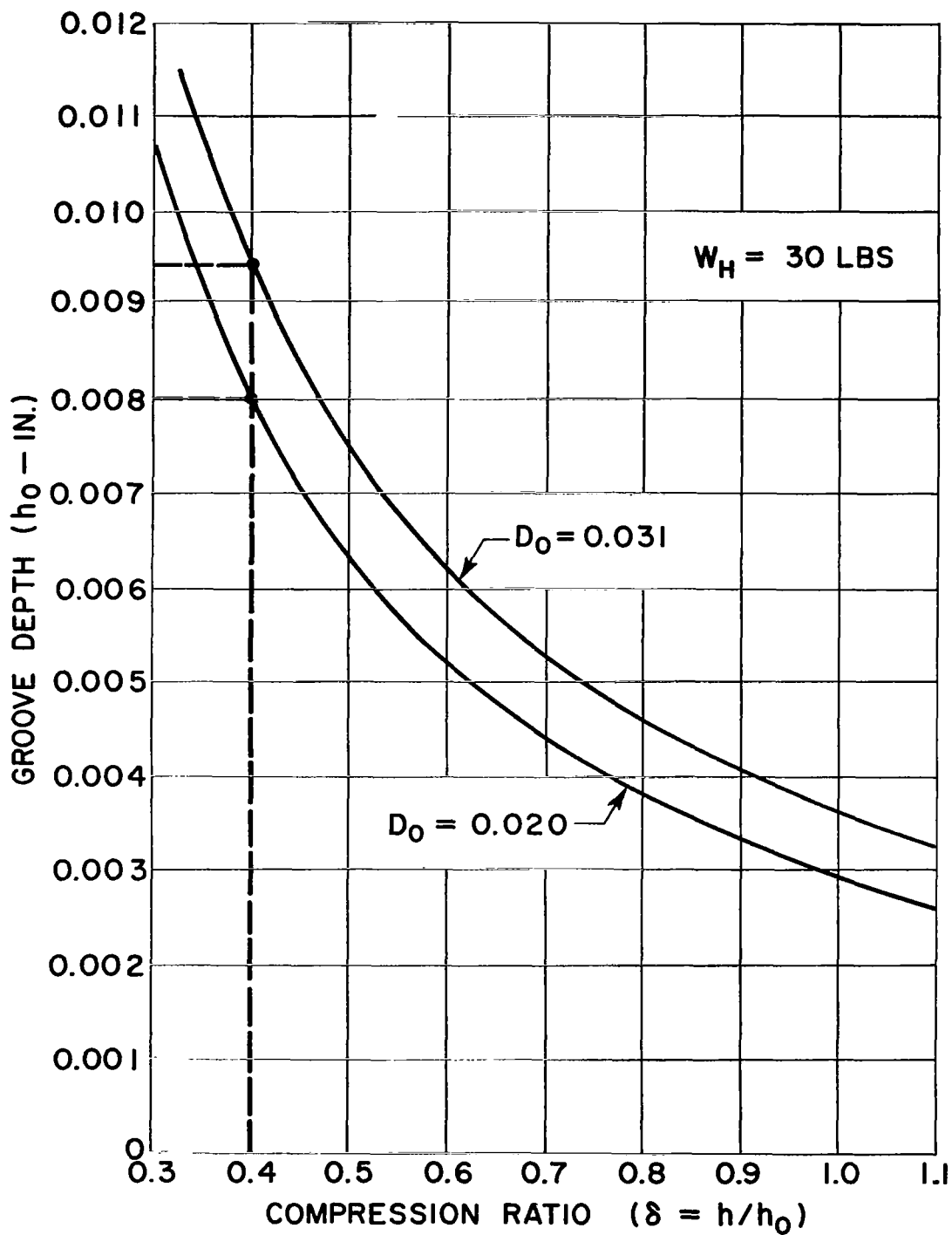


Figure 37 - Groove Depth vs Compression Ratio - $W_H = 30 \text{ lbs.}$

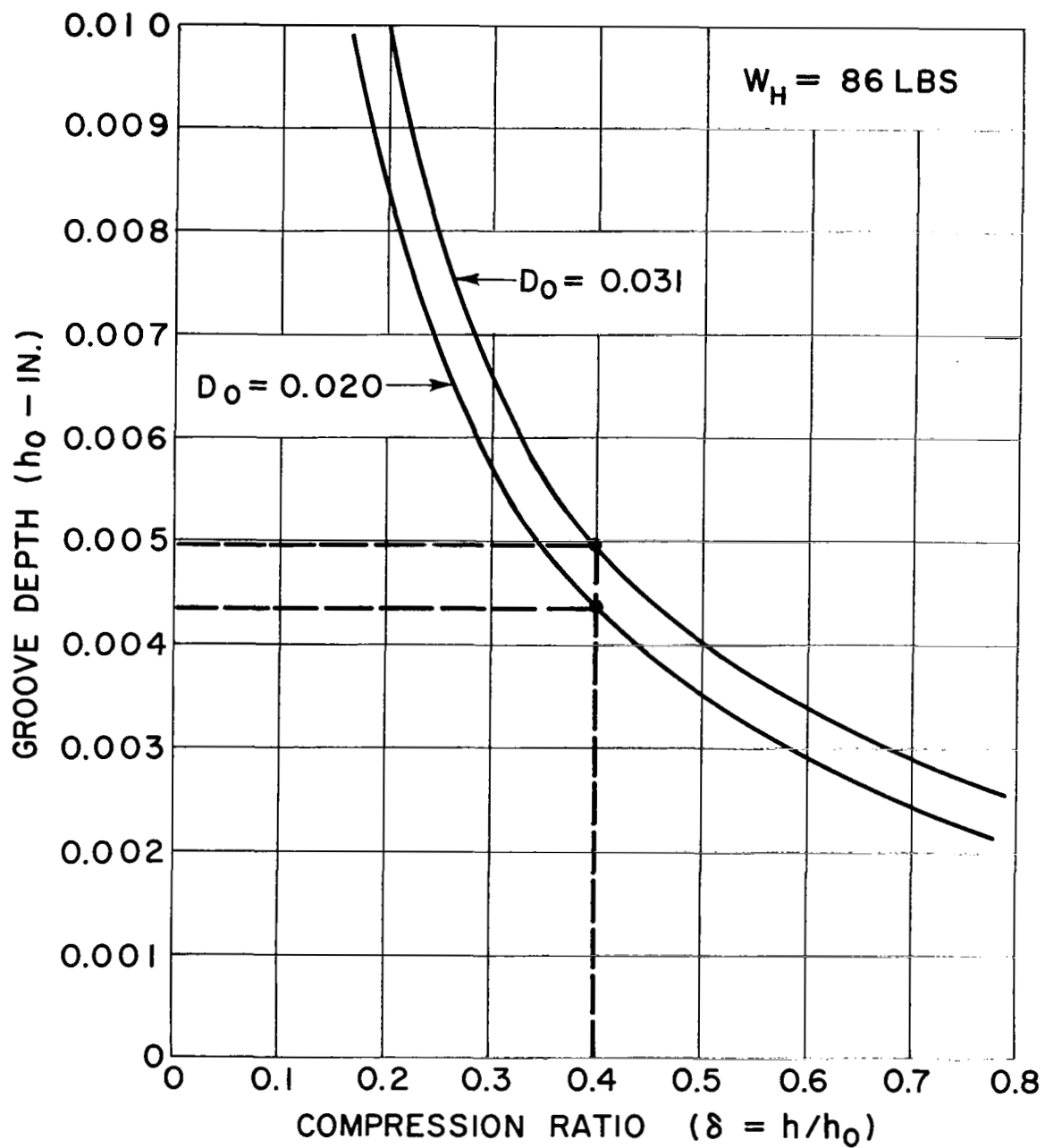


Figure 38 - Groove Depth vs Compression Ratio - $W_H = 86$ lbs.

<u>Load</u> <u>lbs.</u>	<u>Orifice Diameter</u> <u>in.</u>	<u>Optimum Groove Depth</u> <u>in.</u>
30.0	0.020	0.0080
-	0.031	0.0095
86.0	0.020	0.0044
-	0.031	0.005

Once the optimum groove depths were determined the computer program was run for the four orifice-groove depth combinations described above. The outputs for these programs are shown in Figures 39 through 42; the input and nomenclature for these programs are also shown on these Figures. The critical depths of the spiral groove listed in the output represents that depth above which bearing instability would be initiated in the form of pneumatic hammer. The general tendency is for this depth to decrease as the total bearing load increases. If at the maximum operating load of 86 lbs the critical depth is less than the actual spiral groove depth, then the bearing will not operate stably and this particular configuration must then be eliminated from consideration. This criterion eliminated the 0.020 in. orifice diameter 0.008 in. groove depth configuration, and the 0.031 in. orifice diameter 0.0095 in. groove depth configuration. Of the remaining two combinations the 0.031 in. orifice diameter in conjunction with the 0.005 in. spiral groove depth configuration was selected because it provides a significant increase in operating clearance. It does however, require greater flow than the 0.020 in. orifice bearing but the absolute value of flow for both bearings is very small and well within specified limits. It is noted that both acceptable combinations have groove depths optimized for the 86 lb load condition; both groove depths optimized for the 30 lb condition were unstable at the high load condition.

The results of the computer program have been put into a series of plots so that performance can be readily ascertained. Figure 43 displays variation in load capacity of the thrust bearing

HYBRID BEARING SPIRAL GROOVE HYDRODYNAMIC ANNULAR HYDROSTATIC									
I	WEP	WT	PREP	PRHY	CRDEP	DELTA	H	Q	
1	1.00000	1.07522	6.03853	6.04143	3.55267	1.98350	0.01587	0.95309E-05	
2	3.00000	3.37743	6.11560	6.13022	0.67907	1.14124	0.00913	0.54810E-05	
3	5.00000	5.83692	6.19267	6.22492	0.31405	0.88090	0.00705	0.42279E-05	
4	7.00000	8.44244	6.26974	6.32532	0.18890	0.74185	0.00593	0.35575E-05	
5	9.00000	11.87795	6.34681	6.42727	0.12919	0.65187	0.00521	0.31229E-05	
6	11.00000	13.76466	6.42388	6.53041	0.09539	0.58747	0.00470	0.28110E-05	
7	13.00000	16.46793	6.50695	6.63458	0.07413	0.53836	0.00431	0.25726E-05	
8	15.00000	19.19503	6.57802	6.73967	0.05975	0.49927	0.00399	0.23822E-05	
9	17.00000	21.74432	6.65508	6.84561	0.04951	0.46716	0.00374	0.22253E-05	
10	19.00000	24.71477	6.73215	6.95237	0.04191	0.44014	0.00352	0.20927E-05	
11	21.00000	27.53580	6.80922	7.05992	0.03611	0.41698	0.00334	0.19785E-05	
12	23.00000	30.31707	6.88629	7.16825	0.03155	0.39681	0.00317	0.18787E-05	
13	25.00000	33.14850	6.96336	7.27736	0.02791	0.37902	0.00303	0.17902E-05	
14	27.00000	36.00014	7.04043	7.38724	0.02494	0.36317	0.00291	0.17110E-05	
15	29.00000	38.87217	7.11750	7.49791	0.02249	0.34891	0.00279	0.16393E-05	
16	31.00000	41.76488	7.19457	7.60938	0.02045	0.33599	0.00269	0.15740E-05	
17	33.00000	44.67866	7.27163	7.72166	0.01872	0.32420	0.00259	0.15141E-05	
18	35.00000	47.61397	7.34870	7.83477	0.01724	0.31337	0.00251	0.14587E-05	
19	37.00000	50.57133	7.42577	7.94873	0.01597	0.30338	0.00243	0.14073E-05	
20	39.00000	53.22034	7.50284	8.05004	0.01484	0.29411	0.00235	0.13593E-05	
21	41.00000	55.62976	7.57991	8.14366	0.01383	0.28548	0.00228	0.13143E-05	
22	43.00000	58.05552	7.65698	8.23713	0.01295	0.27741	0.00222	0.12719E-05	
23	45.00000	60.47826	7.73405	8.33049	0.01217	0.26943	0.00216	0.12318E-05	
24	47.00000	62.89859	7.81112	8.42376	0.01148	0.26273	0.00210	0.11939E-05	
25	49.00000	65.31737	7.88818	8.51695	0.01087	0.25596	0.00205	0.11578E-05	
26	51.00000	67.73422	7.96525	8.61010	0.01032	0.24958	0.00200	0.11233E-05	
27	53.00000	70.15053	8.04232	8.70321	0.00983	0.24352	0.00195	0.10904E-05	
28	55.00000	72.56647	8.11939	8.79630	0.00939	0.23776	0.00190	0.10589E-05	
29	57.00000	74.98254	8.19646	8.88941	0.00899	0.23225	0.00186	0.10285E-05	
30	59.00000	77.39713	8.27353	8.98253	0.00864	0.22700	0.00182	0.99931E-06	
31	61.00000	79.81670	8.35060	9.07569	0.00832	0.22196	0.00178	0.97114E-06	
32	63.00000	82.23567	8.42767	9.16890	0.00803	0.21712	0.00174	0.94390E-06	
33	65.00000	84.65648	8.50473	9.26218	0.00777	0.21248	0.00170	0.91752E-06	
34	67.00000	87.07755	8.58180	9.35556	0.00753	0.20803	0.00166	0.89194E-06	
35	69.00000	89.55531	8.65887	9.44903	0.00732	0.20368	0.00163	0.86708E-06	
36	71.00000	91.93421	8.73594	9.54263	0.00713	0.19951	0.00160	0.84290E-06	
37	73.00000	94.36670	8.81301	9.63636	0.00696	0.19547	0.00156	0.81934E-06	
38	75.00000	96.80324	8.89038	9.73025	0.00681	0.19156	0.00153	0.79635E-06	
39	77.00000	99.24433	8.96715	9.82432	0.00667	0.18776	0.00150	0.77390E-06	
40	79.00000	101.69045	9.04422	9.91858	0.00655	0.18407	0.00147	0.75193E-06	
41	81.00000	104.14215	9.12128	10.01305	0.00645	0.18047	0.00144	0.73042E-06	
42	83.00000	106.59999	9.19835	10.10776	0.00636	0.17697	0.00142	0.70933E-06	
43	85.00000	109.06456	9.27542	10.20273	0.00628	0.17355	0.00139	0.68864E-06	
44	87.00000	111.53649	9.35249	10.29799	0.00621	0.17022	0.00136	0.66830E-06	
45	89.00000	114.01648	9.42956	10.39355	0.00616	0.16695	0.00134	0.64830E-06	
46	91.00000	116.50524	9.50663	10.48946	0.00612	0.16375	0.00131	0.62861E-06	
47	93.00000	119.03359	9.58370	10.58573	0.00609	0.16061	0.00128	0.60921E-06	
48	95.00000	121.51239	9.66077	10.68243	0.00606	0.15753	0.00126	0.59007E-06	
49	97.00000	124.03259	9.73783	10.77952	0.00607	0.15453	0.00124	0.57117E-06	
50	99.00000	126.56523	9.81490	10.87711	0.00608	0.15151	0.00121	0.55249E-06	
51	101.00000	129.11147	9.89197	10.97523	0.00610	0.14857	0.00119	0.53402E-06	
52	103.00000	131.67258	9.96904	11.07392	0.00613	0.14566	0.00117	0.51573E-06	
53	105.00000	134.25001	10.04611	11.17324	0.00617	0.14279	0.00114	0.49761E-06	
54	107.00000	136.84536	10.12319	11.27325	0.00623	0.13994	0.00112	0.47964E-06	
55	109.00000	139.46043	10.20025	11.37402	0.00630	0.13711	0.00110	0.46180E-06	
56	111.00000	142.09730	10.27732	11.47563	0.00639	0.13433	0.00107	0.44407E-06	
57	113.00000	144.75831	10.35438	11.57817	0.00650	0.13151	0.00105	0.42643E-06	
58	115.00000	147.44618	10.43145	11.68175	0.00662	0.12872	0.00103	0.40888E-06	
59	117.00000	150.16495	10.50852	11.78648	0.00676	0.12594	0.00101	0.39138E-06	
60	119.00000	152.91558	10.58559	11.89251	0.00693	0.12314	0.00099	0.37393E-06	

INPUTD₀ = ORIFICE DIAMETER = .020 inR = GAS CONSTANT = 179045 in²/sec²

γ = SPECIFIC HEAT RATIO = 1.668

T = ABSOLUTE TEMPERATURE = 760°R

μ = VISCOSITY = 4.3 × 10⁻⁹ lb-sec²/inP_s = SUPPLY PRESSURE = 12 PSIAP_a = AMBIENT PRESSURE = 6 PSIA

W = SHAFT SPEED = 1256 RAD/SEC

h₀ = GROOVE DEPTH = .008NOMENCLATURE FOR OUTPUT

WEP = EXTERNALLY PRESSURIZED BEARING

LOAD CAPACITY - LBS

WT = HYBRID BEARING LOAD CAPACITY - LBS

PREP = PRESSURE IMMEDIATELY DOWNSTREAM

OF ORIFICES (RECESS PRESSURE) PSIA

PRHY = EQUIVALENT HYBRID BEARING

RECESS PRESSURE - PSIA

CRDEP = CRITICAL DEPTH OF SPIRAL

GROOVE - IN

DELTA = COMPRESSION RATIO (RATIO OF
OPERATING CLEARANCE TO
GROOVE DEPTH)

H = OPERATING CLEARANCE - IN

Q = MASS FLOW - $\frac{\text{lbs-sec}}{\text{in.}}$ Figure 39 - Program Output - Hybrid Thrust Bearing D₀ = .020, h₀ = .008

HYBRID BEARING SPIRAL GROOVE HYDRODYNAMIC ANNULAR HYDROSTATIC									
I	WEP	WT	PREP	PRHY	CRDEP	DELTA	H	Q	
1	1.00000	1.05027	6.03853	6.04047	3.55014	3.60636	0.01587	0.95309E-05	
2	3.00000	3.21070	6.11560	6.12372	0.67838	2.07497	0.00913	0.54810E-05	
3	5.00000	5.49719	6.19267	6.21183	0.31340	1.60164	0.00705	0.42279E-05	
4	7.00000	7.80919	6.26974	6.30092	0.18817	1.34881	0.00593	0.35575E-05	
5	9.00000	10.13857	6.34681	6.39068	0.12844	1.18523	0.00521	0.31229E-05	
6	11.00000	12.48178	6.42388	6.48098	0.09464	1.06812	0.00470	0.28110E-05	
7	13.00000	14.88986	6.50095	6.57377	0.07340	0.97884	0.00431	0.25726E-05	
8	15.00000	17.49347	6.57802	6.67410	0.05912	0.90777	0.00399	0.23822E-05	
9	17.00000	20.12575	6.65508	6.77553	0.04894	0.84939	0.00374	0.22253E-05	
10	19.00000	22.78457	6.73215	6.87799	0.04140	0.80026	0.00352	0.20927E-05	
11	21.00000	25.46835	6.80922	6.98141	0.03564	0.75814	0.00334	0.19785E-05	
12	23.00000	28.17605	6.88629	7.08575	0.03113	0.72146	0.00317	0.18787E-05	
13	25.00000	30.90701	6.96336	7.19098	0.02751	0.68913	0.00303	0.17902E-05	
14	27.00000	33.66081	7.04043	7.29710	0.02457	0.66031	0.00291	0.17110E-05	
15	29.00000	36.43727	7.11750	7.40409	0.02215	0.63439	0.00279	0.16393E-05	
16	31.00000	39.23634	7.19457	7.51195	0.02012	0.61089	0.00269	0.15740E-05	
17	33.00000	42.05816	7.27163	7.62068	0.01840	0.58946	0.00259	0.15141E-05	
18	35.00000	44.90294	7.34870	7.73031	0.01694	0.56977	0.00251	0.14587E-05	
19	37.00000	47.77100	7.42577	7.84083	0.01569	0.55160	0.00243	0.14073E-05	
20	39.00000	50.66279	7.50284	7.95226	0.01460	0.53475	0.00235	0.13593E-05	
21	41.00000	53.57882	7.57991	8.06463	0.01365	0.51906	0.00228	0.13143E-05	
22	43.00000	56.51967	7.65698	8.17795	0.01282	0.50438	0.00222	0.12719E-05	
23	45.00000	59.48602	7.73405	8.29226	0.01209	0.49060	0.00216	0.12318E-05	
24	47.00000	62.47864	7.81112	8.40758	0.01145	0.47763	0.00210	0.11939E-05	
25	49.00000	65.49835	7.88818	8.52394	0.01088	0.46538	0.00205	0.11578E-05	
26	51.00000	68.54608	7.96525	8.64138	0.01037	0.45378	0.00200	0.11233E-05	
27	53.00000	71.62283	8.04232	8.75994	0.00992	0.44277	0.00195	0.10904E-05	
28	55.00000	74.72970	8.11939	8.87966	0.00952	0.43228	0.00190	0.10589E-05	
29	57.00000	77.86786	8.19646	9.00059	0.00916	0.42228	0.00186	0.10285E-05	
30	59.00000	81.03861	8.27353	9.12277	0.00884	0.41272	0.00182	0.99931E-06	
31	61.00000	84.24333	8.35060	9.24626	0.00855	0.40356	0.00178	0.97114E-06	
32	63.00000	87.48353	8.42767	9.37112	0.00829	0.39477	0.00174	0.94390E-06	
33	65.00000	90.76586	8.50473	9.49741	0.00806	0.38632	0.00170	0.91752E-06	
34	67.00000	94.07705	8.58180	9.62520	0.00786	0.37818	0.00166	0.89194E-06	
35	69.00000	97.43404	8.65887	9.75456	0.00768	0.37033	0.00163	0.86708E-06	
36	71.00000	100.83390	8.73594	9.88557	0.00752	0.36274	0.00160	0.84290E-06	
37	73.00000	104.27887	8.81301	10.01832	0.00738	0.35540	0.00156	0.81934E-06	
38	75.00000	107.77141	8.89008	10.15290	0.00726	0.34828	0.00153	0.79635E-06	
39	77.00000	111.31418	8.96715	10.28942	0.00715	0.34138	0.00150	0.77390E-06	
40	79.00000	114.91008	9.04422	10.42799	0.00706	0.33466	0.00147	0.75193E-06	
41	81.00000	118.56230	9.12128	10.56872	0.00699	0.32813	0.00144	0.73042E-06	
42	83.00000	122.27429	9.19835	10.71176	0.00693	0.32177	0.00142	0.70933E-06	
43	85.00000	126.04988	9.27542	10.85725	0.00689	0.31555	0.00139	0.68864E-06	
44	87.00000	129.89326	9.35249	11.00536	0.00686	0.30948	0.00136	0.66830E-06	
45	89.00000	133.80905	9.42956	11.15625	0.00684	0.30355	0.00134	0.64830E-06	
46	91.00000	137.79317	9.50663	11.29359	0.00682	0.29773	0.00131	0.62861E-06	
47	93.00000	141.84726	9.58370	11.40557	0.00679	0.29202	0.00128	0.60921E-06	
48	95.00000	145.96435	9.66077	11.51829	0.00678	0.28642	0.00126	0.59007E-06	
49	97.00000	146.15316	9.73783	11.63181	0.00678	0.28091	0.00124	0.57117E-06	
50	99.00000	149.11860	9.81490	11.74619	0.00679	0.27548	0.00121	0.55249E-06	
51	101.00000	152.11176	9.89197	11.86153	0.00681	0.27013	0.00119	0.53402E-06	
52	103.00000	155.13197	9.96904	11.97791	0.00685	0.26484	0.00117	0.51573E-06	
53	105.00000	158.18184	10.04611	12.09544	0.00690	0.25961	0.00114	0.49761E-06	
54	107.00000	161.26429	10.12318	12.21422	0.00696	0.25443	0.00112	0.47964E-06	
55	109.00000	164.38260	10.20025	12.33438	0.00705	0.24930	0.00110	0.46180E-06	
56	111.00000	167.54055	10.27732	12.45607	0.00715	0.24419	0.00107	0.44407E-06	
57	113.00000	170.74239	10.35438	12.57945	0.00726	0.23911	0.00105	0.42643E-06	
58	115.00000	173.99305	10.43145	12.70471	0.00740	0.23404	0.00103	0.40888E-06	
59	117.00000	177.29327	10.50852	12.83208	0.00756	0.22897	0.00101	0.39138E-06	
60	119.00000	180.64669	10.58559	12.96180	0.00775	0.22390	0.00099	0.37393E-06	

INPUT

D_o = ORIFICE DIAMETER = 0.020 INCH
 R = GAS CONSTANT = 179045 IN²/SEC²
 γ = SPECIFIC HEAT RATIO = 1.668
 T = ABSOLUTE TEMPERATURE = 760°R
 μ = VISCOSITY = 4.3 x 10⁻⁹ LB-SEC²/IN
 P_s = SUPPLY PRESSURE = 12 PSIA
 P_a = AMBIENT PRESSURE = 6 PSIA
 W = SHAFT SPEED = 1256 RAD/SEC
 h_o = GROOVE DEPTH = 0.0044

NOMENCLATURE FOR OUTPUT

WEP = EXTERNALLY PRESSURIZED BEARING
 LOAD CAPACITY - LBS.
 WT = HYBRID BEARING LOAD CAPACITY - LBS.
 PREP = PRESSURE IMMEDIATELY DOWNSTREAM
 OF ORIFICES (RECESS PRESSURE) - PSIA
 PRHY = EQUIVALENT HYBRID BEARING
 RECESS PRESSURE - PSIA
 CRDEP = CRITICAL DEPTH OF SPIRAL
 GROOVE - INCHES
 DELTA = COMPRESSION RATIO (RATIO OF
 OPERATING CLEARANCE TO
 GROOVE DEPTH)
 H = OPERATING CLEARANCE - INCHES
 Q = MASS FLOW - $\frac{\text{lbs-sec}}{\text{in.}}$

Figure 40 - Program Output - Hybrid Thrust Bearing $D_o = .031$, $h_o = .0095$

HYBRID BEARING SPIRAL GROOVE HYDRODYNAMIC ANNULAR HYDROSTATIC									
I	WEP	WT	PREP	PRHY	CRDEP	DELTA	H	Q	
1	1.000000	3.11281	6.03853	6.33978	4.41943	3.95107	0.01976	0.18392E-04	
2	3.000000	3.11281	6.11560	6.11995	3.84478	2.27332	0.31137	0.10577E-04	
3	5.000000	5.29081	6.19267	6.20388	3.38770	1.75475	0.00877	0.81586E-05	
4	7.000000	7.48648	6.26974	6.28849	0.23381	1.47775	0.00739	0.68650E-05	
5	9.000000	9.69408	6.34681	6.37356	0.15947	1.29852	0.00649	0.60263E-05	
6	11.000000	11.91106	6.42388	6.45899	0.11741	1.17022	0.00585	0.54246E-05	
7	13.000000	14.13609	6.50095	6.54473	0.09096	1.07241	0.00536	0.49645E-05	
8	15.000000	16.37545	6.57802	6.63102	0.07308	0.99454	0.00497	0.45971E-05	
9	17.000000	18.76738	6.65508	6.72319	0.06041	0.93058	0.00465	0.42942E-05	
10	19.000000	21.17713	6.73215	6.81605	0.05102	0.87676	0.00438	0.40384E-05	
11	21.000000	23.67358	6.80922	6.90955	0.04384	0.83061	0.00415	0.38181E-05	
12	23.000000	26.24597	6.88629	7.00367	0.03822	0.79043	0.00395	0.36254E-05	
13	25.000000	28.89378	6.96336	7.09838	0.03372	0.75500	0.00377	0.34547E-05	
14	27.000000	30.97670	7.04043	7.19367	0.03006	0.72342	0.00362	0.33017E-05	
15	29.000000	33.46454	7.11750	7.28954	0.02704	0.69503	0.00348	0.31635E-05	
16	31.000000	35.96724	7.19457	7.38598	0.02452	0.66927	0.00335	0.30374E-05	
17	33.000000	38.48484	7.27163	7.48299	0.02238	0.64580	0.00323	0.29218E-05	
18	35.000000	41.01745	7.34870	7.58058	0.02056	0.62424	0.00312	0.28149E-05	
19	37.000000	43.56528	7.42577	7.67876	0.01900	0.60433	0.00302	0.27157E-05	
20	39.000000	46.12851	7.50284	7.77753	0.01764	0.58587	0.00293	0.26230E-05	
21	41.000000	48.70752	7.57991	7.87691	0.01646	0.56867	0.00284	0.25362E-05	
22	43.000000	51.30265	7.65698	7.97692	0.01543	0.55259	0.00276	0.24544E-05	
23	45.000000	53.91432	7.73405	8.07755	0.01452	0.53750	0.00269	0.23771E-05	
24	47.000000	56.54300	7.81112	8.17885	0.01371	0.52329	0.00262	0.23039E-05	
25	49.000000	59.18922	7.88818	8.28082	0.01300	0.50987	0.00255	0.22342E-05	
26	51.000000	61.85354	7.96525	8.38349	0.01237	0.49716	0.00249	0.21678E-05	
27	53.000000	64.53661	8.04232	8.48688	0.01180	0.48507	0.00243	0.21042E-05	
28	55.000000	67.23122	8.11939	8.59102	0.01129	0.47360	0.00237	0.20433E-05	
29	57.000000	69.94182	8.19646	8.69594	0.01084	0.46265	0.00231	0.19848E-05	
30	59.000000	72.66553	8.27353	8.80166	0.01044	0.45217	0.00226	0.19284E-05	
31	61.000000	75.40113	8.35060	8.90823	0.01007	0.44214	0.00221	0.18740E-05	
32	63.000000	78.25958	8.42767	9.01568	0.00975	0.43251	0.00216	0.18215E-05	
33	65.000000	81.14073	8.50473	9.12406	0.00946	0.42325	0.00212	0.17706E-05	
34	67.000000	83.92729	8.58180	9.23339	0.00920	0.41433	0.00207	0.17212E-05	
35	69.000000	86.72290	8.65887	9.34374	0.00896	0.40573	0.00203	0.16732E-05	
36	71.000000	89.64007	8.73594	9.45515	0.00876	0.39741	0.00199	0.16266E-05	
37	73.000000	92.58426	8.81301	9.56768	0.00857	0.38937	0.00195	0.15811E-05	
38	75.000000	95.55532	8.89028	9.68138	0.00841	0.38157	0.00191	0.15368E-05	
39	77.000000	98.54806	8.96715	9.79633	0.00827	0.37401	0.00187	0.14934E-05	
40	79.000000	101.55324	9.04422	9.91260	0.00815	0.36665	0.00183	0.14510E-05	
41	81.000000	104.58859	9.12128	10.03026	0.00805	0.35950	0.00180	0.14095E-05	
42	83.000000	107.66034	9.19835	10.14937	0.00796	0.35252	0.00176	0.13688E-05	
43	85.000000	110.81293	9.27542	10.27011	0.00790	0.34572	0.00173	0.13289E-05	
44	87.000000	113.98904	9.35249	10.39250	0.00784	0.33907	0.00170	0.12896E-05	
45	89.000000	117.21165	9.42956	10.51668	0.00781	0.33256	0.00166	0.12510E-05	
46	91.000000	120.48403	9.50663	10.64278	0.00779	0.32619	0.00163	0.12131E-05	
47	93.000000	123.80981	9.58370	10.77093	0.00778	0.31994	0.00160	0.11756E-05	
48	95.000000	127.19303	9.66077	10.90130	0.00779	0.31383	0.00157	0.11387E-05	
49	97.000000	130.63821	9.73783	11.03406	0.00782	0.30780	0.00154	0.11022E-05	
50	99.000000	134.14345	9.81490	11.16940	0.00786	0.30181	0.00151	0.10662E-05	
51	101.000000	137.71248	9.89197	11.28412	0.00790	0.29595	0.00148	0.10305E-05	
52	103.000000	139.84860	9.96904	11.38898	0.00794	0.29016	0.00145	0.99523E-06	
53	105.000000	142.59068	10.04611	11.49464	0.00800	0.28443	0.00142	0.96026E-06	
54	107.000000	145.35579	10.12318	11.60119	0.00808	0.27876	0.00139	0.92558E-06	
55	109.000000	148.14626	10.20025	11.70872	0.00817	0.27313	0.00137	0.89114E-06	
56	111.000000	150.96472	10.27732	11.81733	0.00828	0.26753	0.00134	0.85693E-06	
57	113.000000	153.81423	10.35438	11.92714	0.00842	0.26196	0.00131	0.82290E-06	
58	115.000000	156.69824	10.43145	12.03827	0.00858	0.25641	0.00128	0.78903E-06	
59	117.000000	159.62081	10.50852	12.15089	0.00877	0.25086	0.00125	0.75527E-06	
60	119.000000	162.58664	10.58559	12.26517	0.00898	0.24533	0.00123	0.72159E-06	

INPUT

D_o = ORIFICE DIAMETER = 0.031 INCH
 R = GAS CONSTANT = 179045 IN²/SEC²
 γ = SPECIFIC HEAT RATIO = 1.668
 T = ABSOLUTE TEMPERATURE = 760°R.
 μ = VISCOSITY = 4.3×10^{-9} LB·SEC²/IN.
 P_s = SUPPLY PRESSURE = 12 PSIA
 P_a = AMBIENT PRESSURE = 6 PSIA
 ω = SHAFT SPEED = 1256 RAD/SEC
 h_o = GROOVE DEPTH = 0.005

NOMENCLATURE FOR OUTPUT

WEP = EXTERNALLY PRESSURIZED BEARING
 LOAD CAPACITY - LBS.
 WT = HYBRID BEARING LOAD CAPACITY - LBS.
 PREP = PRESSURE IMMEDIATELY DOWNSTREAM
 OF ORIFICES (RECESS PRESSURE) - PSIA
 PRHY = EQUIVALENT HYBRID BEARING
 RECESS PRESSURE - PSIA
 CRDEP = CRITICAL DEPTH OF SPIRAL
 GROOVE - INCHES
 DELTA = COMPRESSION RATIO (RATIO
 OF OPERATING CLEARANCE TO
 GROOVE DEPTH
 H = OPERATING CLEARANCE - INCHES
 Q = MASS FLOW - $\frac{\text{lbs-sec}}{\text{in.}}$

Figure 41 - Program Output - Hybrid Thrust Bearing $D_o = .020$, $h_o = .0044$

HYBRID BEARING SPIRAL GROOVE HYDRODYNAMIC ANNULAR HYDROSTATIC										
	WEP	WT	PREP	PRHY	CRDEP	DELTA	H	Q		
1	1.00000	1.04482	6.03853	6.04026	4.41975	2.07952	0.01976	0.18392E-04		
2	3.00000	3.23835	6.11560	6.12479	0.84472	1.19649	0.01137	0.10577E-04		
3	5.00000	5.50313	6.19267	6.21206	0.39020	0.92355	0.00877	0.81586E-05		
4	7.00000	7.88689	6.26974	6.30392	0.23438	0.77776	0.00739	0.68650E-05		
5	9.00000	10.29731	6.34681	6.39680	0.16006	0.68343	0.00649	0.60263E-05		
6	11.00000	12.72844	6.42388	6.49048	0.11801	0.61591	0.00585	0.54246E-05		
7	13.00000	15.17713	6.50095	6.58484	0.09155	0.56443	0.00536	0.49645E-05		
8	15.00000	17.64151	6.57802	6.67980	0.07367	0.52344	0.00497	0.45971E-05		
9	17.00000	20.12746	6.65508	6.77533	0.06093	0.48978	0.00465	0.42942E-05		
10	19.00000	22.61327	6.73215	6.87137	0.05149	0.46145	0.00438	0.40384E-05		
11	21.00000	25.11951	6.80922	6.96796	0.04427	0.43716	0.00415	0.38181E-05		
12	23.00000	27.63896	6.88629	7.06505	0.03862	0.41602	0.00395	0.36254E-05		
13	25.00000	30.17153	6.96336	7.16264	0.03409	0.39737	0.00377	0.34547E-05		
14	27.00000	32.71724	7.04043	7.26074	0.03041	0.38075	0.00362	0.33017E-05		
15	29.00000	35.27619	7.11750	7.35935	0.02736	0.36580	0.00348	0.31635E-05		
16	31.00000	37.84856	7.19457	7.45847	0.02482	0.35226	0.00335	0.30374E-05		
17	33.00000	40.43459	7.27163	7.55812	0.02267	0.33990	0.00323	0.29218E-05		
18	35.00000	43.03455	7.34870	7.65831	0.02084	0.32855	0.00312	0.28149E-05		
19	37.00000	45.64879	7.42577	7.75905	0.01926	0.31807	0.00302	0.27157E-05		
20	39.00000	48.27779	7.50284	7.86035	0.01789	0.30835	0.00293	0.26230E-05		
21	41.00000	50.92555	7.57991	7.96123	0.01670	0.29930	0.00284	0.25362E-05		
22	43.00000	53.58348	7.65698	8.06439	0.01562	0.29084	0.00276	0.24544E-05		
23	45.00000	56.25492	7.73405	8.16748	0.01467	0.28289	0.00269	0.23771E-05		
24	47.00000	58.93973	7.81112	8.27250	0.01382	0.27542	0.00262	0.23039E-05		
25	49.00000	61.63679	7.88818	8.37348	0.01307	0.26835	0.00255	0.22342E-05		
26	51.00000	64.34589	7.96525	8.47042	0.01240	0.26166	0.00249	0.21678E-05		
27	53.00000	67.06634	8.04232	8.56334	0.01181	0.25531	0.00243	0.21042E-05		
28	55.00000	69.79818	8.11939	8.65166	0.01127	0.24927	0.00237	0.20433E-05		
29	57.00000	72.54130	8.19646	8.73509	0.01079	0.24350	0.00231	0.19848E-05		
30	59.00000	75.29508	8.27353	8.81304	0.01035	0.23799	0.00226	0.19284E-05		
31	61.00000	78.05922	8.35060	8.89610	0.00996	0.23270	0.00221	0.18740E-05		
32	63.00000	80.83379	8.42767	8.97903	0.00961	0.22764	0.00216	0.18215E-05		
33	65.00000	83.61855	8.50473	9.06177	0.00929	0.22276	0.00212	0.17706E-05		
34	67.00000	86.41341	8.58180	9.14517	0.00900	0.21807	0.00207	0.17212E-05		
35	69.00000	89.21836	8.65887	9.22933	0.00874	0.21354	0.00203	0.16732E-05		
36	71.00000	92.03341	8.73594	9.31418	0.00851	0.20917	0.00199	0.16266E-05		
37	73.00000	94.85846	8.81301	9.39962	0.00830	0.20493	0.00195	0.15811E-05		
38	75.00000	97.69351	8.89008	9.48573	0.00812	0.20083	0.00191	0.15368E-05		
39	77.00000	100.53856	8.96715	9.57249	0.00795	0.19685	0.00187	0.14934E-05		
40	79.00000	103.39361	9.04422	9.66080	0.00781	0.19298	0.00183	0.14510E-05		
41	81.00000	106.25866	9.12128	9.74947	0.00768	0.18921	0.00180	0.14095E-05		
42	83.00000	109.13371	9.19835	9.83834	0.00757	0.18554	0.00176	0.13688E-05		
43	85.00000	112.01876	9.27542	9.92749	0.00747	0.18196	0.00173	0.13289E-05		
44	87.00000	114.91381	9.35249	10.01680	0.00739	0.17846	0.00170	0.12896E-05		
45	89.00000	117.81886	9.42956	10.10630	0.00733	0.17503	0.00166	0.12510E-05		
46	91.00000	120.73391	9.50663	10.19601	0.00728	0.17168	0.00163	0.12131E-05		
47	93.00000	123.65896	9.58370	10.28592	0.00724	0.16839	0.00160	0.11756E-05		
48	95.00000	126.59401	9.66077	10.37603	0.00722	0.16516	0.00157	0.11387E-05		
49	97.00000	129.53906	9.73783	10.46634	0.00721	0.16198	0.00154	0.11022E-05		
50	99.00000	132.49411	9.81490	10.55685	0.00722	0.15885	0.00151	0.10662E-05		
51	101.00000	135.45916	9.89197	10.64756	0.00724	0.15576	0.00148	0.10305E-05		
52	103.00000	138.43421	9.96904	10.73847	0.00728	0.15271	0.00145	0.99523E-06		
53	105.00000	141.41926	10.04611	10.82958	0.00733	0.14970	0.00142	0.96026E-06		
54	107.00000	144.41431	10.12318	10.92089	0.00740	0.14671	0.00139	0.92558E-06		
55	109.00000	147.41936	10.20025	11.01240	0.00748	0.14375	0.00137	0.89114E-06		
56	111.00000	150.43441	10.27732	11.10411	0.00759	0.14081	0.00134	0.85693E-06		
57	113.00000	153.45946	10.35439	11.19602	0.00771	0.13788	0.00131	0.82290E-06		
58	115.00000	156.48451	10.43146	11.28813	0.00786	0.13495	0.00128	0.78903E-06		
59	117.00000	159.50956	10.50853	11.38044	0.00803	0.13203	0.00125	0.75527E-06		
60	119.00000	162.53461	10.58559	11.47295	0.00822	0.12911	0.00123	0.72159E-06		

00441 LINES OUTPUT.

INPUT

D_o = ORIFICE DIAMETER = 0.031 INCH.
 R = GAS CONSTANT = 179045 IN²/SEC²
 γ = SPECIFIC HEAT RATIO = 1.668
 T = ABSOLUTE TEMPERATURE = 760°R
 μ = VISCOSITY = 4.3 × 10⁻⁹ LB-SEC²/IN.
 P_s = SUPPLY PRESSURE = 12 PSIA
 P_a = AMBIENT PRESSURE = 6 PSIA
 ω = SHAFT SPEED = 1256 RAD/SEC
 h_o = GROOVE DEPTH = 0.0095

NOMENCLATURE FOR OUTPUT

WEP = EXTERNALLY PRESSURIZED BEARING
 LOAD CAPACITY - LBS
 WT = HYBRID BEARING LOAD CAPACITY - LBS.
 PREP = PRESSURE IMMEDIATELY DOWNSTREAM
 OF ORIFICES (RECESS PRESSURE) - PSIA.
 PRHY = EQUIVALENT HYBRID BEARING
 RECESS PRESSURE - PSIA
 CRDEP = CRITICAL DEPTH OF SPIRAL
 GROOVE - INCHES
 DELTA = COMPRESSION RATIO (RATIO
 OF OPERATING CLEARANCE
 TO GROOVE DEPTH
 H = OPERATING CLEARANCE - INCHES
 Q = MASS FLOW - $\frac{\text{lb-sec}}{\text{in.}}$

Figure 42 - Program Output - Hybrid Thrust Bearing $D_o = .031$, $h_o = .005$

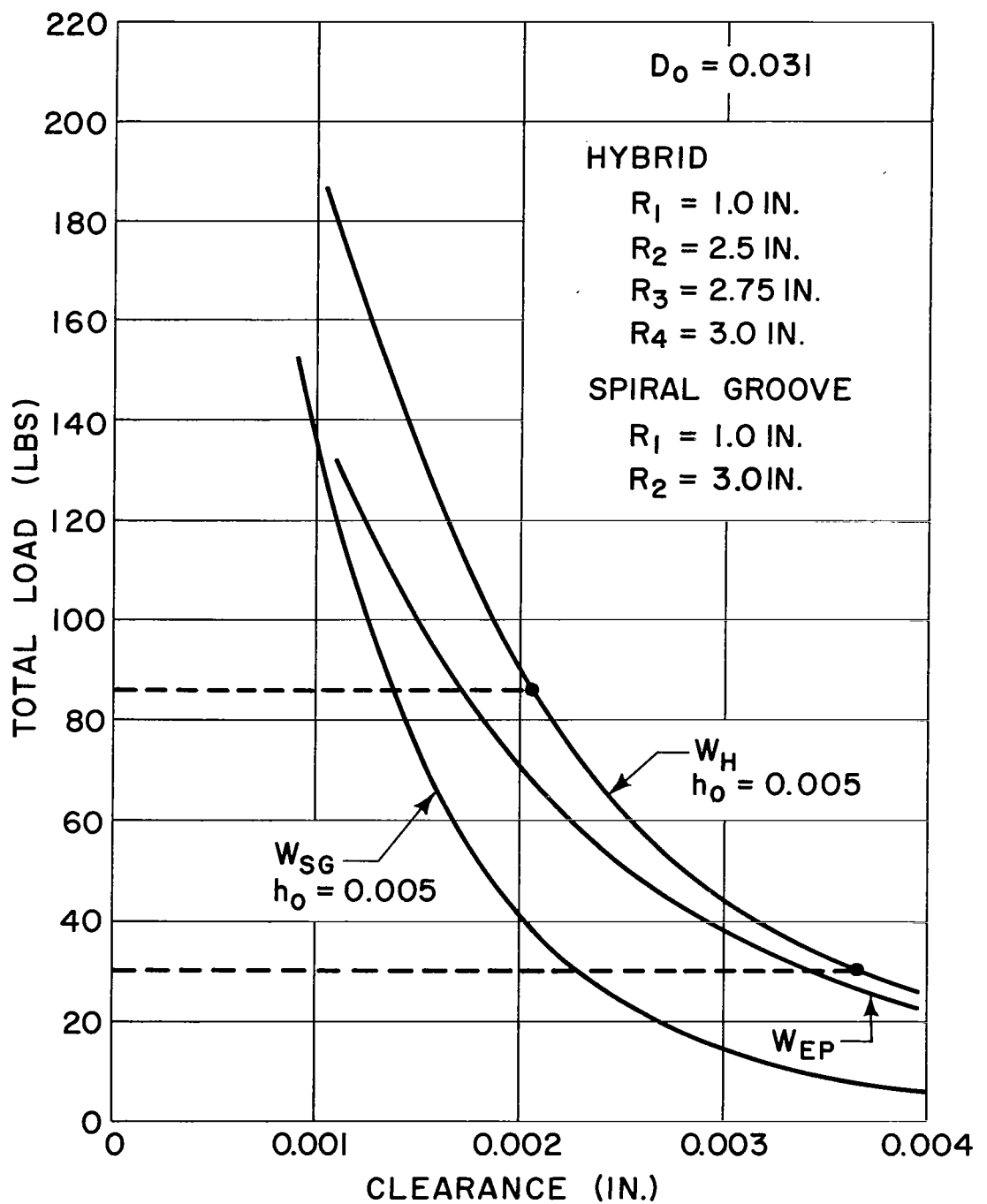


Figure 43 - Load vs Clearance - Hybrid Thrust Bearing ($R_2 = 3.0 \text{ in}$ for W_{SG} curve)

versus clearance. In addition to showing this variation for the hybrid bearing the load-versus-clearance relationship is also indicated for a purely hydrostatic bearing and also for a bearing operating without hydrostatic action or a purely hydrodynamic bearing. The curve labeled W_{EP} indicates the performance for the pure externally pressurized bearing and the curve labeled W_{SG} shows the relationship for the hydrodynamic or spiral groove bearing. The particular spiral groove bearing curve relates to a bearing that would replace the hybrid bearing and thus the outside radius of the spiral bearing corresponds to the outside radius of the hybrid bearing. It is evident that external pressurization adds considerably to the load capacity of the bearing.

On Figure 44 the same curves are displayed, only in this case the spiral groove curve pertains to a bearing geometry whose outside radius would be the same as the outside radius of the spiral groove portion of the hybrid bearing. The curves on this plot then display the contribution of the separate effects of hydrodynamic and hydrostatic action. It is again obvious that external pressurization plays a considerable role in enhancing the load capacity of a hybrid bearing. The value of the slope of the load deflection curve is equivalent to bearing axial stiffness. As described in the analytical section, the tilting (or torsional) stiffness can be derived as a specific combination of the axial stiffness of the separate externally pressurized and hydrodynamic bearings. Bearing stiffnesses are shown on Figure 45, where stiffness is plotted against clearance. Perhaps the most important consideration with regard to axial stiffness is what effect it has on the natural frequency of the rotor bearing system. This frequency has been calculated to vary between 3000 and 6750 rpm within the load limits of 30 and 90 lbs., respectively. These frequencies are safely below the bearing operating rpm and during transient operation should be traversed without difficulty. The major requirements of the tilting stiffness is that it be large enough to overcome the tilting resistance of the bearing alignment structure that has been designed to produce a resistance of approximately 20,000 in.-lb/rad. As can be seen from the graph the tilting

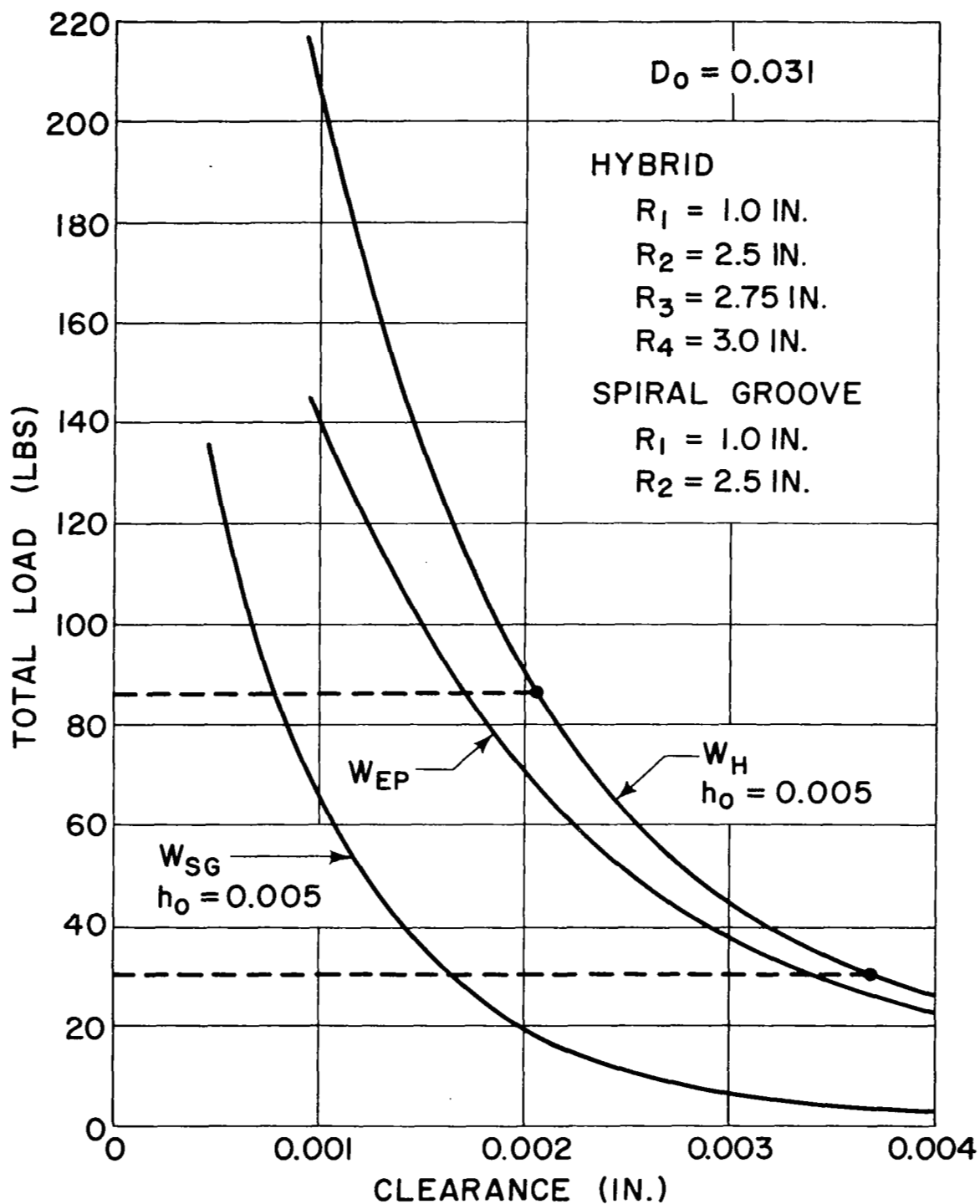


Figure 44 - Load vs Clearance - Hybrid Thrust Bearing ($R_2 = 2.5 \text{ in}$ for W_{SG} curve)

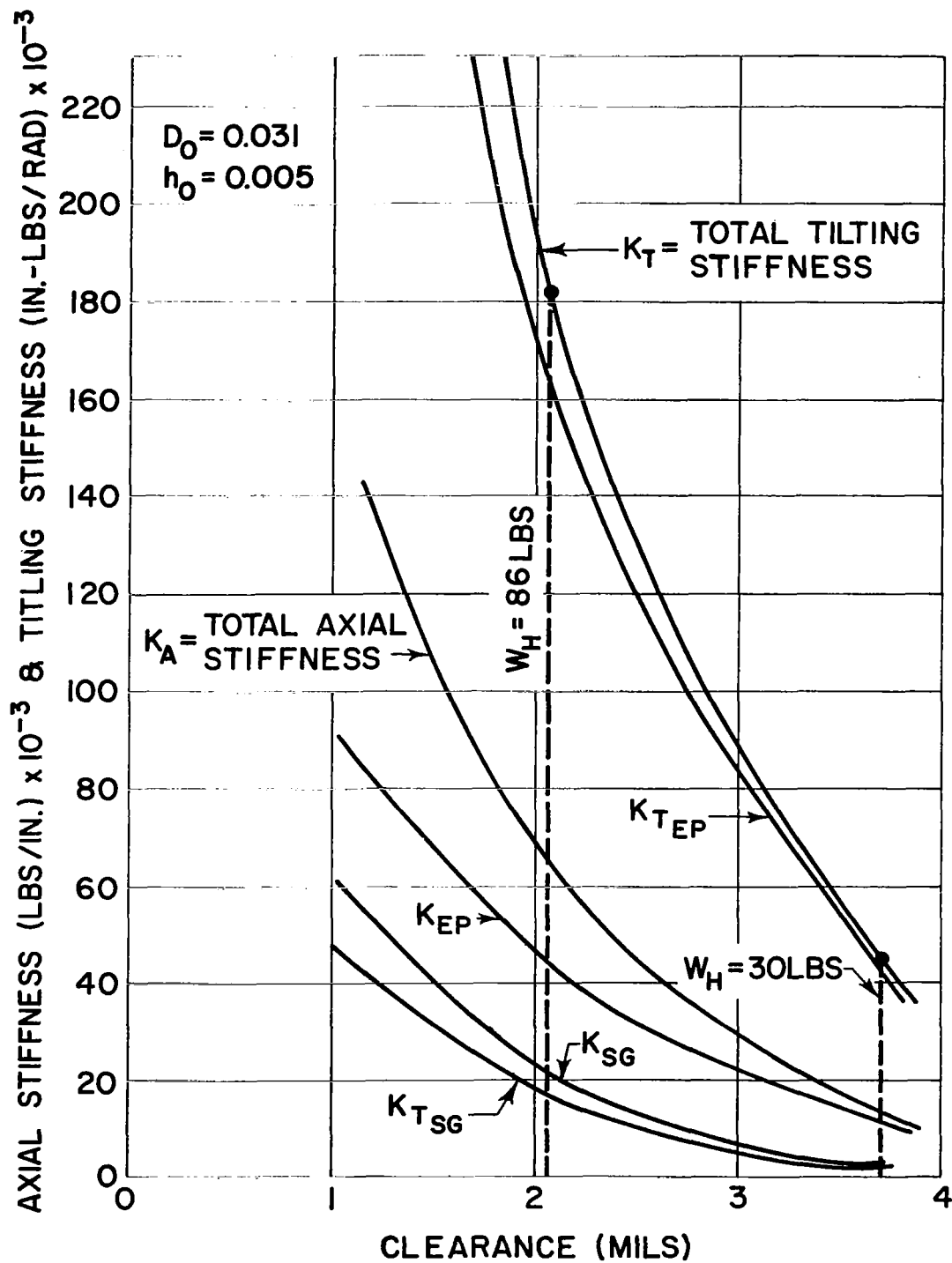


Figure 45 - Stiffness vs Clearance - Hybrid Thrust Bearing

stiffness of the bearing is quite adequate and provides sufficient margin over that of the aligning structure. It should be noted that even though the theoretical results indicate that safe operation is probable, experience indicates that care should be exercised during the actual installation of the thrust bearing assembly to ensure that excessive misaligning torques are not accidentally introduced.

The flow requirements of the bearing are shown on Figure 46. This graph shows the flow requirements of both the bearing with 0.031 in. orifice diameter and a bearing with a 0.020 in. orifice diameter. Although the 0.031 in. orifice diameter requires considerably more flow than a 0.020 in. orifice diameter, the absolute magnitudes of each are very small in relation to the specification limitations. The desirability of maintaining clearances as great as possible dictates the use of the 0.031 in. diameter orifice size.

Calculations of the viscous friction horsepower were completed in the manner described in the analytical section. Results are plotted on Figure 47. The curve indicates a very desirable level of friction dissipation, well within the limits of the specifications. The curve shows two plots. One is with the hybrid bearing configuration and the other represents a purely hydrostatic bearing, without any recesses or grooves (inherently compensated). Thus, the grooving not only increases load capacity or operating clearances but also provides a bearing which produces less viscous dissipation than would be provided by an alternate bearing that generates load capacity only by external pressurization.

In the interest of completeness load-vs-clearance and stiffness-vs-clearance curves are included for the 0.020 in. orifice diameter and the 0.0044 in. groove depth bearing (optimized for 86 lb load) on Figure 48 and 49, respectively.

As a matter of interest, we have obtained from a separate computer program, developed for other studies, a curve of critical recess depth versus load for a hydrostatic bearing that is orifice compensated.

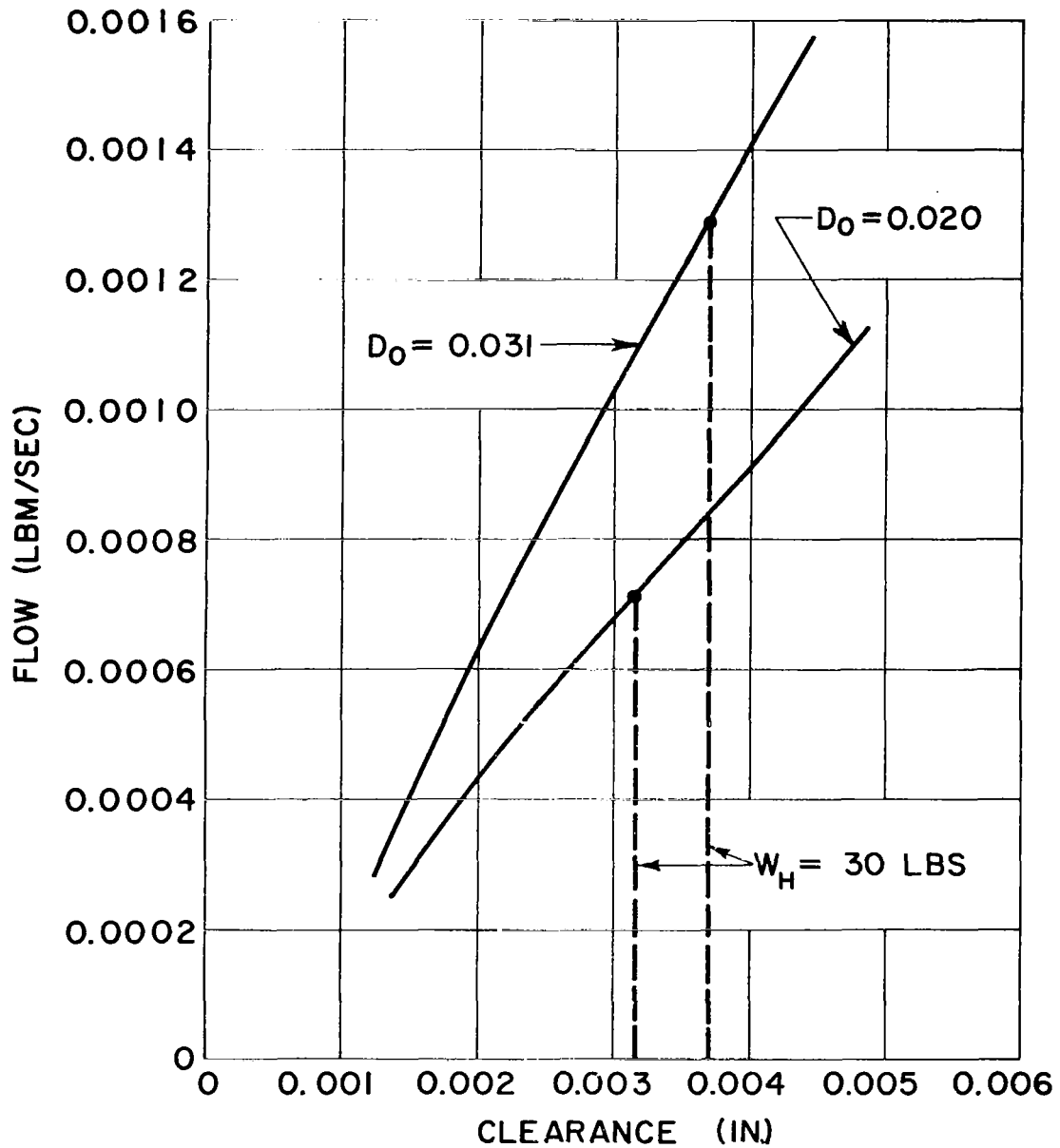


Figure 46 - Flow vs Clearance - Hybrid Thrust Bearing

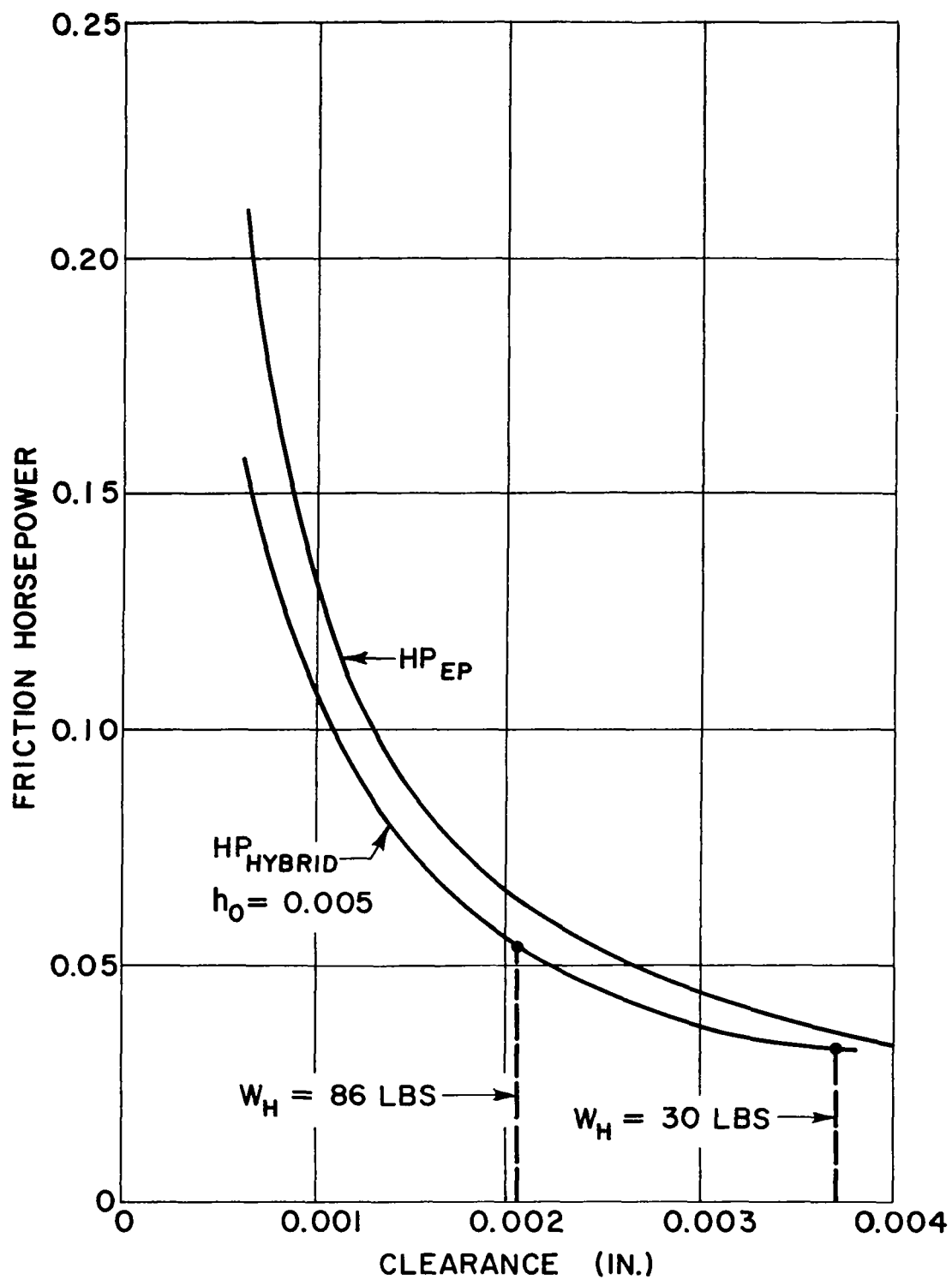


Figure 47 - Friction Horsepower vs Clearance - Hybrid Thrust Bearing

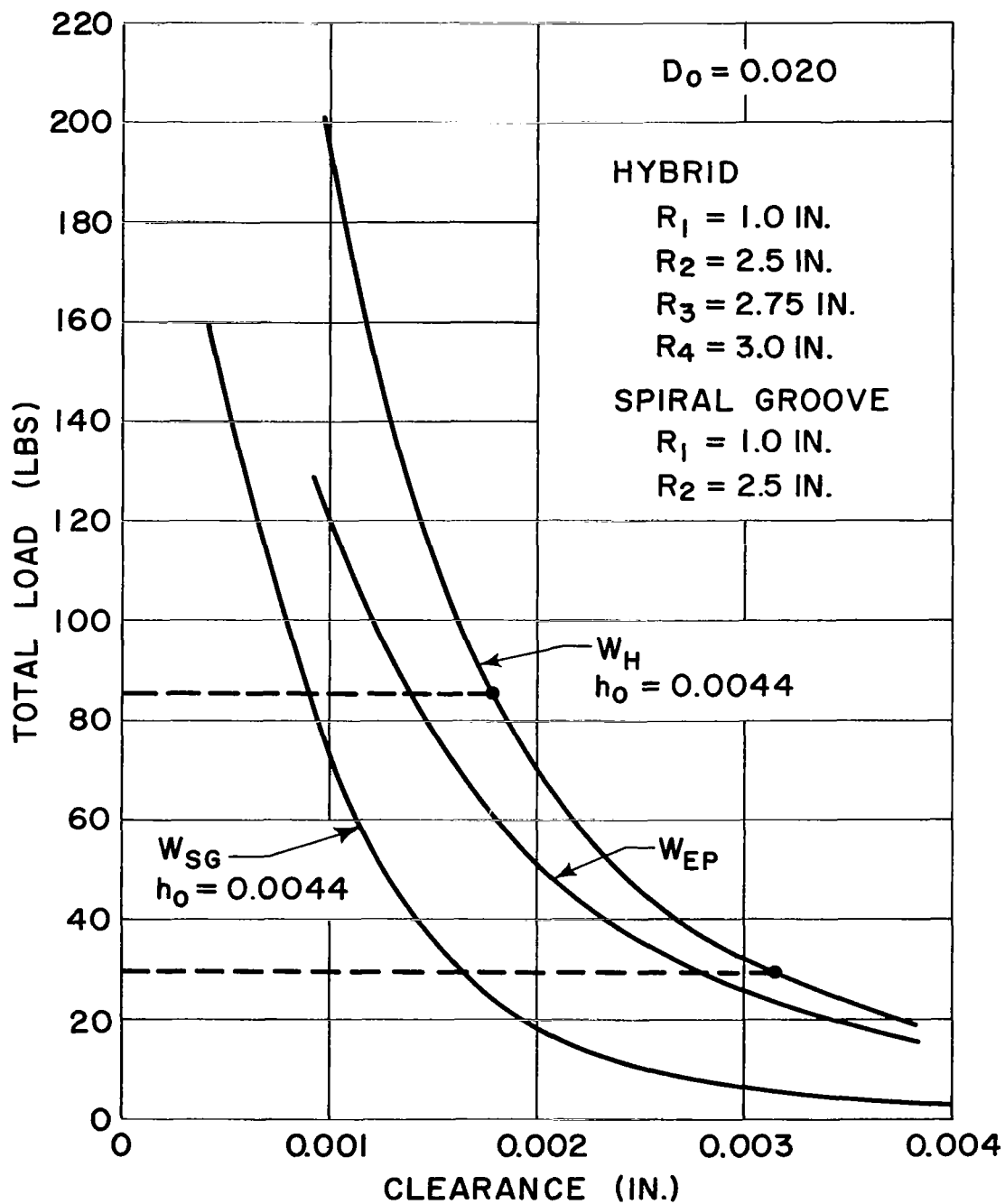


Figure 48 - Load vs Clearance - Hybrid Thrust Bearing ($D_0 = .020$)

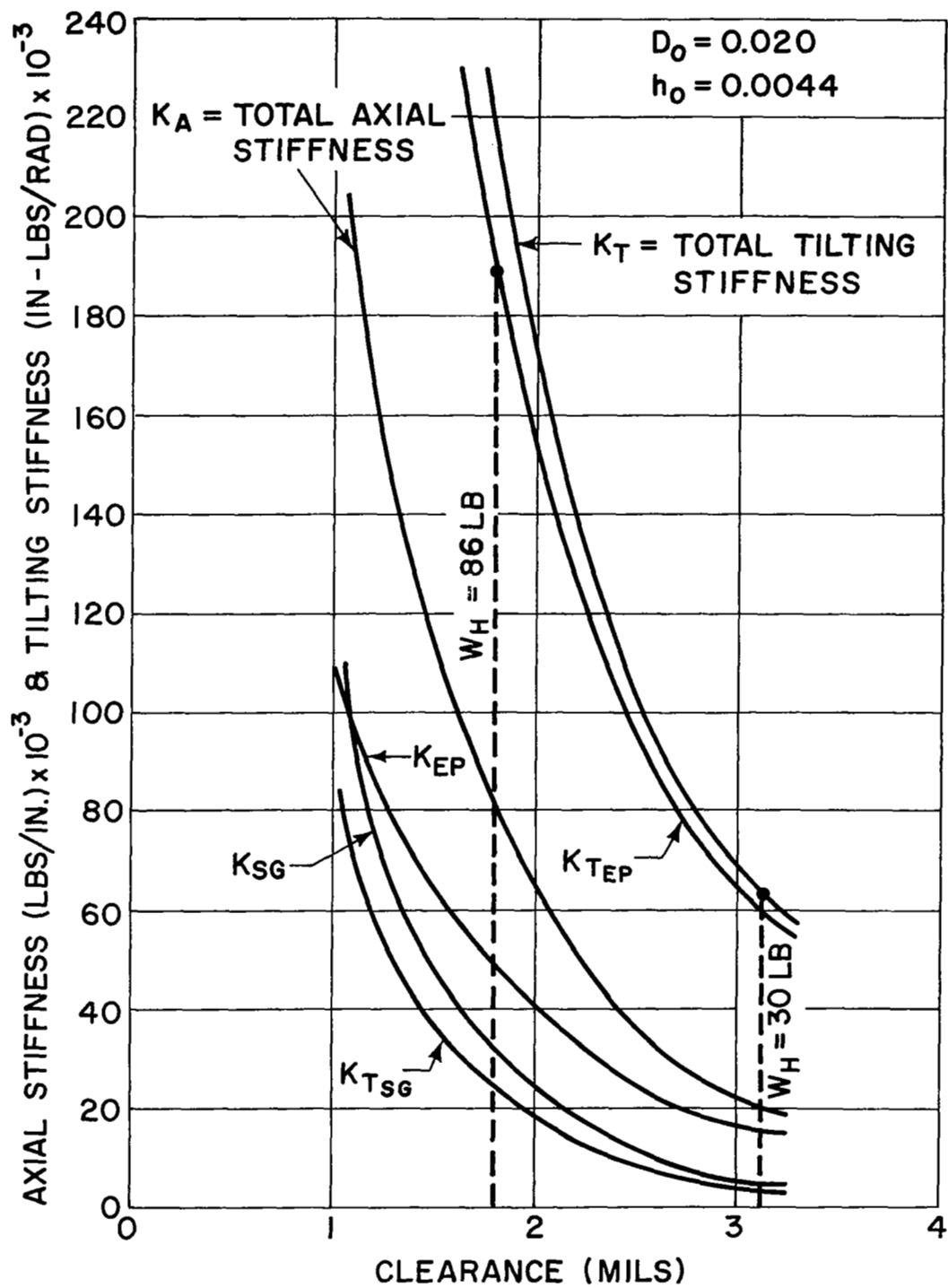


Figure 49 - Stiffness vs Clearance - Hybrid Thrust Bearing ($D_o = .020$)

This means that the recess volume is large in comparison with the clearance volume. A comparison of the critical recess depths of the hybrid bearing described herein and an orifice compensated bearing of like dimensions are shown on Figure 50. It is noted that the effect of inherent compensation considerably increases the recess depth at which pneumatic hammer is initiated.

The calculations shown in the Appendix were made to determine the effect of synchronous vibration and the effect of thermal distortion. As described in the analytical section, by synchronous vibrations we are referring to the swashing effect due to the misalignment of the thrust runner with the shaft axis. Calculations indicate that the relative swash will be approximately equal the initial misalignment. If the thrust runner is installed normal to the shaft axis with a maximum run-out of 0.0003 inches, it is believed that satisfactory operation would result. In regard to thermal distortions they appear to cause no problem. The maximum amount of dishing of the thrust bearing is approximately 2×10^{-5} inches which should be insignificant in affecting the performance of the bearing. A summary sheet, Table III tabulates all the pertinent performance parameters for varying loads for both acceptable bearing configurations.

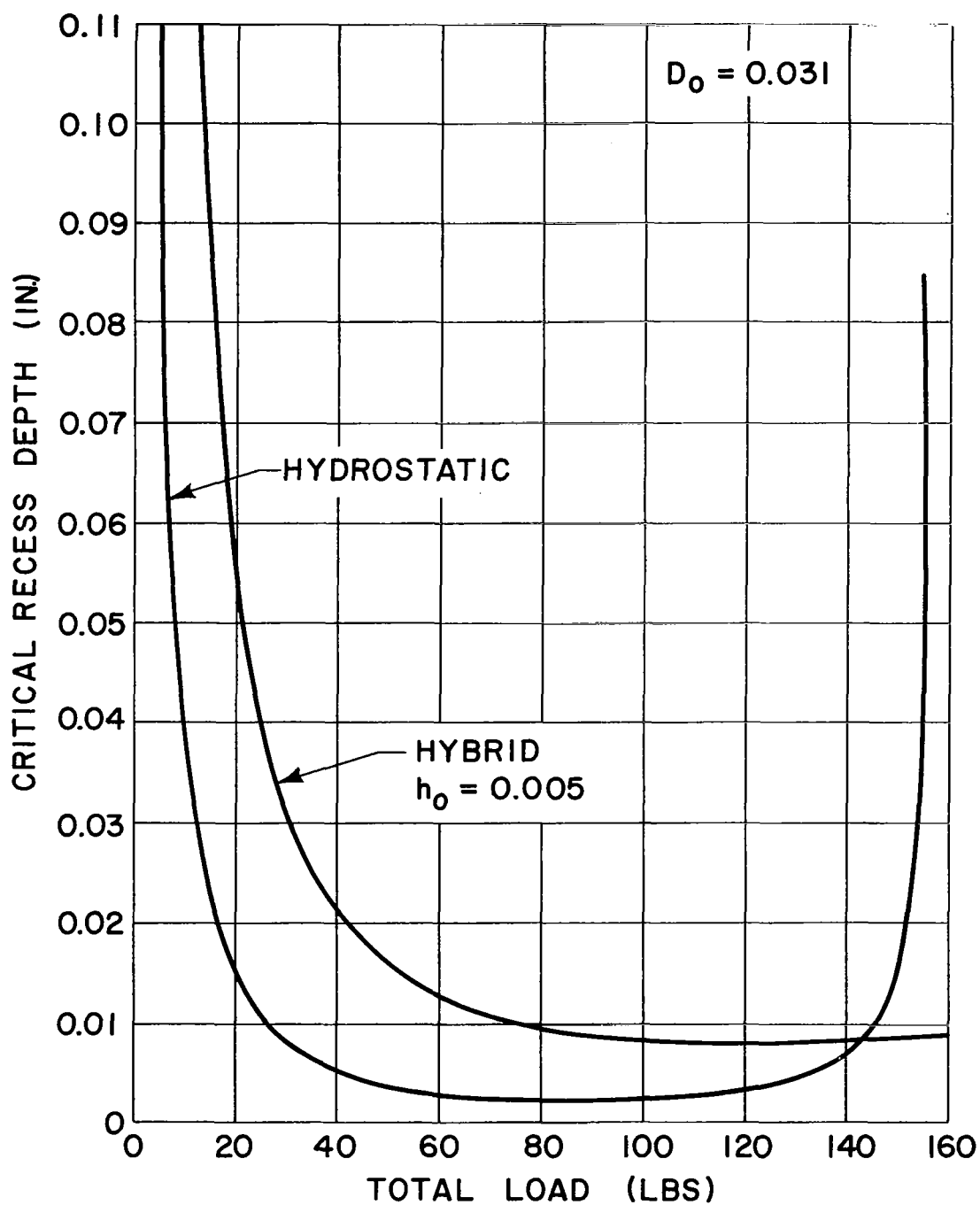


Figure 50 - Comparison of Critical Recess Depths Between Orifice Compensated and Inherently Compensated Thrust Bearings

Table IIIa

BEARING OPTIMIZED FOR 86 lb. LOAD, ORIFICE DIAMETER = 0.020 in.,
GROOVE DEPTH = 0.00435 in.

<u>Load</u> lb	<u>Clearance</u> mils	<u>Flow</u> lbm/sec x 10 ⁴	<u>Power</u> <u>Loss</u> h.p.	<u>Axial</u> <u>Stiffness</u> lb/in	<u>Natural</u> <u>Frequency</u> rpm
30	3.100	7.0	.036	21,000	3680
40	2.675	6.0	.0405	30,000	4390
50	2.400	5.4	.0430	41,500	5180
60	2.175	4.8	.050	53,000	5842
70	2.00	4.3	.055	65,000	6480
80	1.850	4.0	.058	79,500	7160
90	1.725	3.5	.067	88,500	7560

Bearing tilting stiffness at 30 lb. load: 64,385 in. lb/rad

Table IIIb

BEARING OPTIMIZED FOR 86 lb. LOAD, ORIFICE DIAMETER = 0.031 in.,
GROOVE DEPTH = 0.005 in.

<u>Load</u> lb	<u>Clearance</u> mils	<u>Flow</u> lbm/sec x 10 ⁴	<u>Power</u> <u>Loss</u> h.p.	<u>Axial</u> <u>Stiffness</u> lb/in	<u>Natural</u> <u>Frequency</u> rpm
30	3.700	13.0	.033	14,000	3000
40	3.175	11.0	.035	25,000	4010
50	2.800	9.5	.040	34,500	4720
60	2.550	8.5	.044	44,000	5330
70	2.325	7.6	.048	52,500	5820
80	2.150	6.9	.052	60,000	6220
90	2.00	6.3	.055	70,500	6750

Bearing tilting stiffness at 30 lb. load: 45,420 in. lb/rad

K. Bi-Directional Pair - Analytical Results

The computer output for the opposed pair of bearings used for startup and shut-down is shown on Figure 51 thru 54. The output is generated for the bearing operating at 12000 rpm and operating at zero speed. A smooth transitional effect is assumed between these limiting speeds. In the output, negative loads refer to loads directed toward the hybrid bearing while positive loads refer to loads directed toward the reaction bearing. These positive and negative loads are indicated in the column labeled Total Loads. Stability is indicated by either F or T. F(false) means the bearing is unstable, T(true) means the bearing is stable.

As can be seen from the output there are no problems with stability unless extremely high loads are applied toward the hybrid bearing. Within the normal operating range stability does not seem to be a problem. With a 20 lb. supply pressure, the annular reaction bearing supports a 100 lb. load although clearances become rather tight. No determinations at higher supply pressures were made but it appears that stability might become a problem, and thus higher supply pressures should be implemented with caution. It is noted that the hybrid bearing used is the one with 0.031 in. diameter orifices (the recommended configuration). Performance of the bi-directional pair has been plotted from the computer output. Figures 55 and 56 are load versus clearance curves for zero and 12000 rpm conditions. Plotted on these curves are the separate variations of each bearing and the combination of both bearings. As can be seen from a comparison of these two curves the effects of rotation are not very significant. This is to be expected, since increases in supply pressure, above the 12 psi which is a normal operating supply pressure for the hybrid bearing, will cause hydrostatic effects to become increasingly dominating. Figure 57 shows the variations of the flows for the separate bearings versus clearance and the combined total flow versus clearance.

It is noted here that the flows are considerably higher than for normal operation and are approaching the specification limits on flow as set for continuous operating conditions. Startup and shut-down operation however, are for very short periods of time; thus the

I	LOAD ANN.	LOAD STEP	LOAD HYB.	TOT. LOAD	PR ANN.	PR STEP	PR HYBRID	DELTA	STAB
HA	IS GREATER THAN H								
HA	IS GREATER THAN H								
HA	IS GREATER THAN H								
HA	IS GREATER THAN H								
5	2.5000	344.4538	437.0939	-434.5939	6.3183	19.2566	22.8219	0.1154	F
6	3.0000	188.9710	226.6127	-223.6127	6.3820	13.2727	14.7214	0.2840	F
7	3.5000	111.3112	128.1168	-124.6168	6.4456	10.2893	10.9369	0.4154	F
8	4.0000	76.9874	86.6126	-82.6126	6.5093	8.9667	9.3376	0.5215	T
9	4.5000	59.0705	65.4848	-60.9848	6.5730	8.2762	8.5234	0.6096	T
10	5.0000	48.2866	52.9534	-47.9534	6.6366	7.8607	8.0405	0.6843	T
11	5.5000	41.1552	44.7486	-39.2486	6.7003	7.5859	7.7244	0.7487	T
12	6.0000	36.1188	38.9965	-32.9965	6.7639	7.3918	7.5027	0.8049	T
13	6.5000	32.3852	34.7568	-28.2568	6.8276	7.2479	7.3393	0.8547	T
14	7.0000	29.5127	31.5099	-24.5099	6.8913	7.1373	7.2142	0.8991	T
15	7.5000	27.2369	28.9473	-21.4473	6.9549	7.0496	7.1155	0.9390	T
16	8.0000	25.3904	26.8750	-18.8750	7.0186	6.9784	7.0356	0.9752	T
17	8.5000	23.8628	25.1862	-16.6862	7.0822	6.9195	6.9705	1.0082	T
18	9.0000	22.5781	23.8085	-14.8085	7.1459	6.8790	6.9174	1.0385	T
19	9.5000	21.4825	22.6346	-13.1346	7.2096	6.8278	6.8722	1.0664	T
20	10.0000	20.5370	21.6223	-11.6223	7.2732	6.7914	6.8332	1.0922	T
21	10.5000	19.7126	20.7400	-10.2400	7.3369	6.7596	6.7992	1.1162	T
22	11.0000	18.9871	19.9642	-8.9642	7.4006	6.7317	6.7693	1.1386	T
23	11.5000	18.3636	19.2764	-7.7764	7.4642	6.7069	6.7428	1.1595	T
24	12.0000	17.7698	18.6623	-6.6623	7.5279	6.6847	6.7191	1.1792	T
25	12.5000	17.2521	18.1104	-5.6104	7.5915	6.6648	6.6979	1.1976	T
26	13.0000	16.7849	17.6117	-4.6117	7.6552	6.6468	6.6787	1.2151	T
27	13.5000	16.3603	17.1586	-3.6586	7.7189	6.6304	6.6612	1.2315	T
28	14.0000	15.9726	16.7450	-2.7450	7.7825	6.6155	6.6453	1.2471	T
29	14.5000	15.6172	16.3660	-1.8660	7.8462	6.6018	6.6307	1.2619	T
30	15.0000	15.2902	16.0172	-1.0172	7.9098	6.5892	6.6172	1.2760	T
31	15.5000	14.9873	15.6950	-0.1950	7.9735	6.5775	6.6048	1.2894	T
32	16.0000	14.7076	15.3966	0.6034	8.0372	6.5667	6.5933	1.3022	T
33	16.5000	14.4472	15.1192	1.3808	8.1008	6.5567	6.5826	1.3144	T
34	17.0000	14.2045	14.8606	2.1354	8.1645	6.5474	6.5726	1.3260	T
35	17.5000	13.9776	14.6190	2.8810	8.2281	6.5386	6.5633	1.3372	T
36	18.0000	13.7650	14.3921	3.6073	8.2918	6.5304	6.5546	1.3479	T
37	18.5000	13.5653	14.1832	4.3198	8.3555	6.5221	6.5464	1.3582	T
38	19.0000	13.3775	13.9853	5.0197	8.4191	6.5155	6.5387	1.3681	T
39	19.5000	13.2003	13.7918	5.7082	8.4828	6.5087	6.5315	1.3777	T
40	20.0000	13.0330	13.6138	6.3862	8.5465	6.5022	6.5246	1.3868	T
41	20.5000	12.8746	13.4453	7.0547	8.6101	6.4961	6.5181	1.3957	T
42	21.0000	12.7245	13.2857	7.7143	8.6738	6.4903	6.5120	1.4042	T
43	21.5000	12.5819	13.1341	8.3659	8.7374	6.4848	6.5061	1.4125	T
44	22.0000	12.4464	12.9901	9.0099	8.8011	6.4796	6.5006	1.4204	T
45	22.5000	12.3174	12.8529	9.6471	8.8648	6.4746	6.4953	1.4281	T
46	23.0000	12.1944	12.7222	10.2778	8.9284	6.4699	6.4902	1.4356	T
47	23.5000	12.0770	12.5974	10.9026	8.9921	6.4654	6.4854	1.4428	T
48	24.0000	11.9648	12.4782	11.5218	9.0557	6.4611	6.4808	1.4498	T
49	24.5000	11.8574	12.3641	12.1359	9.1194	6.4569	6.4764	1.4566	T
50	25.0000	11.7546	12.2549	12.7451	9.1831	6.4530	6.4722	1.4632	T

NOMENCLATURE

LOAD ANN = REACTION BRG. LOAD (LBS)

LOAD STEP = EXT. PRESS. LOAD-(LBS)

LOAD HYB = HYBRID LOAD-(LBS)

TOT. LOAD = NET LOAD (LBS)

PR ANN = REACTION BRG RECESS PRESS (PSIA)

PR STEP = EXT. PRESS RECESS PRESS. (PSIA)

PR HYBRID = HYBRID EQUIVALENT RECESS PRESS -(PSIA)

DELTA = COMPRESSION RATIO = h/h_0

STAB = STABLE

T = TRUE

F = FALSE

HA = REACTION BRG. CLEARANCE (IN)

Figure 51 - Program Output I - Bi-Directional Pair (N = 12,000 RPM)

I	ANNULAR FLOW	STEP FLOW	TOTAL FLOW	ANNULAR CLEARANCE	STEP CLEARANCE
HA IS GREATER THAN H					
HA IS GREATER THAN H					
HA IS GREATER THAN H					
HA IS GREATER THAN H					
5	0.14624E-C4	0.33059E-C6	0.14959E-04	0.94229E-02	0.57707E-C3
6	0.13221E-C4	0.20644E-C5	0.15384E-04	0.85798E-02	0.14202E-C2
7	0.12303E-C4	0.32196E-C5	0.15520E-04	0.79230E-C2	0.20770E-02
8	0.11477E-C4	0.45482E-C5	0.15525E-04	0.73924E-C2	0.26076E-02
9	0.10793E-C4	0.47320E-C5	0.15525E-04	0.69520E-02	0.30480E-02
10	0.10213E-C4	0.53117E-C5	0.15525E-04	0.65786E-02	0.34214E-02
11	0.97173E-C5	0.58114E-C5	0.15525E-04	0.62567E-02	0.37433E-02
12	0.92766E-C5	0.62482E-C5	0.15525E-04	0.59754E-02	0.40246E-02
13	0.88905E-C5	0.66342E-C5	0.15525E-04	0.57267E-02	0.42733E-02
14	0.85459E-C5	0.69798E-C5	0.15525E-04	0.55047E-02	0.44953E-02
15	0.82358E-C5	0.72889E-C5	0.15525E-04	0.53050E-02	0.46950E-02
16	0.77549E-C5	0.75679E-C5	0.15525E-04	0.51239E-02	0.48761E-02
17	0.76983E-C5	0.78263E-C5	0.15525E-04	0.49589E-02	0.50411E-02
18	0.74635E-C5	0.80613E-C5	0.15525E-04	0.48075E-02	0.51925E-02
19	0.72440E-C5	0.82779E-C5	0.15525E-04	0.46679E-02	0.53321E-02
20	0.70443E-C5	0.84783E-C5	0.15525E-04	0.45388E-C2	0.54612E-02
21	0.68602E-C5	0.86646E-C5	0.15525E-04	0.44189E-02	0.55811E-02
22	0.66845E-C5	0.88383E-C5	0.15525E-04	0.43070E-C2	0.56930E-02
23	0.65240E-C5	0.90007E-C5	0.15525E-04	0.42024E-02	0.57976E-02
24	0.63716E-C5	0.91531E-C5	0.15525E-04	0.41042E-02	0.58958E-02
25	0.62283E-C5	0.92965E-C5	0.15525E-04	0.40118E-02	0.59882E-02
26	0.60931E-C5	0.94317E-C5	0.15525E-04	0.39247E-02	0.60753E-02
27	0.59653E-C5	0.95595E-C5	0.15525E-04	0.38424E-02	0.61576E-02
28	0.58442E-C5	0.96805E-C5	0.15525E-04	0.37645E-02	0.62355E-02
29	0.57294E-C5	0.97954E-C5	0.15525E-04	0.36905E-C2	0.63095E-02
30	0.56202E-C5	0.99046E-C5	0.15525E-04	0.36201E-02	0.63799E-02
31	0.55162E-C5	0.10039E-04	0.15525E-04	0.35531E-02	0.64469E-02
32	0.54173E-C5	0.10138E-C4	0.15525E-04	0.34892E-C2	0.65108E-02
33	0.53222E-C5	0.10203E-C4	0.15525E-04	0.34282E-02	0.65718E-02
34	0.52316E-C5	0.10293E-C4	0.15525E-04	0.33698E-C2	0.66302E-02
35	0.51447E-C5	0.10380E-C4	0.15525E-04	0.33139E-02	0.66861E-02
36	0.50613E-C5	0.10463E-C4	0.15525E-04	0.32603E-C2	0.67397E-02
37	0.49815E-C5	0.10543E-C4	0.15525E-04	0.32088E-C2	0.67912E-02
38	0.49047E-C5	0.10620E-C4	0.15525E-04	0.31593E-02	0.68407E-02
39	0.48307E-C5	0.10694E-C4	0.15525E-04	0.31116E-02	0.68884E-02
40	0.47595E-C5	0.10763E-C4	0.15525E-04	0.30658E-02	0.69342E-02
41	0.46909E-C5	0.10834E-C4	0.15525E-04	0.30215E-02	0.69785E-02
42	0.46246E-C5	0.10900E-C4	0.15525E-04	0.29789E-02	0.70211E-02
43	0.45606E-C5	0.10964E-C4	0.15525E-04	0.29377E-02	0.70623E-02
44	0.44998E-C5	0.11026E-C4	0.15525E-04	0.28978E-C2	0.71022E-02
45	0.44414E-C5	0.11086E-C4	0.15525E-04	0.28593E-C2	0.71407E-02
46	0.43811E-C5	0.11144E-C4	0.15525E-04	0.28220E-C2	0.71780E-02
47	0.43251E-C5	0.11200E-C4	0.15525E-04	0.27859E-C2	0.72141E-02
48	0.42707E-C5	0.11254E-C4	0.15525E-04	0.27509E-C2	0.72491E-02
49	0.42180E-C5	0.11307E-C4	0.15525E-04	0.27169E-02	0.72831E-02
50	0.41668E-C5	0.11358E-C4	0.15525E-04	0.26840E-02	0.73160E-02

ANNULAR Flow = REACTION BRG
Flow- $\frac{\text{lbs-sec}}{\text{in.}}$

STEP Flow = HYBRID BRG. Flow
 $\frac{\text{lbs-sec}}{\text{in.}}$

TOTAL Flow = NET FLOW
 $\frac{\text{lbs-sec}}{\text{in.}}$

ANNULAR CLEARANCE = REACTION
BRG CLEAR. (IN)

STEP CLEARANCE = HYBRID
BRG. CLEARANCE (IN)

Figure 52 - Program Output II - Bi-Directional Pair (N = 12,000 RPM)

I	LOAD ANN.	LOAD STEP	LOAD HYB.	TOT. LOAD	PR ANN.	PR STEP	PR HYBRID	DELTA	STAB
1	20.0000	13.3333	13.6138	6.3862	8.5465	6.5022	6.5246	1.3868	T
2	22.0000	12.4464	12.9901	9.0099	8.8011	6.4796	6.5006	1.4204	T
3	24.0000	11.9648	12.4782	11.5218	9.0557	6.4611	6.4808	1.4498	T
4	26.0000	11.5614	12.0497	13.9503	9.3104	6.4455	6.4643	1.4758	T
5	28.0000	11.2181	11.6850	16.3150	9.5650	6.4323	6.4503	1.4990	T
6	30.0000	10.9215	11.3704	18.6296	9.8197	6.4209	6.4381	1.5199	T
7	32.0000	10.6612	11.0942	20.9058	10.0743	6.4108	6.4275	1.5390	T
8	34.0000	10.4300	10.8488	23.1512	10.3290	6.4019	6.4181	1.5565	T
9	36.0000	10.2227	10.6293	25.3713	10.5836	6.3939	6.4096	1.5727	T
10	38.0000	10.0354	10.4304	27.5696	10.8383	6.3867	6.4019	1.5878	T
11	40.0000	9.8651	10.2499	29.7501	11.0930	6.3801	6.3950	1.6019	T
12	42.0000	9.7092	10.0847	31.9153	11.3476	6.3741	6.3886	1.6151	T
13	44.0000	9.5658	9.9328	34.0672	11.6023	6.3686	6.3828	1.6275	T
14	46.0000	9.4332	9.7923	36.2077	11.8569	6.3635	6.3773	1.6392	T
15	48.0000	9.3100	9.6618	38.3382	12.1115	6.3588	6.3723	1.6504	T
16	50.0000	9.1950	9.5401	40.4599	12.3662	6.3543	6.3676	1.6610	T
17	52.0000	9.0873	9.4260	42.5740	12.6208	6.3502	6.3632	1.6711	T
18	54.0000	8.9860	9.3188	44.6812	12.8755	6.3463	6.3591	1.6807	T
19	56.0000	8.8904	9.2176	46.7824	13.1301	6.3426	6.3552	1.6900	T
20	58.0000	8.8000	9.1219	48.8781	13.3848	6.3391	6.3515	1.6989	T
21	60.0000	8.7143	9.0310	50.9690	13.6394	6.3358	6.3480	1.7075	T
22	62.0000	8.6322	8.9443	53.0557	13.8941	6.3326	6.3447	1.7158	T
23	64.0000	8.5539	8.8616	55.1384	14.1487	6.3296	6.3415	1.7238	T
24	66.0000	8.4790	8.7823	57.2177	14.4034	6.3267	6.3384	1.7316	T
25	68.0000	8.4069	8.7060	59.2940	14.6580	6.3240	6.3355	1.7392	T
26	70.0000	8.3374	8.6326	61.3674	14.9127	6.3213	6.3327	1.7466	T
27	72.0000	8.2703	8.5615	63.4385	15.1673	6.3187	6.3299	1.7539	T
28	74.0000	8.2051	8.4926	65.5074	15.4220	6.3162	6.3273	1.7610	T
29	76.0000	8.1417	8.4256	67.5744	15.6766	6.3137	6.3247	1.7680	T
30	78.0000	8.0799	8.3602	69.6398	15.9313	6.3114	6.3222	1.7750	T
31	80.0000	8.0193	8.2962	71.7038	16.1859	6.3090	6.3197	1.7818	T
32	82.0000	7.9597	8.2332	73.7668	16.4406	6.3067	6.3173	1.7886	T
33	84.0000	7.9029	8.1711	75.8289	16.6952	6.3045	6.3149	1.7954	T
34	86.0000	7.8426	8.1095	77.8905	16.9499	6.3022	6.3125	1.8023	T
35	88.0000	7.7845	8.0481	79.9519	17.2045	6.3000	6.3101	1.8092	T
36	90.0000	7.7263	7.9865	82.0135	17.4592	6.2977	6.3078	1.8161	T
37	92.0000	7.6674	7.9244	84.0756	17.7138	6.2955	6.3054	1.8233	T
38	94.0000	7.6075	7.8611	86.1389	17.9685	6.2932	6.3029	1.8306	T
39	96.0000	7.5460	7.7961	88.2039	18.2231	6.2908	6.3004	1.8382	T
40	98.0000	7.4818	7.7283	90.2717	18.4777	6.2883	6.2978	1.8463	T
41	100.0000	7.4137	7.6564	92.3436	18.7324	6.2857	6.2950	1.8549	T
42	102.0000	7.3397	7.5783	94.4217	18.9870	6.2828	6.2920	1.8645	T
43	104.0000	7.2562	7.4901	96.5098	19.2417	6.2796	6.2886	1.8754	T
44	106.0000	7.1558	7.3842	98.6158	19.4963	6.2757	6.2845	1.8888	T
45	1.8.0000	7.1170	7.2377	100.7623	19.7510	6.2704	6.2789	1.9078	T

PRA/PS IS GREATER THAN 1

LOAD ANN.= REACTION BRG. LOAD (LBS)
 LOAD STEP=EXT. PRESS LOAD -(LBS)
 LOAD HYB= HYBRID LOAD -(LBS)
 TOT. LOAD= NET LOAD (LBS)
 PR. ANN= REACTION BRG RECESS PRESS (PSIA)
 PR. STEP= EXT. PRESS BRG - RECESS PRESS (PSIA)
 PR HYBRID= HYBRID EQUIVALENT RECESS
 PRESS - (PSIA)
 DELTA = COMPRESSION RATIO = h/h_0
 STAB = STABLE
 T=TRUE
 F=FALSE
 HA= REACTION BRG CLEARANCE (IN)

Figure 53 - Program Output III - Bi-Directional Pair (N = 12,000 RPM)

	ANNULAR FLOW	STEP FLOW	TOTAL FLOW	ANNULAR CLEARANCE	STEP CLEARANCE	
1	0.47595E-05	0.10765E-04	0.15525E-04	0.30658E-02	0.69342E-02	
2	0.44588E-05	0.11026E-04	0.15525E-04	0.28978E-02	0.71022E-02	ANNULAR Flow = REACTION BRG
3	0.42707E-05	0.11254E-04	0.15525E-04	0.27509E-02	0.72491E-02	Flow $\frac{\text{lbs-sec}}{\text{in.}}$
4	0.40769E-05	0.11456E-04	0.15525E-04	0.26209E-02	0.73791E-02	
5	0.38887E-05	0.11636E-04	0.15525E-04	0.25048E-02	0.74952E-02	
6	0.37243E-05	0.11798E-04	0.15525E-04	0.24003E-02	0.75997E-02	
7	0.35764E-05	0.11946E-04	0.15523E-04	0.23305E-02	0.76950E-02	STEP Flow = HYBRID BRG. Flow
8	0.34363E-05	0.12082E-04	0.15519E-04	0.22173E-02	0.77827E-02	$\frac{\text{lbs-sec}}{\text{in.}}$
9	0.33046E-05	0.12208E-04	0.15513E-04	0.21363E-02	0.78637E-02	
10	0.31811E-05	0.12325E-04	0.15505E-04	0.20609E-02	0.79391E-02	
11	0.30618E-05	0.12434E-04	0.15496E-04	0.19906E-02	0.80094E-02	
12	0.29492E-05	0.12537E-04	0.15486E-04	0.19246E-02	0.80754E-02	
13	0.28409E-05	0.12633E-04	0.15474E-04	0.18625E-02	0.81375E-02	TOTAL Flow = NET Flow
14	0.27370E-05	0.12724E-04	0.15461E-04	0.18038E-02	0.81962E-02	$\frac{\text{lbs-sec}}{\text{in.}}$
15	0.26366E-05	0.12811E-04	0.15448E-04	0.17481E-02	0.82519E-02	
16	0.25399E-05	0.12893E-04	0.15433E-04	0.16952E-02	0.83048E-02	
17	0.24463E-05	0.12971E-04	0.15417E-04	0.16447E-02	0.83553E-02	
18	0.23546E-05	0.13046E-04	0.15401E-04	0.15965E-02	0.84035E-02	
19	0.22656E-05	0.13118E-04	0.15384E-04	0.15501E-02	0.84499E-02	
20	0.21787E-05	0.13187E-04	0.15366E-04	0.15056E-02	0.84944E-02	ANNULAR CLEARANCE = REACTION
21	0.20937E-05	0.13254E-04	0.15348E-04	0.14627E-02	0.85373E-02	BRG CLEARANCE (IN)
22	0.20103E-05	0.13318E-04	0.15329E-04	0.14212E-02	0.85788E-02	
23	0.19284E-05	0.13381E-04	0.15309E-04	0.13810E-02	0.86190E-02	
24	0.18478E-05	0.13441E-04	0.15289E-04	0.13420E-02	0.86580E-02	
25	0.17684E-05	0.13500E-04	0.15269E-04	0.13040E-02	0.86960E-02	
26	0.16899E-05	0.13558E-04	0.15248E-04	0.12669E-02	0.87331E-02	STEP CLEARANCE = HYBRID
27	0.16124E-05	0.13614E-04	0.15227E-04	0.12306E-02	0.87694E-02	BRG. CLEARANCE (IN)
28	0.15356E-05	0.13670E-04	0.15205E-04	0.11949E-02	0.88051E-02	
29	0.14593E-05	0.13724E-04	0.15183E-04	0.11598E-02	0.88402E-02	
30	0.13836E-05	0.13778E-04	0.15162E-04	0.11252E-02	0.88748E-02	
31	0.13082E-05	0.13831E-04	0.15139E-04	0.10909E-02	0.89091E-02	
32	0.12331E-05	0.13884E-04	0.15117E-04	0.10568E-02	0.89432E-02	
33	0.11577E-05	0.13937E-04	0.15095E-04	0.10228E-02	0.89772E-02	
34	0.10824E-05	0.13990E-04	0.15073E-04	0.98862E-03	0.90114E-02	
35	0.10073E-05	0.14043E-04	0.15051E-04	0.95422E-03	0.90458E-02	
36	0.93145E-06	0.14097E-04	0.15029E-04	0.91935E-03	0.90807E-02	
37	0.85493E-06	0.14153E-04	0.15008E-04	0.88374E-03	0.91163E-02	
38	0.77747E-06	0.14210E-04	0.14987E-04	0.84707E-03	0.91529E-02	
39	0.69891E-06	0.14269E-04	0.14968E-04	0.80892E-03	0.91911E-02	
40	0.61847E-06	0.14331E-04	0.14950E-04	0.76863E-03	0.92314E-02	
41	0.53591E-06	0.14399E-04	0.14935E-04	0.72536E-03	0.92746E-02	
42	0.45029E-06	0.14473E-04	0.14923E-04	0.67765E-03	0.93224E-02	
43	0.36032E-06	0.14558E-04	0.14918E-04	0.62295E-03	0.93770E-02	
44	0.26360E-06	0.14662E-04	0.14925E-04	0.55590E-03	0.94441E-02	
45	0.15456E-06	0.14809E-04	0.14964E-04	0.46086E-03	0.95391E-02	

PRA/PS IS GREATER THAN 1

Figure 54 - Program Output IV - Bi-Directional Pair (N = 12,000 RPM)

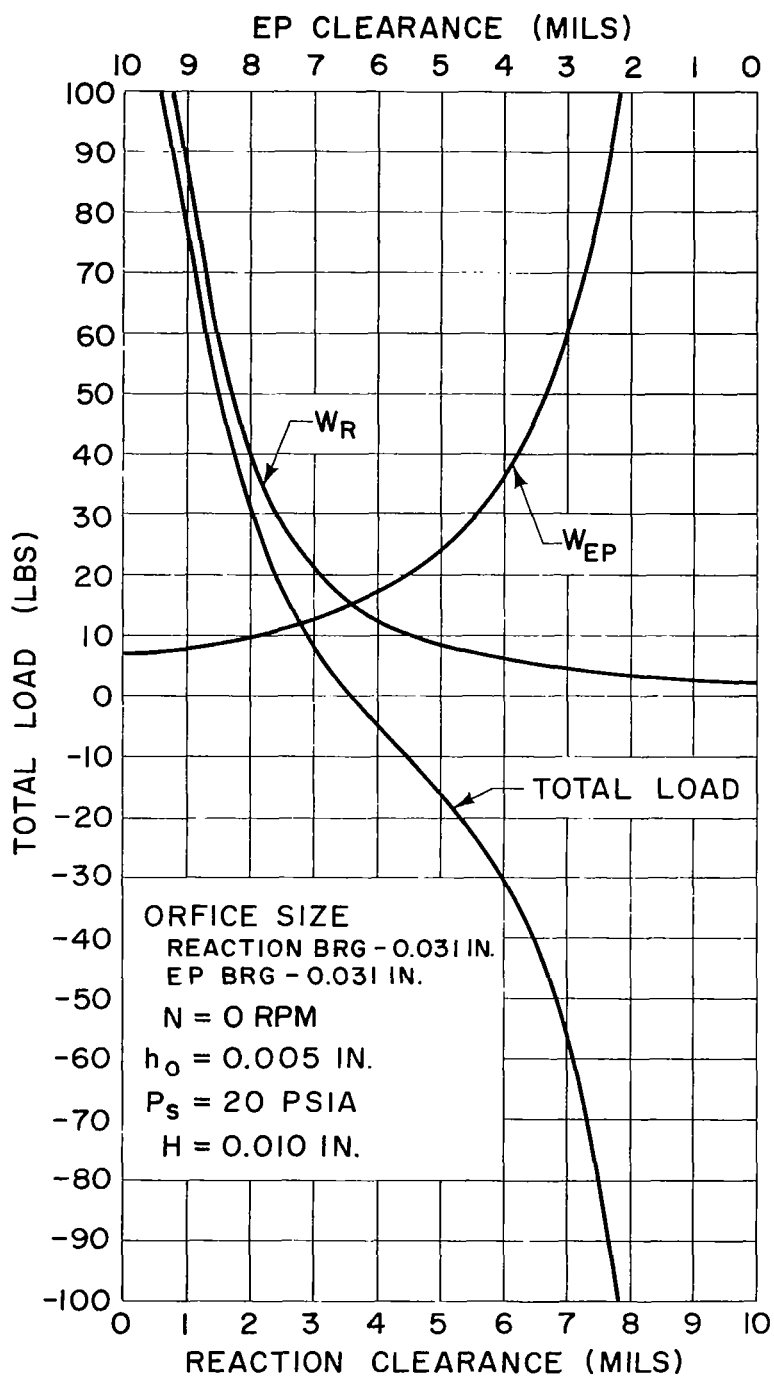


Figure 55 - Load vs Clearance - Bi-Directional Pair (N = 0 RPM)

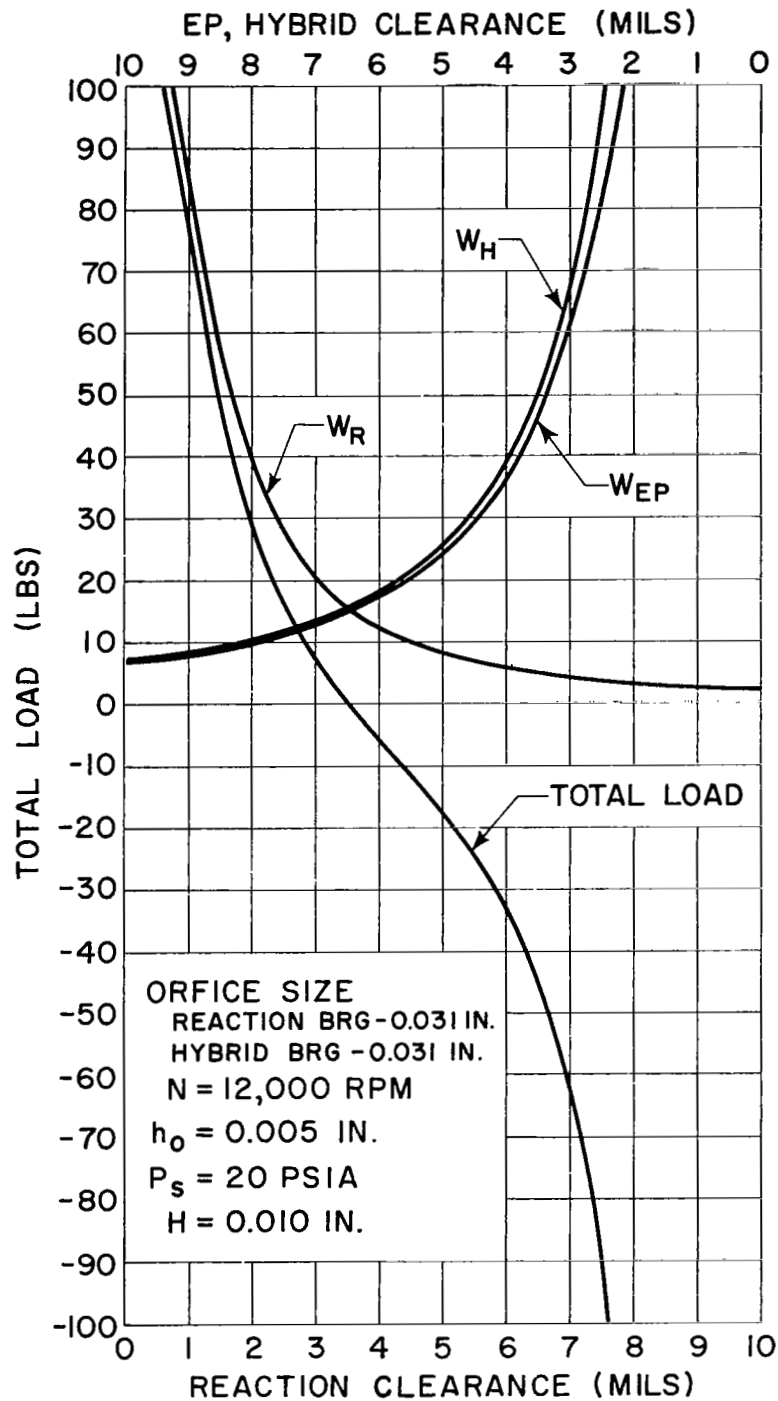


Figure 56 - Load vs Clearance - Bi-Directional Pair ($N = 12,000$ RPM)

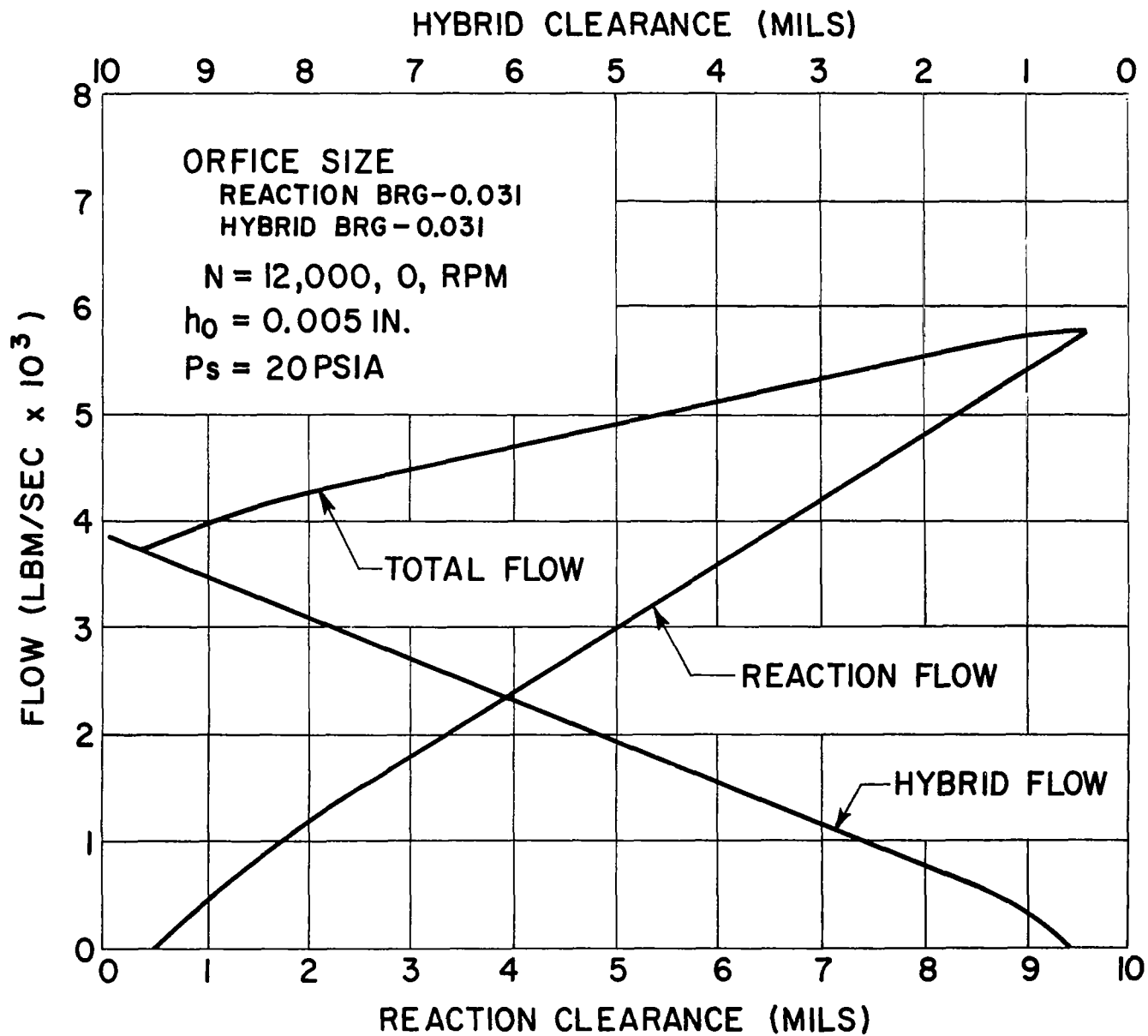


Figure 57 - Flow vs Clearance - Bi-Directional Pair

total flow used by the bi-directional pair is insignificant. Figures 58 and 59 describe the variations in axial stiffness of the bi-directional pair versus clearance and load respectively. The natural frequency of the bearing rotor system, where the gas film of the thrust bearing is considered as a spring, is indicated on Figure 58. These values are well below normal operating speed.

L. Mechanical Design - Hybrid Thrust Bearing

The design configuration of the main hybrid thrust bearing is shown on Figure 60. The bearing consists of essentially two members bolted together. The first member is a manifold in which the gas is introduced and through which the gas is distributed to the other member which is the groove plate. The groove plate contains the spiral groove bearing and the inherently compensated hydrostatic bearing. The groove geometry is specified on Figures 61 and 62. This geometry corresponds precisely to those used in the analytical investigations. As noted on Figure 60 the gas is introduced at the geometric center of the bearing so that incoming gas momentum would not produce any moments on the thrust bearing that would produce misalignment. The orifices are an integral part of the groove plate, and not separate pieces so that true inherent compensation can readily be achieved. To keep mass at a minimum and also to improve thermal conductivity and thus minimize thermal distortion a good grade of aluminum is recommended for the bearing pieces. The grooves can be produced by flame coating the aluminum, appropriately masked, with chrome oxide. Spiral groove bearings have been very successfully produced in this manner by the Linde Division of Union Carbide Corporation. When producing the bearings, caution should be exercised to ensure that groove depths do not exceed values indicated on the drawings. It is preferable to be on the low side of tolerance in regards to groove depth, than on the high side. It was pointed out in the discussion of performance that excessive groove depths produce pneumatic hammer.

The orifice drill diameter is indicated as .028 in. on the drawing, but the edge radii will increase the effective diameter to the design value of 0.031. The self aligning support structure will be designed by Pratt and Whitney Aircraft. Although a 20,000 in.-lb/rad structure is recommended the actual stiffness should be determined empirically. It is recommended that experiments be conducted with a stiff structure and if experimental results indicate that an increase in flexibility is required, the support thickness can be reduced. This procedure will allow proper compensation for variations between predicted and actual values of the film tilting stiffness.

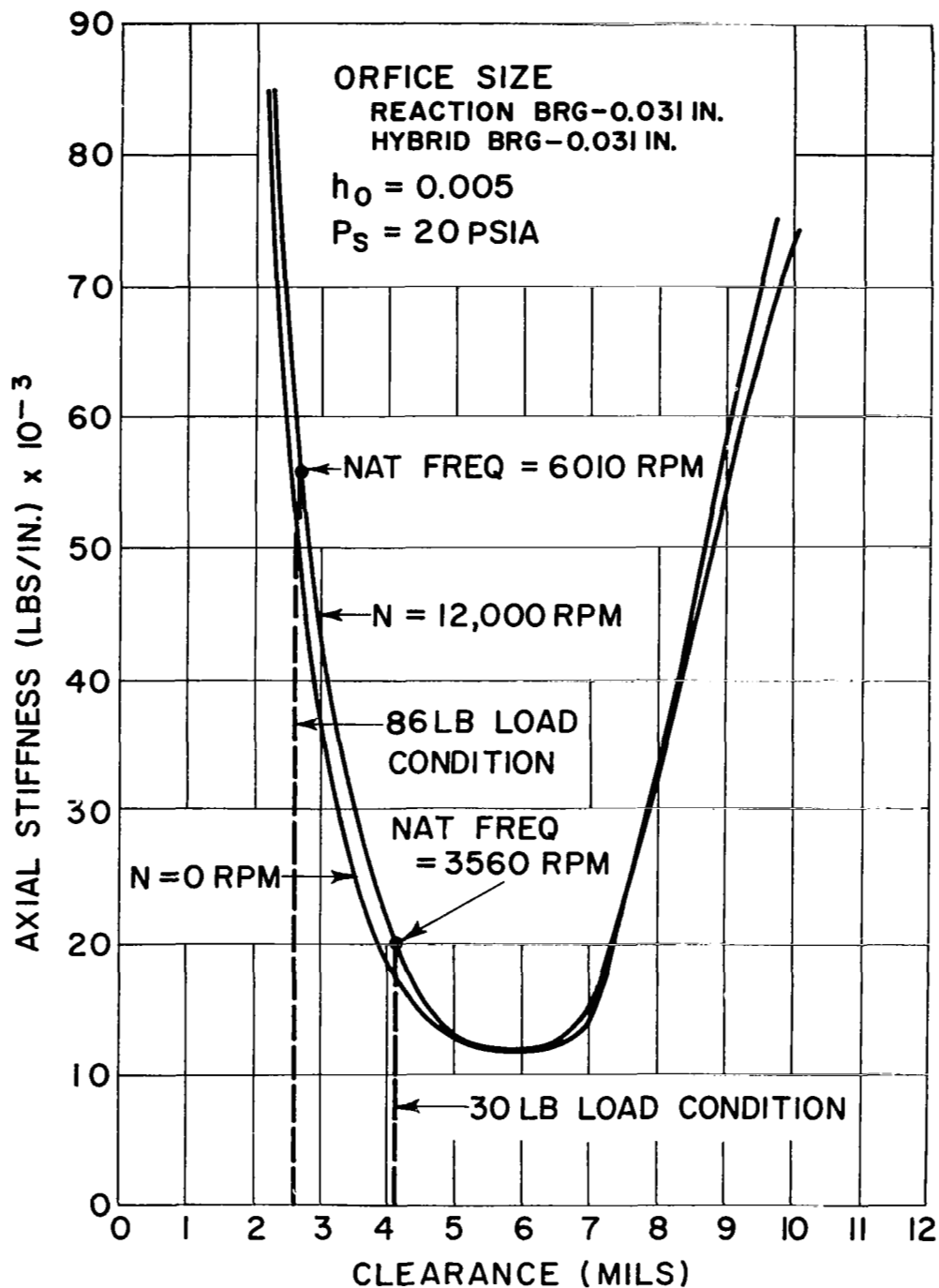


Figure 58 - Axial Stiffness vs Clearance - Bi-Directional Pair

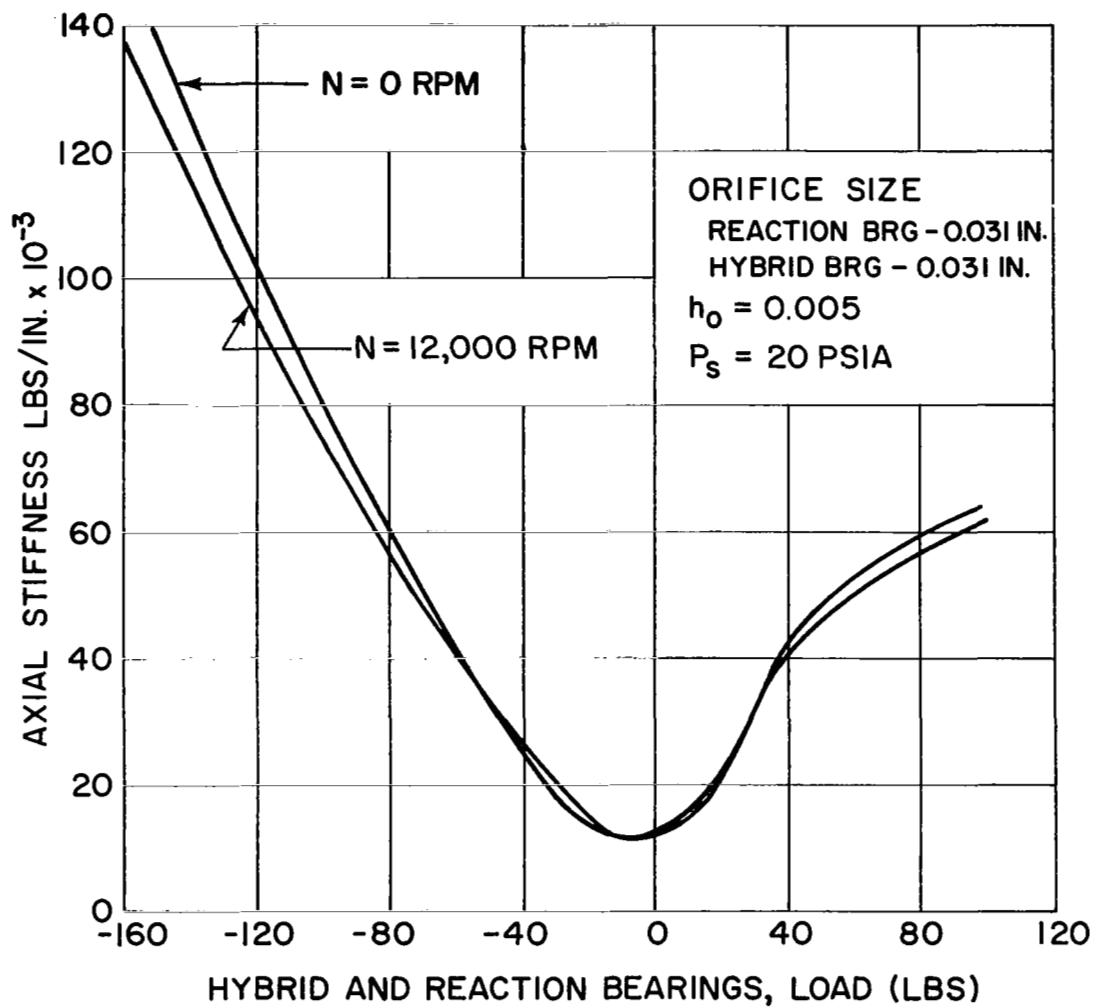


Figure 59 - Axial Stiffness vs Load - Bi-Directional Pair

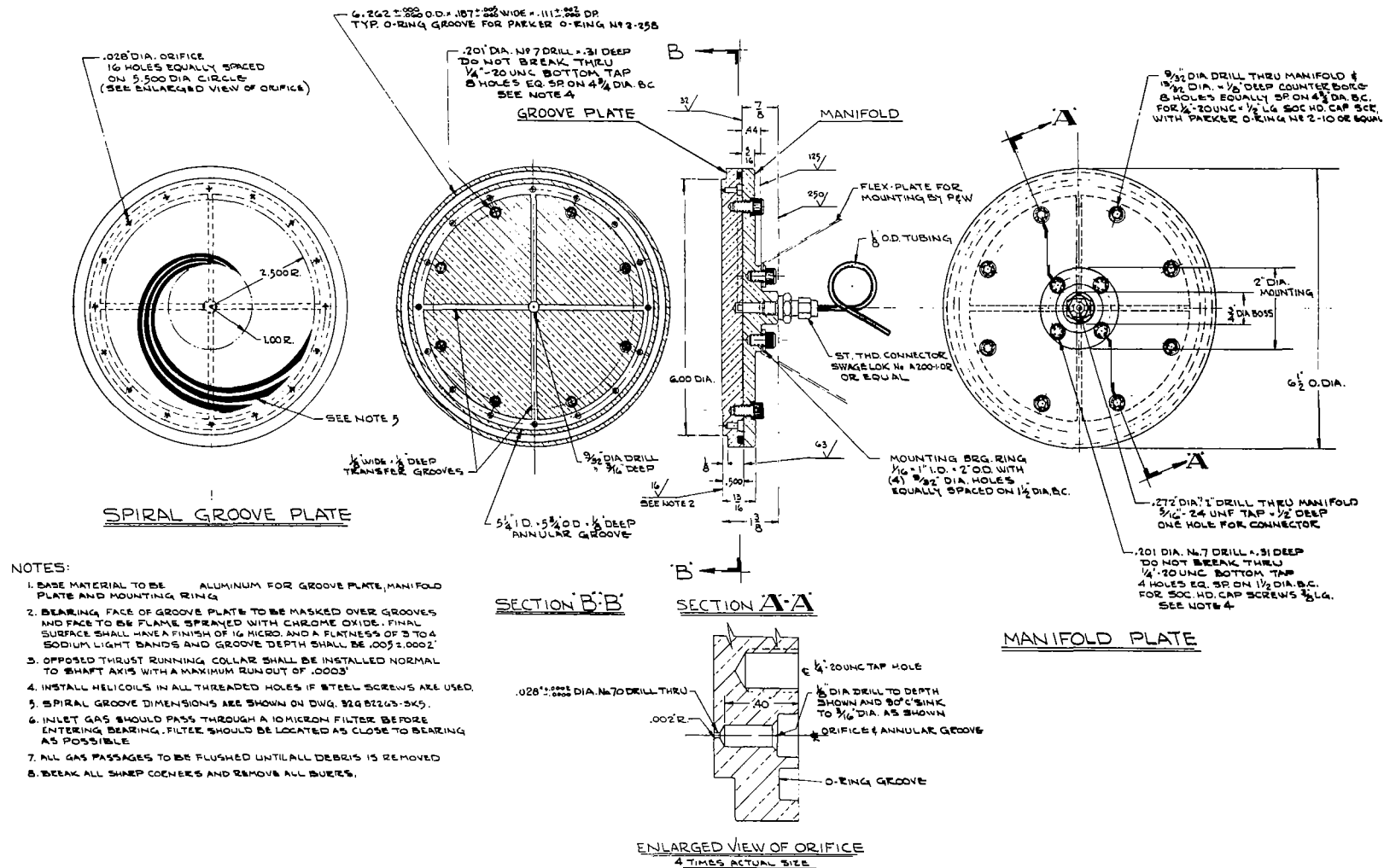
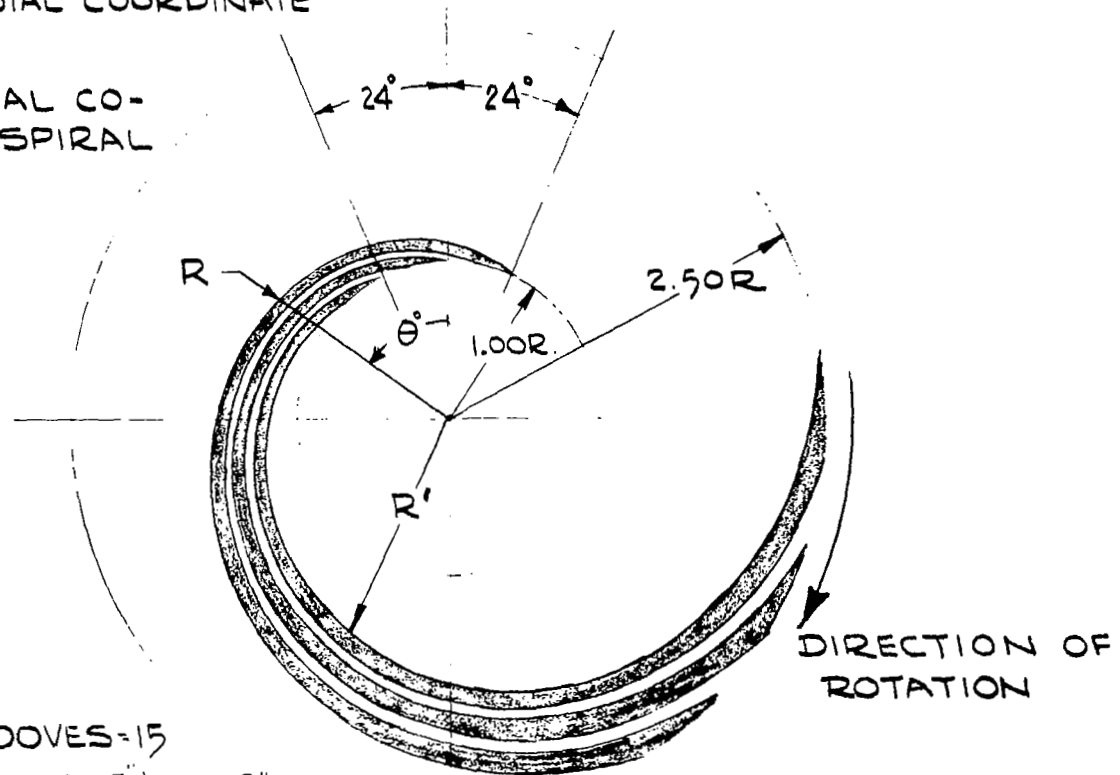


Figure 60 - Mechanical Design - Hybrid Thrust Bearing

R = OUTSIDE RADIAL COORDINATE
OF SPIRAL

R' = INSIDE RADIAL CO-
ORDINATE OF SPIRAL



NUMBER OF GROOVES = 15
GROOVE DEPTH = $.005 \pm .0002$ "
AT A CONSTANT RADIUS
RATIO OF LAND WIDTH/GROOVE WIDTH = 1.16

Figure 61 - Groove Geometry - Hybrid Thrust Bearing

LOGARITHMIC SPIRAL GROOVE

GROOVE COORDINATES		
θ°	R	R'
0	1.000	.958
10	1.039	.995
20	1.080	1.034
30	1.122	1.075
40	1.166	1.117
50	1.212	1.161
60	1.259	1.206
70	1.308	1.253
80	1.359	1.302
90	1.413	1.353
100	1.468	1.406
110	1.525	1.461
120	1.585	1.518
130	1.647	1.577
140	1.711	1.639
150	1.778	1.704
160	1.848	1.770
170	1.920	1.839
180	1.995	1.911
190	2.073	1.986
200	2.154	2.064
210	2.239	2.145
220	2.326	2.228
230	2.417	2.316
240	2.512	2.406
250	2.610	2.500
260	2.712	2.598
270	2.818	2.700
280	2.928	2.805
290	3.043	2.915
300	3.162	3.029

See Figure 61 for Orientation

Fig. 62 - Tabulation of Groove Coordinates - Hybrid Thrust Bearing

M. Conclusions and Recommendations - Hybrid Thrust Bearing

1. The use of a spiral groove hydrodynamic bearing in combination with a central recess, inherently compensated, hydrostatic bearing considerably improves operating performance over that of either a spiral groove or hydrostatic bearing operating individually. It is estimated that the hybrid bearing improves operating clearance and maximum loads by 52% above that of the pure spiral groove hydrodynamic bearing and about 20% above that of the pure hydrostatic bearing. This is accomplished with flow requirements that are less than one-half of 1% of the compressor bleed flow.

2. The orifice size and spiral groove depths have been selected to produce optimum operating clearances at the maximum load and to insure stable operation. It is strongly recommended that due caution be exercised by the manufacturer of the bearings so that groove depths do not exceed the maximum values specified.

3. The bi-directional pair of bearings used for startup and shutdown will allow loads of about 90 pounds to be applied in either direction without difficulty. Exceeding these values will cause rather tight clearances on the reaction bearing and could possibly cause problems in regard to stability on the main hybrid bearing.

4. The bi-directional pair has been designed for a supply pressure of 20 psi. Caution must be exercised if higher supply pressures are desired. The problem here again is with the main hybrid bearing -- if too high a load is applied pneumatic hammer may result.

5. It is recommended that during startup the external pressurization of the opposed pair be activated for a very short time. As soon as loads are applied in the direction of the main hybrid thrust bearing it would be prudent to deactivate the startup system. This will immediately remove the preload of the reaction bearing and thus reduce the total load on the main hybrid bearing with consequent

minimization of stability problems. At shutdown it is recommended that the system be activated near the end of the coastdown cycle, when aerodynamic loads are low. The pre-load of the reaction bearing will then, not produce cumulative high loads on the hybrid bearing.

6. It is recommended that an additional groove plate of identical groove configuration, with 24 orifices of 0.020 in. diameter equally spaced on the orifice circle, be manufactured and tested. Comparative results of the two orifice geometries will determine the error of the theoretical assumption of a line source of pressure emanating from the orifice circle circumference.

IV. REFERENCES

1. "Spiral Groove Bearing", E. A. Muijdermann. Phd. Thesis March, 1964 University of Delft, Netherlands.
2. "Self-Excited Vibrations of an Air-Lubricated Thrust Bearing", L. Licht, D. D. Fuller, B. Sternlicht, ASME Transactions, Vol. 80, No. 2, 1958.
3. "Air-Hammer Instability Pressurized-Journal Gas Bearings", L. Licht, Journal of Basic Engineering, June 1961.
4. "Gas Film Lubrication", W. A. Gross, John Wiley and Sons, Copyright 1962.
5. "Lubrication for Engineers", D. D. Fuller, John Wiley and Sons, copyright 1956.
6. "The Determination of the characteristics of Hydrostatic Bearings through the use of the Electric Analog Field Plotter", A. Loeb, ASLE Transactions, Vol. 1, No. 1, April 1958.
7. "Extension of the Conducting Sheet Analogy to Externally Pressurized Gas Bearings", L. Licht, Journal of Basic Engineering, June 1961.
8. "Cast Bronze Hydrostatic Bearing Design Manual" H. C. Rippel, published by Cast Bronze Bearing Institute, Inc., Jan. 1964
9. "The Gas Lubricated Spiral - Groove Thrust Bearing" S. Whitley, L. G. Williams, United Kingdom Atomic Energy Authority Industrial Group, I. G. Report 28(RD/CA), 1959.
10. Mechanical Vibrations - J. P. DenHartog, Fourth Edition - McGraw Hill Book Co, 1956.
11. Theoretical and Experimental Analysis of Hydrostatic Thrust Bearings - Elwell, R.C., Sternlicht, B. Transactions ASME, Journal of Basic Engineering, September 1960.

APPENDIX A

CALCULATIONS OF SYNCHRONOUS VIBRATIONS AND THERMAL DISTORTIONS

SYNCHRONOUS VIBRATIONS OF THRUST BEARING

Transverse Moment of Inertia of Thrust Bearing

$$I_T = M[R^2 + (a^2/3)]/4$$

R = Outside Radius = 3.25 inches

a = Thickness = 0.8125 inch

M = Bearing Mass

Material = Aluminum

γ' = Weight Density = 0.1 lbs/in³

V = Volume = $\pi R^2 a = \pi(3.25)^2(0.8125) = 26.947$ in³

W = Weight = (26.947)(0.1) = 2.695 lbs

M = Mass = $w/g = \frac{2.695}{386} = 6.968 \times 10^{-3}$ lb-sec²/in.

$$I_T = \frac{6.968 \times 10^{-3}}{4} [3.25^2 + 0.8125^2/3]$$

$$I_T = 18.783 \times 10^{-3} \text{ lb-in.-sec}^2$$

K_{TB} = Tilting Stiffness of Bearing = 46,000 in.-lb/rad. @ 30 lbs load

K_{TS} = Tilting Stiffness of Bearing Support = 20,000 in.-lb/rad

K_T = Total Tilting Stiffness = 66,000 in.-lb/rad

$$\omega_c^2 = K_T/I_T = \frac{66,000 \times 10^3}{18.783} = 3.51 \times 10^6, \quad \omega_c = 1.87 \times 10^3 \text{ rad/sec}$$

$$\omega = 12,000 \times \frac{2\pi}{60} = 1260 \text{ rad/sec}$$

$$\omega^2 = 15.8 \times 10^5 \text{ rad}^2/\text{sec}^2$$

ϵ_{\max} = max. relative swash

ϵ_o = max. absolute swash of rotating plate

ξ = max. absolute swash of stationary plate

$$\epsilon_{\max} = \epsilon_o \left(\frac{\omega^2}{\omega_c^2 - \omega^2} \right)$$

$$\epsilon_{\max} = \epsilon_o \left(\frac{15.8}{35.1 - 15.8} \right) + \frac{15.8}{19.3} \quad \epsilon_o = \underline{\underline{.82 \epsilon_o}}$$

$$\xi_{\max} = \frac{\epsilon_o}{1 - \frac{\omega^2 I_T}{K_T}} = \frac{\epsilon_o}{1 - \frac{15.8(18.783) \times 10^{-1}}{66}} = \frac{\epsilon_o}{1 - .45} = \underline{\underline{+1.820 \epsilon_o}}$$

THERMAL DISTORTIONS

$$y_{\max} = \frac{Pa}{6K\pi} = \frac{HP \times 2545\alpha}{6K\pi}$$

P = Power consumption in BTU/HR.

α = Coefficient of thermal expansion IN./IN. °F

K = Thermal conductivity

HP = 0.054 @ 86 LB. Load

$\alpha = 13.2 \times 10^{-6}$ IN./IN. - °F

$K = 70 \text{ BTU/HR. FT}^2 - \text{°F/FT} = 5.38 \frac{\text{BTU}}{\text{HR.} - \text{IN.}^2 - \frac{\text{°F}}{\text{IN.}}}$

$$y_{\max} = \frac{(.054)(2545)(13.2 \times 10^{-6})}{6 (5.38)(3.14)} = 1.79 \times 10^{-5} \text{ IN.}$$

APPENDIX B
FINAL DESIGN AND PERFORMANCE
OF THRUST BEARING

As the design of the Turbine - Alternator progressed a re-evaluation of the thrust balance indicated that it would be necessary to increase the thrust bearing load capacity. This resulted in some major alterations to the specifications, namely

- a) Total load = 250 lbs. (at Startup)
- b) Bearing Max Diameter = 7 in.
- c) Ambient Pressure , $P_a = 6$ psia
- d) Aerodynamic Load = 80 lbs.

Using the computer program discribed in the text, it was possible to establish a bearing configuration that would satisfy requirements. The geometry, gas requirements and performance for the Main Thrust and Reaction Bearings are tabulated below:

MAIN THRUST BEARING

Outside Radius, $R_4 = 3.5$ in.
Orifice Radius, $R_3 = 3.25$ in.
Spiral Groove outside radius, $R_2 = 3.00$ in.
Spiral Groove inside radius, $R_1 = 1.2$ in.
Groove Depth, $h_o = .0057$ in.
Orifice diameter, $D_o = .031$ in.
No. of orifices, $N_o = 36$

REACTION BEARING

Outside radius, $R_4 = 3.5$ in.
Inside radius, $R_1 = 2.0$ in.
Inner orifice radius, $R_2 = 2.735$ in.
Outer orifice radius, $R_3 = 2.766$ in.
Orifice diameter, $D_o = .031$ in.
No. of orifices, $N_o = 36$

Gas Conditions

Supply Pressure, $P_s = 16$ psia max.

Exceeding this pressure could initiate pneumatic hammer.

Performance					
<u>Condition</u>	<u>Load</u> <u>lbs.</u>	<u>Flow</u> <u>lbs/sec</u>	<u>Main Brg.</u> <u>Clearance</u> <u>in.</u>	<u>Reaction Brg.</u> <u>Clearance</u> <u>in.</u>	<u>RPM</u>
Startup (Vertical Attitude)	254	.0103	.00132	.00868	0
Normal (Zero G)	80	.004	.0038	.0062	12,000

The Friction Horsepower Loss at normal conditions = .055 H.P.

The Spiral groove configuration is identical with that described in the content of this report except that it starts and ends at larger radii.